MID-AMERICA TRANSPORTATION CENTER

Report # MATC-KU: 157-1

Final Report

WBS: 25-1121-0005-157-1

Quantifying Soil Moisture Reduction by Wicking Geotextile to Minimize Pavement Distresses

Jie Han, PhD, PE, F.ASCE
Roy A Roberts Distinguished Professor
Department of Civil, Environmental, and Architectural Engineering
The University of Kansas

Md Wasif Zaman, PhD
Research Associate

Robert L. Parsons, PhD, PE, F.ASCE
Professor

2024

A Cooperative Research Project sponsored by U.S. Department of Transportation- Office of the Assistant Secretary for Research and Technology

Quantifying Soil Moisture Reduction by Wicking Geotextile to Minimize Pavement Distresses

Jie Han, Ph.D., P.E., F.ASCE
Roy A. Roberts Distinguished Professor
Department of Civil, Environmental, and
Architectural Engineering
The University of Kansas

Md Wasif Zaman, Ph.D.
Research Associate
Department of Civil, Environmental, and
Architectural Engineering
The University of Kansas

Robert L. Parsons, Ph.D., P.E., F.ASCE
Professor
Department of Civil, Environmental, and
Architectural Engineering
The University of Kansas

A Report on Research Sponsored by

Mid-America Transportation Center

University of Nebraska–Lincoln

June 2024

Technical Report Documentation Page

1. Report No. 25-1121-0005-157-1	2. Government Accession No.	3. Recipient's Catalog No.
4. Title and Subtitle Quantifying Soil Moisture Reduction by Wicking Geotextile to Minimize Pavement Distresses		5. Report Date June 2024
		6. Performing Organization Code
7. Author(s) Jie Han, Md. Wasif Zaman, and Robert L. Parsons		8. Performing Organization Report No. 25-1121-0005-157-1
9. Performing Organization Name and Address Mid-America Transportation Center Prem S. Paul Research Center at Whittier School 2200 Vine St. Lincoln, NE 68583-0851		10. Work Unit No. (TRAIS)
		11. Contract or Grant No. 69A3551747107
12. Sponsoring Agency Name and Address Office of the Assistant Secretary for Research and Technology 1200 New Jersey Ave., SE Washington, D.C. 20590		13. Type of Report and Period Covered Final Report 07/01/2022 - 06/30/2023
		14. Sponsoring Agency Code MATC TRB RiP No. 91994-113
15. Supplementary Notes		

16. Abstract

Excessive moisture in pavement foundations including base courses and subgrade is one of the major causes for pavement distresses, which often pose safety risks to vehicles and drivers and increase the cost for maintenance and reconstruction. Moisture can weaken pavement foundations and become a source for freeze-thaw problems in cold regions, which accelerate the deterioration of pavements with time. Therefore, pavement drainage is critical to pavement performance. Typical drainage systems are effective for saturated soils but become less effective or ineffective for unsaturated soils. Wicking geotextile that contains deep-grooved fibers can generate suction when in contact with water and reduce moisture in unsaturated soils. However, the effectiveness of the wicking geotextile in reducing moisture depends on several factors including the percentage of fines in soils. So far, no simple test method is available to evaluate the effectiveness of the geotextile in reducing moisture in soils including those with fines and no fines content limit has been established for the wicking geotextile to be effective. This research evaluated wettability of geotextiles with contact angles and developed a simple soil column test method to quantify the effectiveness of the wicking geotextile in reducing moisture in sands at different fines contents and the influence distances from the geotextile as compared with the non-wicking geotextiles. The measured contact angles for the wicking geotextile decreased quickly to less than 90^{o} and were smaller than those for the non-wicking woven geotextile and the nonwoven geotextile, indicating its better wettability. The soil column tests first determined field capacities of silty sands at different fines contents and then evaluated moisture reduction by geotextiles by measuring moisture contents at different distances from the geotextile location at different time periods. These tests demonstrated the effectiveness of the wicking geotextile and determined the amount of moisture reduction and the distance of influence, and the fines content limit for the wicking geotextile to be effective.

17. Key Words Wettability, field capacity, moisture reduction, silty sand, wicking geotextile	18. Distribution Statement		
19. Security Classif. (of this report) Unclassified	20. Security Classif. (of this page) Unclassified	21. No. of Pages 66	22. Price

Table of Contents

List of Figures

List of Tables

Acknowledgments

The authors would like to thank the former Ph.D. student, Dr. Hao Liu, at the University of Kansas for his great help in making test boxes in the laboratory and appreciate Mr. John Lostumbo of Solmax Inc. for providing the geotextile materials and his technical feedback and suggestions.

Disclaimer

The contents of this report reflect the views of the authors, who are responsible for the facts and the accuracy of the information presented herein. This document is disseminated in the interest of information exchange. The report is funded, partially or entirely, by a grant from the U.S. Department of Transportation's University Transportation Centers Program. However, the U.S. Government assumes no liability for the contents or use thereof.

Abstract

Excessive moisture in pavement foundations including base courses and subgrade is one of the major causes for pavement distresses, which often pose safety risks to vehicles and drivers and increase the cost for maintenance and reconstruction. Moisture can weaken pavement foundations and become a source for freeze-thaw problems in cold regions, which accelerate the deterioration of pavements with time. Therefore, pavement drainage is critical to pavement performance. Typical drainage systems are effective for saturated soils but become less effective or ineffective for unsaturated soils. Wicking geotextile that contains deep-grooved fibers can generate suction when in contact with water and reduce moisture in unsaturated soils. However, the effectiveness of the wicking geotextile in reducing moisture depends on several factors including the percentage of fines in soils. So far, no simple test method is available to evaluate the effectiveness of geotextile in reducing moisture in soils including those with fines and no fines content limit has been established for the wicking geotextile to be effective. This research evaluated wettability of geotextiles with contact angles and developed a simple soil column test method to quantify the effectiveness of the wicking geotextile in reducing moisture in sands at different fines contents and the influence distances from the geotextile as compared with the non-wicking geotextiles. The measured contact angles for the wicking geotextile decreased quickly to less than 90^{o} and were smaller than those for the non-wicking woven geotextile and the nonwoven geotextile, indicating its better wettability. The soil column tests first determined field capacities of silty sands at different fines contents and then evaluated moisture reduction by geotextiles by measuring moisture contents at different distances from the geotextile location at different time periods. These tests demonstrated the effectiveness of the wicking geotextile and

determined the amount of moisture reduction, the distance of influence, and the fines content limit for the wicking geotextile to be effective.

Executive Summary

Excessive moisture in pavement foundations is a major cause for distresses, posing safety risks and increasing maintenance costs. Traditional drainage systems are effective for saturated soils but less or not effective in unsaturated soils, leading to pavement deterioration, particularly in cold regions where freeze-thaw cycles exacerbate the problem. Wicking geotextile, utilizing deep-grooved fibers to generate suction, shows promise in reducing moisture in unsaturated soils. However, its effectiveness depends on several factors including soil fines content. So far, no standardized test method is available to evaluate its efficacy. This research aimed to develop a simple soil column test method to quantify the effectiveness of the wicking geotextile in reducing moisture in sands with fines. By determining the field moisture capacities of silty sands and assessing the moisture reduction at different distances from the geotextile, this study established the extent of moisture reduction, the influence distance, and the fines content limit for effective geotextile use, thus enhancing pavement performance and reducing maintenance needs.

Chapter 1 Introduction

1.1 Background

Moisture in pavements may come from infiltration from precipitation, capillary rise of groundwater, seepage from higher ground, and vapor movements due to temperature differences as shown in Figure 1.1. It remains within base/subbase courses and subgrade, weakens the soils, and induces ground movement due to freeze-thaw cycles in cold regions, thus causing the distresses of pavements over time. Pavement distresses often pose safety risks to vehicles and drivers and increase the cost for maintenance and reconstruction.

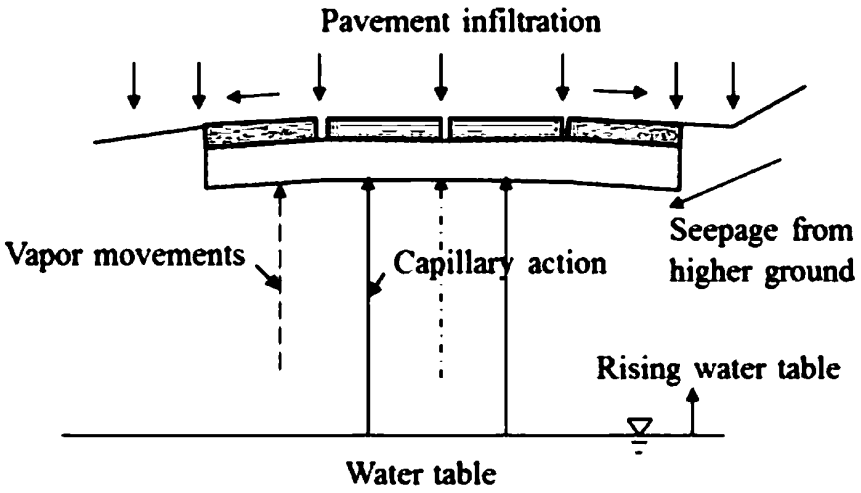

Figure 1.1 Sources of water (FHWA, 1992)

Pavement drainage is critical to maintain pavement performance and minimize pavement distresses. Typical drainage systems including drainage bases and edge drains are effective for saturated soils. However, they become less effective or ineffective for unsaturated soils, which may still have too much moisture and cause pavement distresses. Wicking geotextile that

contains deep-grooved fibers can generate suction when in contact with water and reduce moisture in unsaturated soils.

1.2 Wicking Fibers

While the wicking geotextile is a relatively new product to the geosynthetics community, the concept of wicking has been well known to the garment industry since the late 1950s, mostly for manufacturing performance apparels (e.g., athletic, comfort, and cooling) that can transfer and evaporate body moisture (e.g., sweat) to the environment at a faster rate. Textile engineers and researchers have conducted many investigations on the properties and size/shape of pore structures of fibrous materials. Their studies indicated that wicking fibers can effectively absorb and transfer liquid. However, liquid quantity and transfer mostly depend on the fiber type, pore structure, internal surface, chemical treatment, and liquid property.

A typical fabric has warp and weft directions based on the manufacture process. Wicking ability in two directions may be different. Harnett and Mehta (1984) described four different laboratory tests to evaluate wicking ability of knitted fabrics in different directions: (1) strip test, (2) plate test, (3) spot test, and (4) siphon test. They found the vertical strip test (also known as the column test) is appropriate for tracking movement of water while the horizontal plate test is suitable for simulating a sweating skin surface (Figure 1.2)

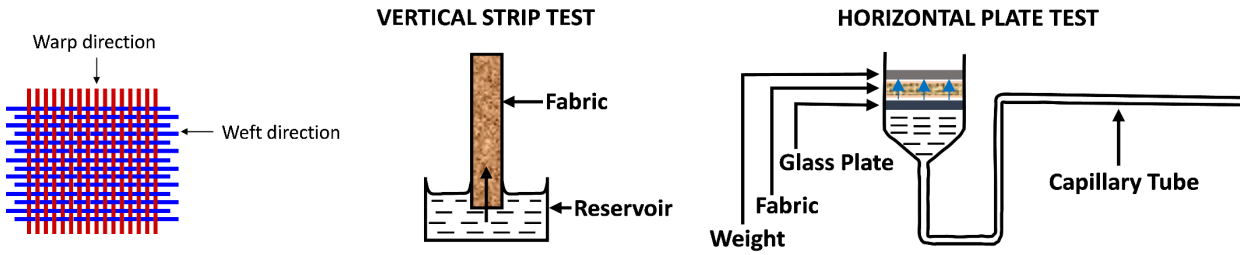

(a) (b) (c)

Figure 1.2 Laboratory tests to measure wick ability in different directions: (a) fiber directions, (b) parallel to the fabric plane, and (c) perpendicular to the fabric plane (Harnett and Mehta, 1984).

1.3 Evolution of Wicking Geotextile from Wicking Fiber

In recent years, geotechnical engineers and researchers have paid attention to removing moisture from unsaturated road sections with the help of geotextiles. To do this, one type of geotextile namely "wicking geotextile" was introduced to the market by providing an improved lateral drainage ability. Wicking geotextile includes special nylon fibers that have four deep grove (4DG) channels as shown in Figure 1.3, to produce a high capillary force to absorb and wick water out of road sections. Recent studies on the wicking geotextile have proved its effectiveness to remove moisture from unsaturated soil and hence, increase the overall roadway performance. Various laboratory experiments and field monitoring have taken place to quantify the behavior and working mechanisms of the wicking geotextile.

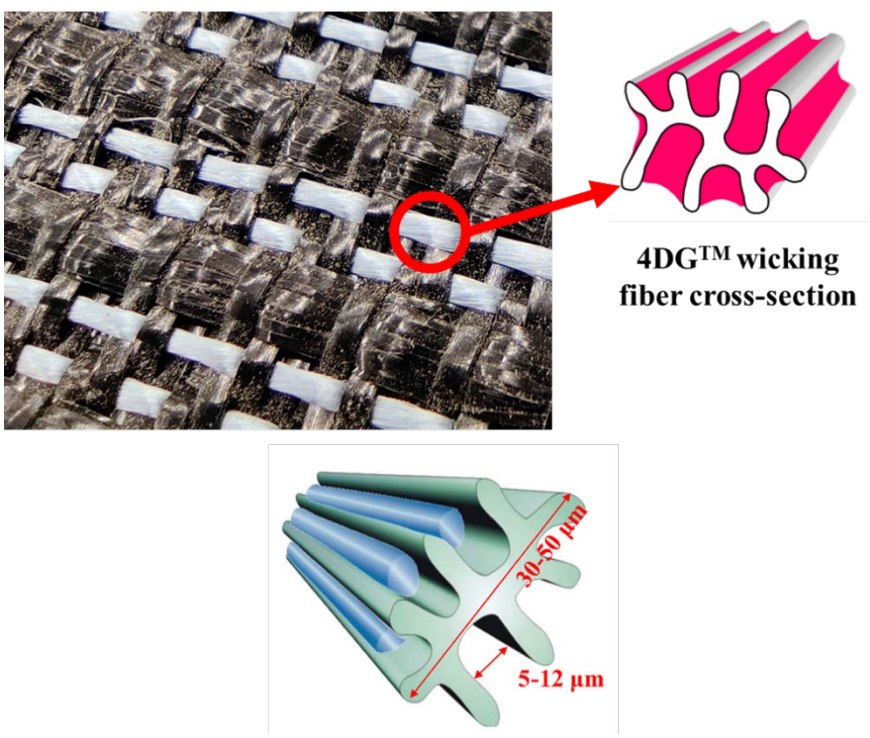

Figure 1.3 Photograph (top-left) of the wicking geotextile and schematic (top-right and bottom) of the deep-grooved nylon wicking fiber (Guo, 2017)

The deep-grooved fibers are weaved into the geotextile in the machine direction. For roadway applications, these deep-grooved fibers are perpendicular to the traffic direction. Compared with non-wicking woven geotextiles, wicking geotextile presents two advantages: (1) greater transmissivity under saturated conditions and (2) the ability to "wick" water out of the soil when the soil is unsaturated. As a result, the inclusion of a wicking geotextile in roadway structures not only provides reinforcement as non-wicking woven geotextiles but also enhances drainage under both saturated and unsaturated conditions (Guo, 2017).

1.4 Surface Wettability

Wetting is a foremost requirement for starting the drainage or wicking process in a fibrous material. Wettability of a solid surface can be described by the contact angle of a liquid on that surface, which is the angle forming between the tangent of the liquid surface and the

horizontal specimen surface. When liquid is on an ideal solid surface, such as glass, metal, and ceramic, it will reach an equilibrium shape dependent on the contact angle. Marmur (2006) pointed out "the ideal surface for a contact angle is smooth, rigid, chemically homogeneous, insoluble, and non-reactive." Geotextiles consist of individual fibers and are different from solid media; therefore, they do not have an ideal surface. When liquid is on a fibrous surface, such as a textile fabric, liquid penetrates the fabric over time. In this case, the contact angle decreases until the liquid droplet fully disappears into the material. Kutilek and Nielsen (1994) concluded that the magnitude of the contact angle could be used to define wetting of solids in three categories as follows: (1) when the contact angle $\theta = 0°$, the surface is completely wet and the solid can be considered fully hydrophilic; (2) when $0° < \theta < 90°$, the solid is considered partially hydrophilic since partial wetting of the surface occurs; and (3) when $\theta \geq 90°$, the surface exhibits non-wetting and the solid is considered hydrophobic.

1.5 Benefit of Moisture Reduction from Soil

Removal of water (e.g., drainage) in an efficient and timely manner is necessary to improve the short-term and long-term performance of earth structures including slopes, walls, and roadways (Azevedo and Zornberg 2013, Lin et al. 2017, Lin and Zhang 2018, Guo et al. 2019). Non-wicking geotextiles made of synthetic permeable textile materials (e.g., polyester, polyamide, polypropylene, and polyethylene) are not effective in unsaturated soil conditions due to their fiber properties and pore structures (Koerner 2012). Both non-wicking woven and non-woven geotextile fibers are unable to produce enough capillary force that allows them to absorb and transport moisture between soil particles under a certain saturation limit.

To overcome this problem, a wicking geotextile containing special hydrophilic and hygroscopic nylon fibers with deep-grooved channels has been introduced to the market. This

product has demonstrated its excellent moisture wicking ability (i.e., wicking drainage), especially under unsaturated soil conditions as compared with those commonly used woven and non-woven geotextiles in several studies (Zhang et al. 2014, Guo et al. 2017, Wang et al. 2017, Zornberg et al. 2017, Lin and Zhang 2020, Biswas et al. 2021). Capillary water in the soil migrates towards the wicking geotextile due to the suction difference between the unsaturated soil and the wicking geotextile and finally evaporates into the air through the exposed portion of the geotextile to the environment (Zhang et al. 2014, Wang et al. 2017, Guo et al. 2017, Guo et al. 2019) as shown in Figure 1.4. Lin et al. (2017) collected field data of the wicking geotextile buried in Alaskan pavements, showing that the wicking geotextile was able to reduce moisture contents of soils in the pavements during thawing in spring. The test section showed the wicking geotextile successfully prevented water from rising up from the subgrade via capillary action.

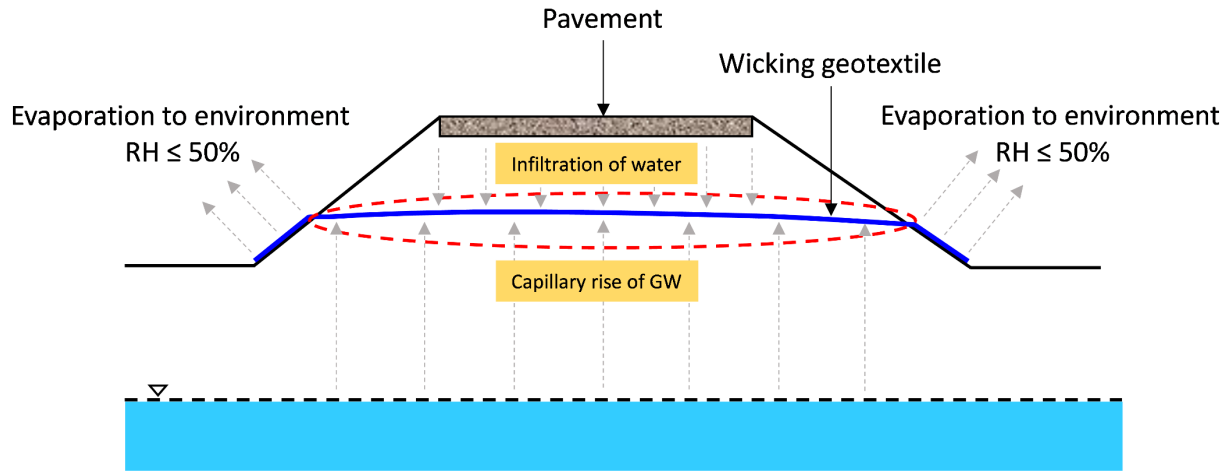

Figure 1.4 Mechanism of the water-wicking geotextile interaction in soil (Guo et al., 2016).

1.6 Problem Statements

Several experimental studies reported that the presence of nylon fibers in the wicking geotextile enhances lateral drainage from unsaturated soils (Azevedo and Zornberg, 2013; Guo et

al., 2017; Lin and Zhang, 2018; Hachem and Zornberg, 2019; Lin et al., 2019). Practical applications of the wicking geotextile have also been reported in several field studies (Lin et al., 2017; Zornberg et al., 2017; Galinmoghadam and Zhang, 2020; Galinmoghadam et al., 2022; Guzman et al., 2021; Biswas et al., 2021; and Liu et al., 2022).

Galinmoghadam and Zhang (2023) reported that wicking geotextile effectively removes moisture from soil containing fines less than 15%. However, the performance of wicking geotextile for moisture reduction in soils prepared at the field moisture capacity condition containing different amounts of fines has not been explored yet. In addition, the interface shear strength and interaction coefficients of wicking geotextile-sands at different fines amounts and moisture contents have not yet been identified. Furthermore, the benefits of wicking geotextile under traffic loading at the field moisture capacity condition of subgrade soil, compared with sections without or with nonwoven geotextile under the same conditions, have not been explored. Therefore, the lack of information about the wicking geotextile's ability to reduce moisture from soil at the field moisture capacity condition with different amounts of fines, interaction coefficients, and the wicking geotextile's performance under cyclic loading at the field moisture capacity condition of subgrade soil limits the development of pavement design guidelines for incorporating the benefits of wicking geotextile, especially when the subgrade soil contains fines.

1.7 Research Objectives

The objectives of this study were to: (1) investigate the wettability of different types of geotextiles; (2) quantify the field capacity amount of water in the silty sands containing different amounts of fines by a simple method; and (3) investigate the amount of moisture reduction and

the influence zone in silty sands placed above and below the wicking geotextile and develop the relationship between the moisture reduction amount and time.

1.8 Organization of Report

This report consists of five chapters. Chapter one presents an introduction including background and problem statements, research objectives, and organization of the report. Chapter two presents the contact angle method to evaluate the surface wettability of wicking geotextile. Chapter three presents the simple laboratory technique to determine the field moisture capacity profiles of silty sand containing different amounts of fines. Chapter four presents the laboratory tests to investigate the wicking geotextile for moisture reduction in silty sands at different fines contents. Chapter five presents the conclusions and future work.

Chapter 2 Evaluating Wettability of Geotextiles with Contact Angles

2.1 Introduction

Wicking woven geotextile is a relatively new product to the geosynthetics industry that contains a special type of hydrophilic and hygroscopic fibers with the fourth-generation deep grooves. This product has demonstrated its excellent moisture wicking ability (i.e. wicking drainage), especially under unsaturated soil conditions as compared to commonly-used woven and nonwoven geotextiles in several studies (Azevedo & Zornberg, 2013; Guo et al., 2017; Guo et al., 2019; Guo et al., 2021; Lin et al., 2017; Lin et al., 2018; Wang et al., 2017; Zhang et al., 2014; Zornberg et al., 2017). Azevedo & Zornberg (2013) showed the efficacy of a wicking woven geotextile to remove water accumulated in capillary barriers that form between layers of two different sized porous materials. Zhang et al. (2014) reported a successful field study of using a wicking geotextile to mitigate freeze-thaw problems in an Alaskan road. Guo et al. (2017) evaluated the water removal rate of the wicking woven geotextile from water tanks in a controlled environment considering vapor pressure, temperature, and relative humidity. Wang et al. (2017) conducted a laboratory study to evaluate the benefits of the wicking geotextile to reduce the moisture content of the soil after simulated rainfalls. Lin et al. (2017) observed that the wicking geotextile was able to reduce the moisture content of an unsaturated soil that might increase during thawing in spring. Yuan (2017) concluded that the wicking geotextile increased the subgrade reaction modulus of a base material after drainage. Guo et al. (2019) showed that the wicking geotextile could effectively remove moisture from a zone ranging from 180 to 250 mm in the aggregate placed above the geotextile. Hachem & Zornberg (2019) experimentally tested the moisture removal ability of a wicking geotextile for capillary rise of ground water at the interface of the base course and the subgrade. Guo et al. (2021) evaluated the performance benefits of the wicking geotextile between a granular base and a fine-grained subgrade to reduce

permanent deformations under cyclic plate loading after simulated rainfalls over the control sections and the non-wicking woven geotextile-improved sections.

Wetting is a foremost requirement for starting the drainage or wicking process in a fibrous material. Wettability of a solid surface can be described by the contact angle of a liquid on that surface, which is the angle forming between the tangent of the liquid surface and the horizontal specimen surface. When liquid is on an ideal solid surface, such as glass, metal, and ceramic, it will reach an equilibrium shape dependent on the contact angle. Marmur (2006) pointed out "the ideal surface is considered to be smooth, rigid, chemically homogeneous, insoluble, and non-reactive." Geotextiles consist of individual fibers and are different from solid media; therefore, they do not have an ideal surface. When liquid is on a fibrous surface, such as a textile fabric, liquid penetrates the fabric over time. In this case, the contact angle decreases until the liquid droplet fully disappears into the material. Kutilek and Nielsen (1994) concluded that the magnitude of the contact angle could be used to define wetting of solids in three categories as follows: (1) when the contact angle $\theta = 0°$, the surface is completely wet and the solid can be considered as being fully hydrophilic; (2) when $0° < \theta < 90°$, the solid is considered being partially hydrophilic since partial wetting of the surface occurs; and (3) when $\theta \geq 90°$, the surface exhibits non-wetting and the solid is considered to be hydrophobic.

Past studies showed that spreading and penetration of a liquid droplet on a porous surface depend on time (Clarke et al. 2002; Kumar & Deshpande 2006; and Sarah & Ulrich 2018). In the literature, three possible mechanisms have been identified for the change of contact angle over time: (i) initial spreading of the droplet, (ii) penetration of the droplet into the channels of fibers and gaps between fibers, and (iii) evaporation of the droplet. Right after a droplet was placed on a surface, the droplet spreads, and the contact angle decreases. The contact angle can also

decrease as the droplet penetrates the channels of fibers and pore spaces between fibers. Due to relative humidity difference from air, the droplet evaporates with time. Additional mechanisms were identified in this study such as the contact angle of the droplet decreases due to the wicking ability of fibers and will be discussed later. If there are wicking fibers, the droplet can disappear due to lateral movement of water in the fiber channels where suction develops. Due to the above mechanisms, the observation time for the contact angle should be limited.

The most common methods to measure contact angles are: (i) the liquid droplet method (Fig. 2.1.a) and (ii) the immersed filament method (Fig. 2.1.b) (also known as the Wilhelmy plate method). The liquid droplet method follows the ASTM D7334 standard where a small droplet (typically, 0.5µL-5µL volume) of specific liquid is dropped onto the specimen surface using a syringe. Once the liquid droplet interacts with the specimen surface, an optical image is scanned and projected on the computer screen to calculate the angle that forms between the tangent of the liquid surface and the horizontal specimen surface. This type of contact angle is important to identify the surface roughness and initial wettability of the specimen.

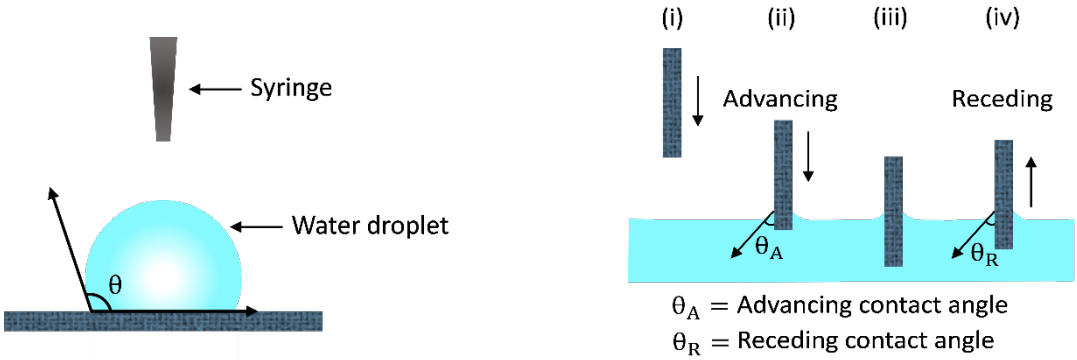

Figure 2.1 Common methods to measure contact angle: (a) the liquid droplet method and (b) the immersed filament method (modified from Kung et al., 2019)

In the immersed filament method, a small strip of the specimen is submerged in a bowl containing liquid at a specific speed and then extracted from the bowl in the same way. Due to the adhesion between the liquid and the specimen molecules, the liquid surface close to the specimen tends to rise and form an angle. During the submersion, the angle is called the advancing contact angle while during the extraction, the angle is called the receding contact angle (Fig. 2.1.b). This type of contact angle is commonly used to investigate the capillary behavior and calculate the wicking height (i.e., travel distance of liquid) using the Washburn capillary flow equation (Washburn, 1921).

Contact angle is a common parameter to determine the wettability and surface roughness of a fabric in the textile industry. Miller & Young (1975) measured the water contact angles on nylon, polyester, and polypropylene monofilaments (rinsed with petroleum ether and air dried) as 71°, 75°, and 86°, respectively. Several studies reported the contact angle as a parameter to evaluate wettability and concluded that fabrics having smaller contact angles can transport liquid faster as the fibers produce larger capillary pressure (Ghali et al., 1994; Le et al., 1996; Chen et al., 2001; and Melki et al., 2019). Shim et al. (2014) investigated the robustness of hydrophobicity of textile fabrics by the contact angle and suggested it as an effective parameter to evaluate wettability.

Chemical and plasma treatment can effectively improve the wettability of a fabric as concluded in past studies. Van Der Meeren et al. (2002) tested the wettability by measuring the contact angle of water on cotton fabrics treated with different conditioners and concluded that chemical treatment significantly improved the wettability. Similarly, Pimanpang et al. (2006) found that liquid's contact angle drastically decreased on silk fabrics after treated with H_2SO_4 solution. Rani et al. (2018) performed a contact angle analysis on both untreated and plasma-

treated silk fabrics and found that the contact angle could be significantly reduced by treating the fabric, indicating better wettability.

Wettability is one of the hydraulic properties of the geotextile important for drainage applications (Rollin & Lombard, 1988). Rollin & Lombard (1988) concluded that water flow may create a gap between the soil and the geotextile if water cannot penetrate the geotextile due to its poor wettability. The European Committee for Standardization (CEN) (2000) developed a standard for determining the initial resistance of a dry geotextile or a dry geotextile-related product against water flow perpendicularly to the plane of the specimen based on the hydraulic head required for initiating the flow. This resistance is different from wettability to be evaluated in this study. Unsaturated soil may still wet the geotextile although there is no hydraulic head. Stormont et al. (1997) studied the water retention functions of four nonwoven polypropylene geotextiles and concluded that the pore size and the geotextile fiber-water contact angle affected the soil moisture retention properties. Henry & Patton (1998) used the immersed filament method to measure the water contact angle on a nonwoven geotextile using a Dynamic Contact Analyzer (DCA). They concluded that contact angle measurement was helpful to investigate the wetting and capillary behavior of water in geotextiles. Later, Stormont & Morris (2000) reported that contact angle measurement provided information to characterize geotextile behavior under unsaturated conditions. They further concluded that the capillary rise or capillary depression was a function of the contact angle of the material as well as the pore structure. Jeon & Bouazza (2007) used plasma treatment on nonwoven geotextiles to improve the hydrophilicity of the geotextile. In other words, plasma treatment on geotextiles was used to achieve better wettability. Bouazza (2014) proposed a capillary rise method to evaluate the wettability of needle-punched nonwoven polyester geotextiles. Bouazza (2014) found the untreated nonwoven geotextiles had

non-wetting behavior since no capillary rise was observed in the laboratory experiment. However, he classified and compared the hydrophobicity and hydrophilicity based on the water droplet method and concluded the untreated nonwoven geotextile as hydrophobic (contact angle=153°). Furthermore, he compared the untreated specimen with the specimen treated by the wet oxidation method that performed better for capillary rising.

Aydilek et al. (2007) suggested to revise the ASTM D6767 standard by including a contact angle as an additional parameter for determining capillary rise of liquid in fibers. They suggested that wettability of the compressed specimen (i.e., disturbed geotextiles) should be investigated to properly quantify the hydraulic behavior of the geotextile. In addition, Elton & Hayes (2007) used the bubble point method (i.e. ASTM D6767) to analyze the pore size distribution (PSD) of geotextiles and concluded that the contact angle was important to accurately estimate PSD. To better design geotextiles for filtration purposes, Elton & Hayes (2008) further investigated the contact angle between the wetting fluid and the geotextile and suggested reconsidering the data reduction of the ASTM D6767. In addition, Fatema & Bhatia (2020) suggested including contact angle measurement in the ASTM D6767 that generally assumes a zero-contact angle between geotextiles and mineral oil.

Based on the above discussion, it can be concluded that a contact angle measured by the liquid droplet method is suitable to determine the surface wettability of fibers, whereas a contact angle measured by the immersed filament method is suitable to predict the liquid capillary rise in the fabric. In the first method, the surface of the fabric gets wet by a droplet while liquid rises vertically in a fabric strip to make it wet in the second method. Definitions of geotextile wettability based on these two methods are not same; therefore, a clear guideline on the significance and applicability of these methods is needed. In this study, the liquid droplet method

was used to measure the water contact angles of geotextiles by an optical tensiometer. Furthermore, the effects of soil particle intrusion and geotextile or fiber deep groove flattening associated with soil compaction on the wettability of geotextiles were investigated and will be discussed later.

2.2 Material and Test Method

In this study, the water droplet method was used to determine the contact angles of water on three types of geotextiles, namely (i) wicking woven (WW) geotextile; (ii) non-wicking woven (NWW) geotextile; and (iii) nonwoven (NW) geotextile (Fig. 2.2.a). Table 2.1 provides the basic properties of the geotextile products used in this study. Among them, the WW geotextile is manufactured with a special type of hydrophilic and hygroscopic fibers. An optical tensiometer, VCA Optima XE (AST Inc.), was used in this study to measure the water contact angle on the geotextile surface (Fig. 2.2.b).

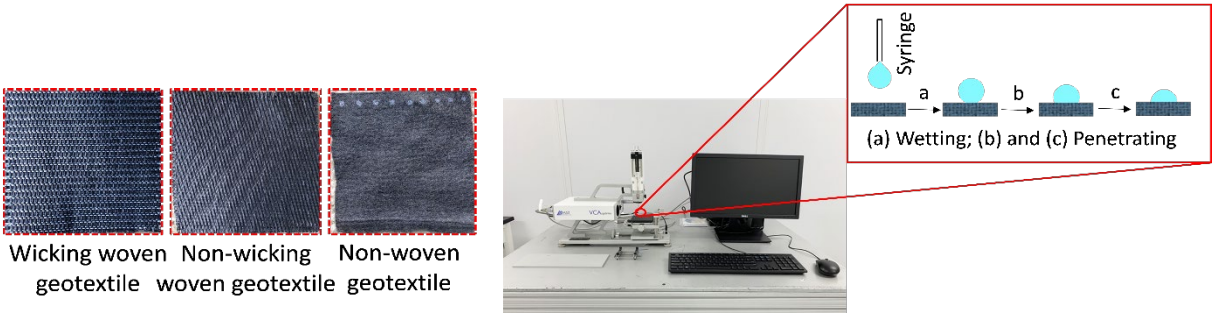

(a) (b)

Figure 2.2 Contact angle test setup: (a) geotextile specimens and (b) optical tensiometer used to measure contact angle.

Since geotextiles are typically placed between soils subjected to compaction, it is important to evaluate a possible particle intrusion effect associated with soil compaction on their

wettability. To investigate a possible compaction effect on the contact angle, a standard Proctor compaction mold was used to compact clean sand on the geotextile specimen to maintain a specific compaction energy. Figure 2.3 shows the gradation of the sand material. The unit masses of the geotextile specimens used in this study were measured according to ASTM D5261 standard and are provided in Table 2.1. The geotextile specimen was placed at the bottom inside the mold and covered by the sand, followed with compaction for one lift at a different lift thickness. Therefore, the geotextile was compacted at sand lift thicknesses of 50, 100, and 150 mm, respectively in three tests. After compaction, the geotextile specimen as a disturbed geotextile was carefully removed from the compaction mold and tested to determine possible contact angle changes of the geotextile after soil compaction under various soil thicknesses. The geotextile specimen without any compaction is referred to as an undisturbed geotextile in this article.

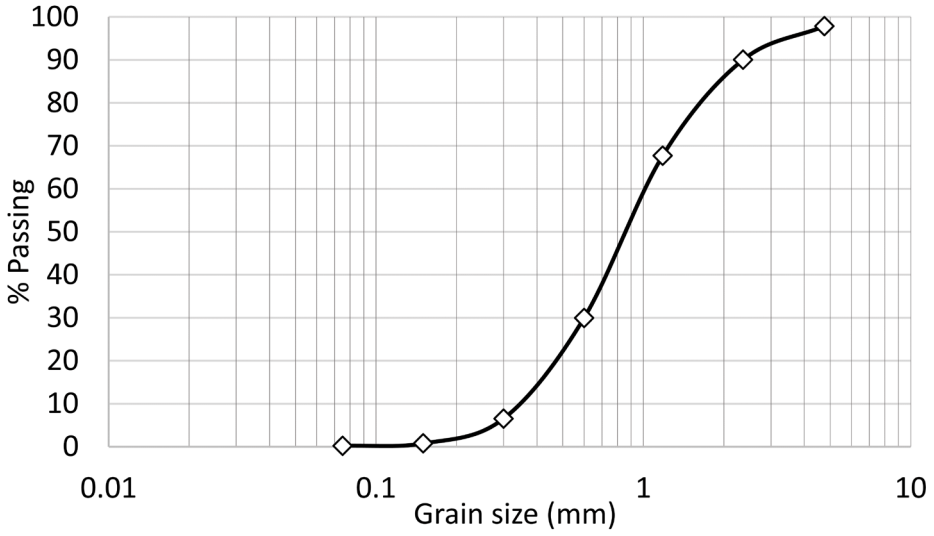

Figure 2.3 Particle size distribution of Kansas river sand.

Table 2.1 Geotextile properties (provided by the manufacturer).

Geotextile	Property	Unit	Value
WW	Apparent opening size	Mm	0.43
	Pore size (O_{50})	Microns	85
	Pore size (O_{95})	Microns	195
	Permittivity	sec^{-1}	0.4
	Flow rate	$l/min/m^2$	1222
	Thickness	Mm	1.24
	Unit mass	g/m^2	497
	Specific gravity of fibers	-	0.96
	Porosity	%	58.6
	Tensile strength (2% strain, MD)	kN/m	7
	Tensile strength (2% strain, CD)	kN/m	15.8
	Wet front movement (vertical)	Mm	152
	Wet front movement (horizontal)	Mm	1862
NWW	Apparent opening size	Mm	0.60
	Permittivity	sec^{-1}	0.4
	Flow rate	$l/min/m^2$	1222
	Thickness	Mm	1.22
	Unit mass	g/m^2	385
	Specific gravity of fibers	-	0.91
	Porosity	%	65.3
	Tensile strength (2% strain, MD)	kN/m	14
	Tensile strength (2% strain, CD)	kN/m	19.3
	Tensile Strength (ultimate)	kN/m	70
NW	Apparent opening size	Mm	0.212
	Permittivity	sec^{-1}	1.5
	Flow rate	$l/min/m^2$	4481
	Thickness	Mm	1.9
	Unit mass	g/m^2	220
	Specific gravity of fibers	-	0.91
	Porosity	%	87.3
	Grab tensile strength	N	712
	Grab elongation	%	50
	Trapezoid tear	N	267
	CBR puncture strength	N	1825

Note: porosity = $1-(M/\rho t)$, M = unit mass, ρ = density of fibers, t = average thickness.

2.3 Results and Discussion

The change of the contact angle of a water droplet on a geotextile surface was recorded for 12 seconds. Within this observation period, the water droplet fully penetrated the WW geotextile whereas the droplet partially penetrated the other two types of geotextiles.

2.3.1 Interaction of water droplets on geotextiles

To observe the interaction of a water droplet on a geotextile, a water droplet (5μL volume) was dropped onto each geotextile surface using a syringe. Figure 2.4 shows the water droplets on the fibers in different geotextiles. On the wicking woven geotextile, the water droplet spread and penetrated rapidly into the deep groove channels of fibers, followed by the lateral movement due to the high capillary force (Fig. 2.4a). Because nylon is a hydrophilic material, water molecules interacted more quickly with the nylon molecules, thus resulting in a smaller contact angle. In addition, the nylon fibers in the wicking geotextile had deep grooves that could generate suction and attract water, therefore, the contact angle decreased quickly, and the water droplet disappeared into the fabric within a few seconds after dropping. In the non-wicking woven geotextile, the water droplet spread on the flatter surface of the fibers and partially penetrated the pores between fibers (Fig. 2.4b). Due to the flatter geometry of the fibers, capillary action did not take place, and the water droplet remained beaded on the geotextile, thus leading to a slower rate of change in the contact angle. In the nonwoven geotextile, many filaments were compressed together to impede spreading and penetration of the water droplet (Fig. 2.4c). Clarke et al. (2002) also concluded that the complex internal geometry of real porous systems inhibits penetration of a wetting liquid. Note that the NWW and NW geotextiles are made of polypropylene fibers, which are hydrophobic. As a result, they had larger contact angles. Since these two geotextiles did not have wicking fibers, the change of contact angles with time

was slow. A geotextile with larger opening sizes might allow a smaller droplet to enter openings. To measure a contact angle and investigate the wettability of a geotextile, a droplet larger than the opening size is suggested.

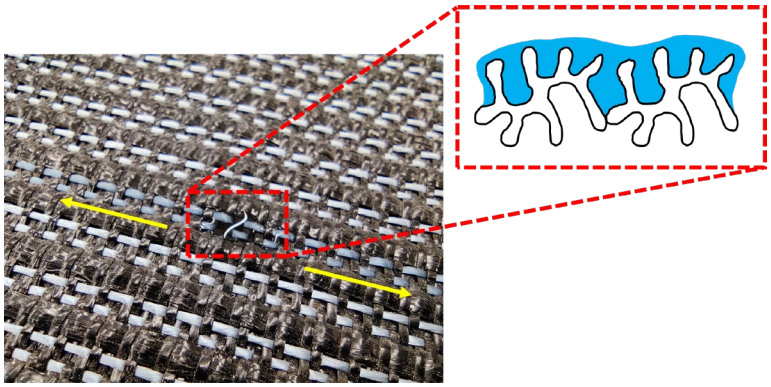

(a) water droplet on the wicking woven geotextile

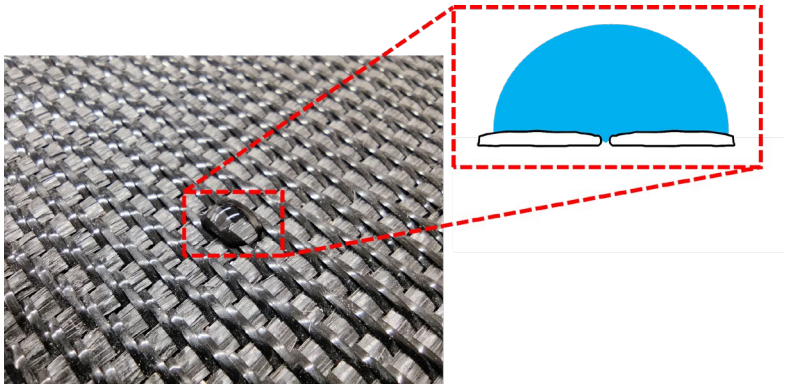

(b) water droplet on the non-wicking woven geotextile

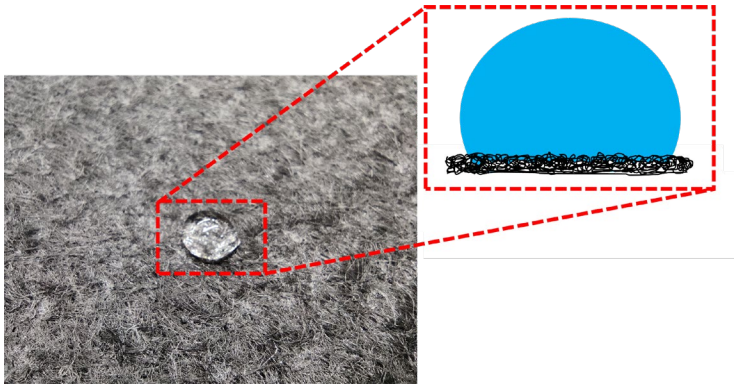

(c) water droplet on the nonwoven geotextile

Figure 2.4 Water droplets on different geotextiles.

2.3.2 Water contact angle on undisturbed geotextile with time

This study investigated surface wettability of undisturbed geotextiles by the water droplet method. According to the ASTM D7334 standard, a small droplet (typically, 0.5µL-5µL volume) of specific liquid should be dropped onto a specimen surface using a syringe. To demonstrate the effect of droplet size, contact angle measurements of a 2µL water droplet (smaller) and a 5µL water droplet (larger) on undisturbed geotextiles were conducted. An optical tensiometer device was used to maintain the same volume of droplet for all the tests. The diameter of the 2µL droplet measured was 1.56 mm while the diameter for the 5µL droplet was 2.12 mm. The apparent opening sizes (i.e., AOS) for the WW, NWW and NW geotextiles were 0.43, 0.60, and 0.212 mm, respectively. It should be noted that the water droplet was dropped on the geotextile fibers to check the fiber surface wettability. The NWW and NW geotextiles were made of polypropylene fibers only while the WW geotextile was made of two types of polymers: polypropylene and nylon. Since nylon is hydrophilic, the water droplet on this type of fiber was absorbed quickly.

Figure 2.5 shows the measured water contact angles using the 2µL water droplet (smaller) and the 5µL water droplet (larger). It is shown that the initial contact angles of the 5µL water droplet on the two woven geotextiles were slightly smaller than those of the 2µL water droplet. The larger water droplet spread more because of its larger volume and weight (Davis & Hocking 2000; Kumar & Deshpande 2006). However, the rate of change of contact angle with time was almost the same. Drelich (1997) found that droplet volume does not have an obvious effect on the contact angle for close-to-ideal surfaces. Geotextiles consist of individual fibers and are different from solid media; therefore, they do not have an ideal surface. However, a larger droplet volume has more effect on the contact angle on a non-ideal surface; therefore, a smaller

droplet (commonly 2µL) is preferred. Furthermore, the water droplet regardless of different size disappeared into the wicking woven geotextile whereas the water droplet remained beaded on the non-wicking woven geotextile. For the nonwoven geotextile, no significant change in the contact angle was observed because the filaments in the nonwoven geotextile did not allow the droplet to spread or penetrate. As discussed earlier, the wicking woven geotextile had one additional mechanism (wicking action) for water interaction with the nylon fibers. This mechanism is well reflected in the measurement technique; therefore, it is not only an appropriate technique for the wicking woven geotextile but also demonstrates the benefit of the wicking geotextile's wicking ability.

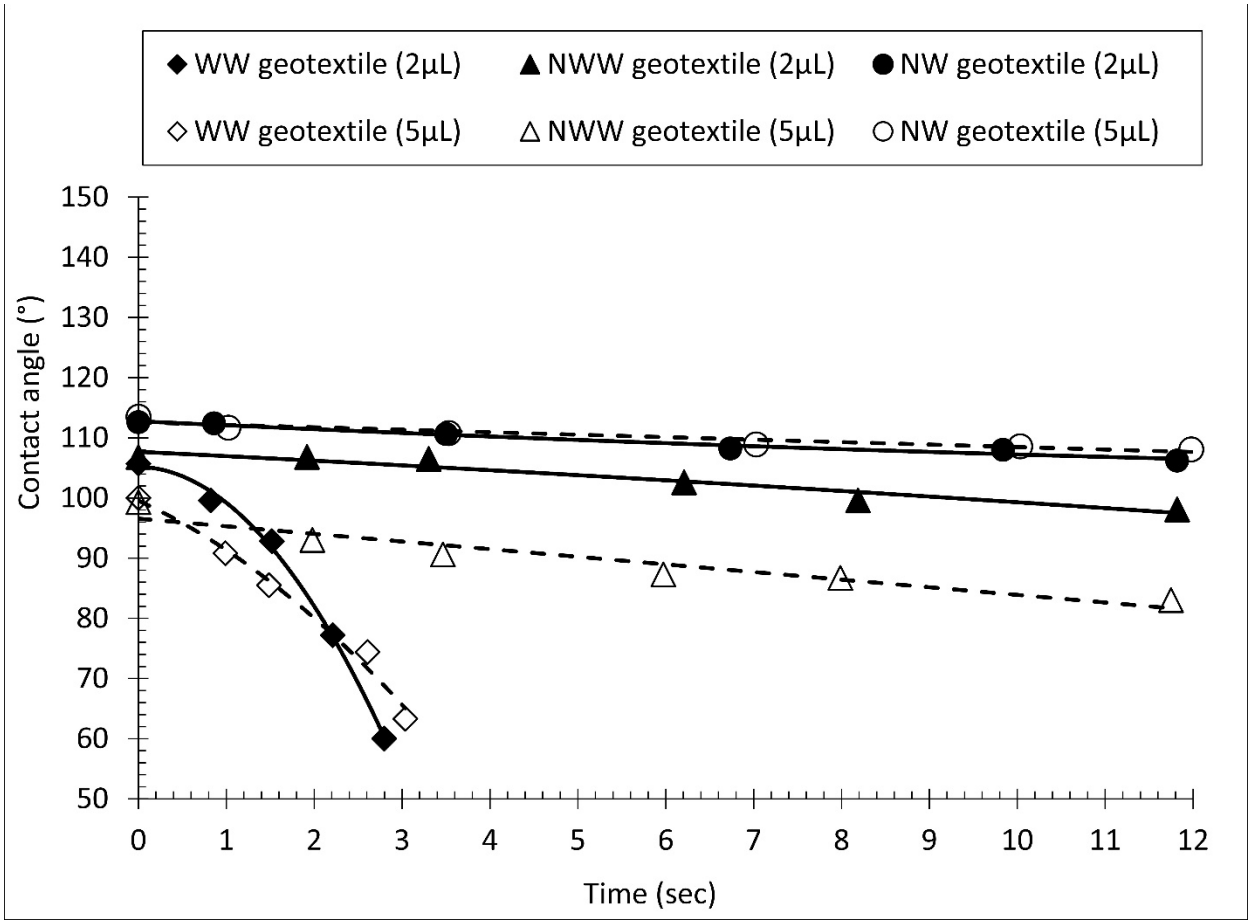

Figure 2.5 Contact angles of water on undisturbed geotextiles.

Even though a water droplet partially entered the NW or NWW geotextile surface during the observation period, since the contact angle remained more than 90° for the 2μL water droplet (smaller) or approximately 90° for the 5μL water droplet (larger), it is still considered a non-wetting surface, i.e., hydrophobic.

2.3.3 Water contact angle on disturbed geotextile

So far, limited studies have reported the compaction effect on wettability of geotextiles with soil. Henry & Patton (1998) observed larger capillary rise in the dirty geotextiles compared to clean or new specimens and reported that soil fines coated the fibers and improved the wettability of the fibers. Their conclusion was based on the water contact angle of the fibers measured by the immersed filament method. Lin et al. (2017) observed flattening of deep grooves in the nylon wicking fibers due to the vertical pressure that reduced wettability of wicking fibers in the geotextile. The following two mechanisms may affect measured contact angles of geotextiles after soil compaction: (i) the contact angle decreases due to the accumulation of fine particles on the surface of a geotextile (also referred as soil intrusion) and (ii) the contact angle increases due to flattening of fibers or a fabric. The overall effect on the contact angle and wettability of a geotextile after soil compaction depends on the dominant effect of one of these two opposite mechanisms, which depend on soil gradation, fabric structure, and compaction energy.

In this study, two types of undisturbed geotextile specimens (one circular with a large size and another rectangular with a small size) were evaluated in the soil compaction tests. One geotextile was first placed, covered by one lift of sand of specific thickness, and then compacted in the compaction mold by the standard Proctor compactor at the compaction energy specified by the ASTM D698 - 12(2021) for compaction of one soil lift. The geotextile specimen was

carefully removed from the compaction mold to determine the mass of soil particles remaining on the geotextile. Table 2.2 shows the comparison of the unit masses of the retained fine particles on two different specimens (i.e., rectangular and circular) after compaction. This comparison shows that the two specimen sizes yielded similar unit masses; however, the NW geotextile retained most soil particles, followed by WW and NWW. Since NW was thicker than other woven geotextiles and had higher porosity and randomly oriented fibers, soil particles could more easily enter and retain in this geotextile during compaction. Table 2.1 shows that WW and NWW had their apparent opening sizes of 0.43 and 0.60 mm, respectively. The ratios of the geotextile apparent opening size to the fine particle size (75 μm) for WW and NWW were 5.7 and 8.0, respectively. Han and Giroud (2016) pointed out that the optimum aperture size for geogrid interlocking with granular material is approximately twice the mean particle size. Therefore, WW with a smaller ratio had a better size ratio for fines retained on the geotextile than NWW. In addition, Table 2.2 shows that at the lift thickness of 100 mm, the amount of fine particles retained on the geotextile was least because the combined effect of the overburden stress and the distributed compaction energy was least. When the soil lift thickness became larger, the overburden stress increased but the distributed compaction energy became lower. The opposite situation happened for the smaller soil lift thickness. In this study, smaller rectangular specimens were used for the contact angle tests.

Table 2.2 Mass of retained soil particles in geotextile after compaction.

Geotextile	Specimen size (mm)	M_1 (g)	M_2 (g)	ΔM (g)	$\Delta M/A$ (g/m^2)
		h = 50 mm			
WW	65 (L) x 65 (W)	2.00	2.11	0.11	26
NWW	65 (L) x 55 (W)	1.36	1.43	0.07	20
NW	70 (L) x 70 (W)	1.01	1.27	0.26	53
WW	96.5 (D)	3.76	3.98	0.22	30
NWW	96.5 (D)	3.00	3.10	0.10	14
NW	96.5 (D)	1.30	1.72	0.42	58
		h = 100 mm			
WW	65 (L) x 65 (W)	2.00	2.11	0.11	26
NWW	65 (L) x 55 (W)	1.36	1.42	0.06	17
NW	70 (L) x 70 (W)	1.01	1.24	0.23	47
WW	96.5 (D)	3.76	3.93	0.17	24
NWW	96.5 (D)	3.00	3.12	0.12	17
NW	96.5 (D)	1.30	1.61	0.31	43
		h = 150 mm			
WW	65 (L) x 65 (W)	2.00	2.21	0.21	50
NWW	65 (L) x 55 (W)	1.36	1.43	0.07	20
NW	70 (L) x 70 (W)	1.01	1.30	0.29	59
WW	96.5 (D)	3.76	4.11	0.35	48
NWW	96.5 (D)	3.00	3.15	0.15	21
NW	96.5 (D)	1.30	1.70	0.40	55

Note: M_1 = mass of geotextile specimen before compaction, M_2 = mass of geotextile specimen after compaction, $\Delta M = M_2 - M_1$ = retained soil mass on geotextiles, A = surface area of the specimen, h = soil thickness, L = length of the specimen, W = width of the specimen, D = diameter of the specimen.

Since the water droplets of two different sizes produced similar results, a water droplet with 2μL volume was preferred and selected for further investigations of contact angles with disturbed geotextiles in this study. Figure 2.6 shows the contact angles of the geotextile specimens after compaction with a lift thickness of 50 mm of clean sand. For this lift thickness, the distributed compaction energy on the geotextile was higher. The NW geotextile sheet or the WW geotextile fibers was flattened by compaction. Even though there was an effect of soil intrusion on reducing contact angles, the effect of flattening the geotextile or fibers was dominant. As a result, among all the specimens, the NW geotextile showed the maximum

hydrophobic behavior after compaction by producing a water contact angle in between 130° and 140° (Fig. 2.6). The contact angle for the NW geotextile increased due to its surface being flattened by compaction. Since the NW geotextile had random fibers, it had a rough surface before compaction. The sheet of the NW geotextile also became flatter after compaction, thus increasing the contact angle. Initially the disturbed WW geotextile had a slightly larger water contact angle than the undisturbed WW geotextile as shown in Figure 2.5. This may result from the flattening of deep grooves in the nylon wicking fibers due to the vertical pressure as observed by Lin et al. (2017). However, the water droplet penetrated the geotextile quickly within a few seconds after water dropping. This result indicates that the WW geotextile after compaction with 50-mm thick sand still had good wettability or water absorption ability. No significant change in the contact angle was observed for the disturbed NWW geotextile as compared to the undisturbed NWW geotextile because the fibers in this geotextile were not flattened and the amount of fine particles on this geotextile was small.

Figure 2.7 shows the contact angles of the geotextile specimens after compaction with a lift thickness of 100 mm of clean sand. The NW geotextile retained more fines than the two previous woven geotextiles. The water droplet could not fully penetrate the NWW and NW geotextiles in this case and the initial water contact angle of the disturbed WW geotextile specimen was larger than that of the undisturbed WW geotextile, as shown in Figure 2.5. This phenomenon happened because of the dominant flattening effect of the wicking fibers compared with the fine particle effect. However, this phenomenon lasted only for a fraction of a second and the water droplet was seen penetrating and vanishing into the WW geotextile quickly. No significant change in the contact angle was observed for the NWW geotextile after compaction with 100 mm of clean sand.

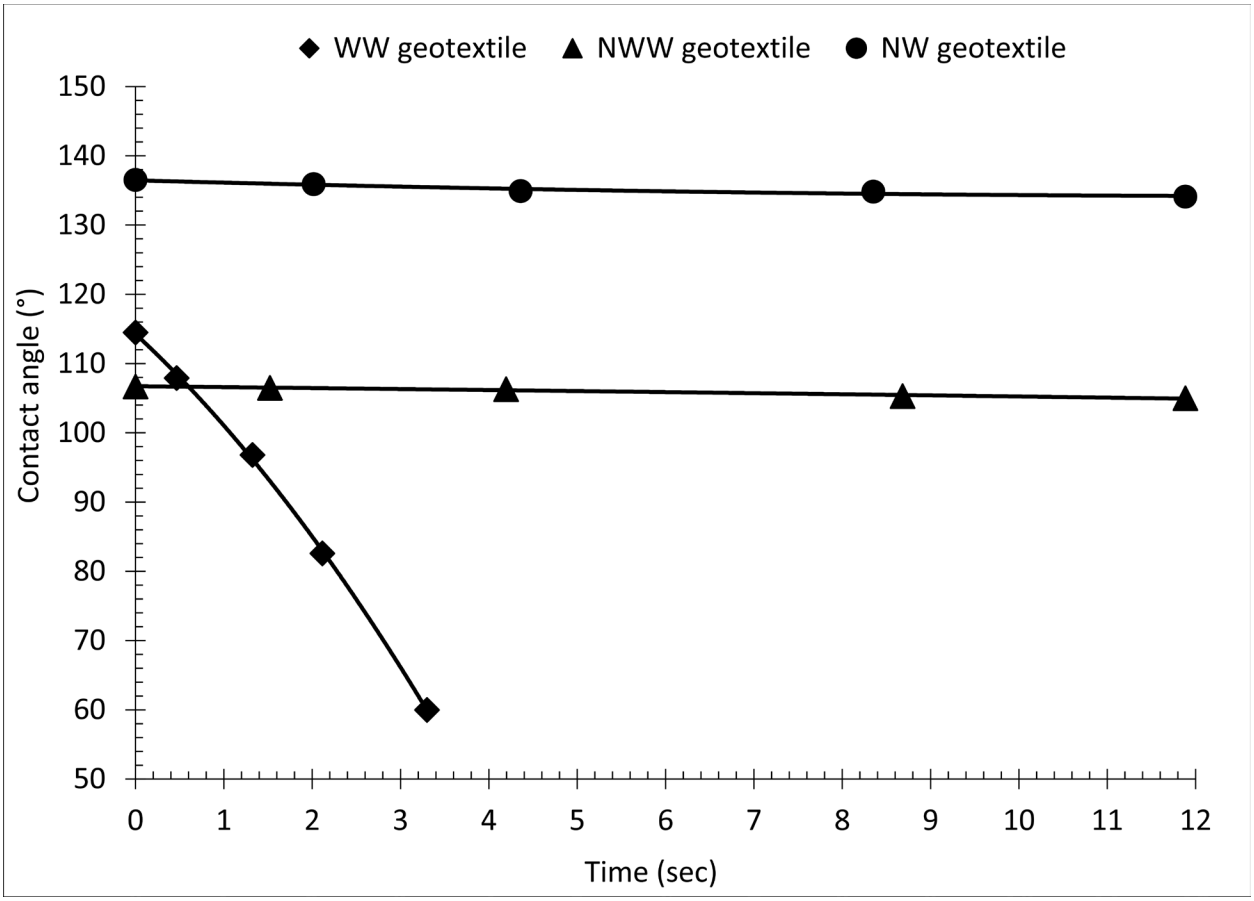

Figure 2.6 Contact angle of water on the disturbed geotextiles compacted with 50 mm thick sand.

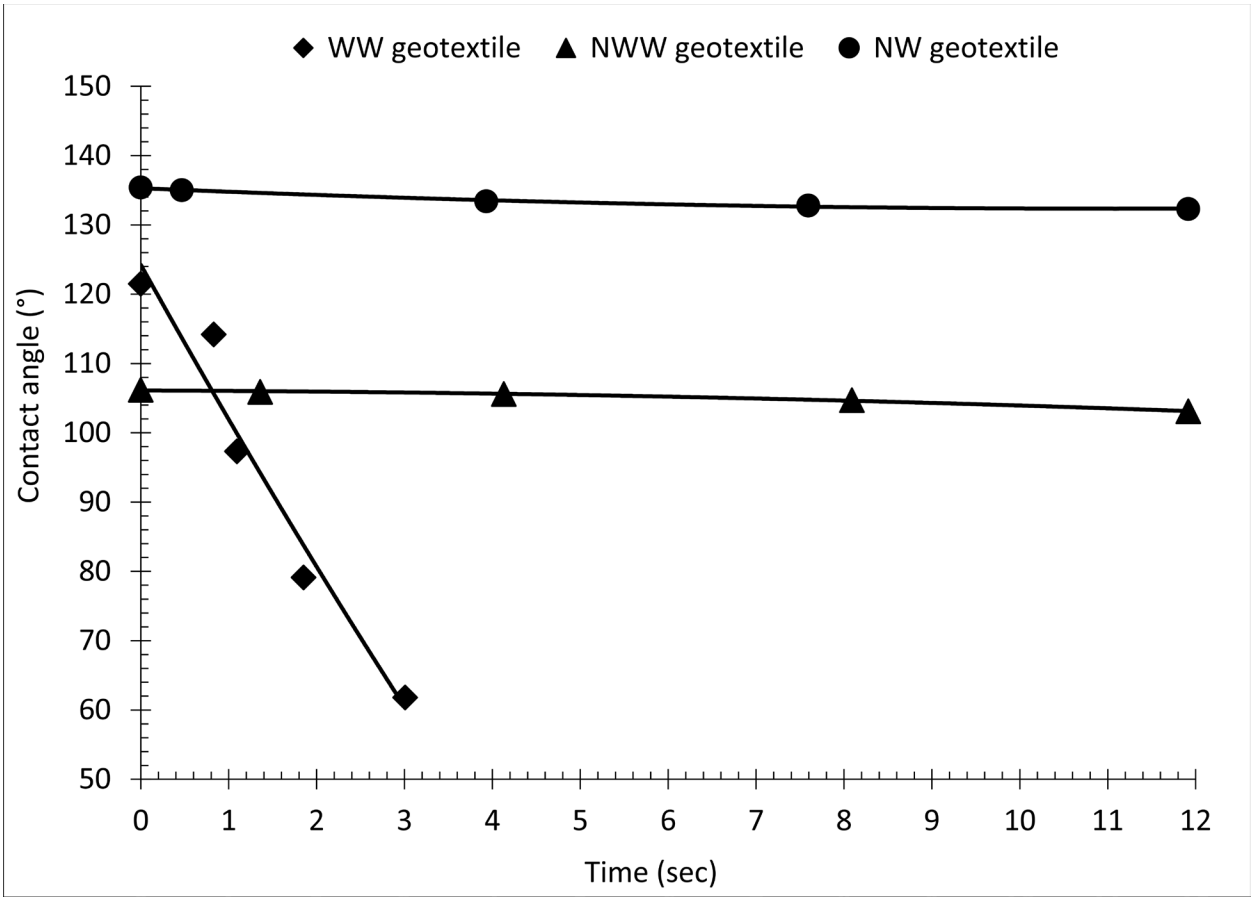

Figure 2.7 Contact angle of water on the disturbed geotextiles compacted with 100 mm thick sand.

Figure 2.8 shows the contact angles of the geotextile specimens after being placed and compacted with a lift thickness of 150 mm of clean sand. As discussed earlier, the water droplet could not fully penetrate the NWW and NW geotextiles in this case. Although, the initial water contact angle was smaller in the WW geotextile than the previous cases, the water droplet took more time to fully penetrate the fibers (Fig. 2.8). This phenomenon can be explained as the amount of soil intrusion in the WW geotextile was more under compaction with the lift thickness of 150 mm as compared with the previous cases in Table 2.2. The effect of soil intrusion played a more dominant effect on the contact angle than the flattening effect of fibers. As a result, the

initial contact angle of the disturbed WW geotextile was smaller than that of the undisturbed WW geotextile as shown in Fig. 2.5. However, it took longer time for the penetration and disappearance of the water droplet into the WW geotextile due to the existence of more fine particles on openings between fibers after compaction as shown in Fig. 2.9. Water droplets needed to penetrate through the fine particles first and then reached the wicking fibers. Similarly, there was more soil intrusion in the NWW and NW geotextiles after compaction with the lift thickness of 150 mm as shown in Table 2.2; therefore, they had more effect on the reduction of contact angles than the effect of flattening the geotextile compared with the phenomenon in the previous cases.

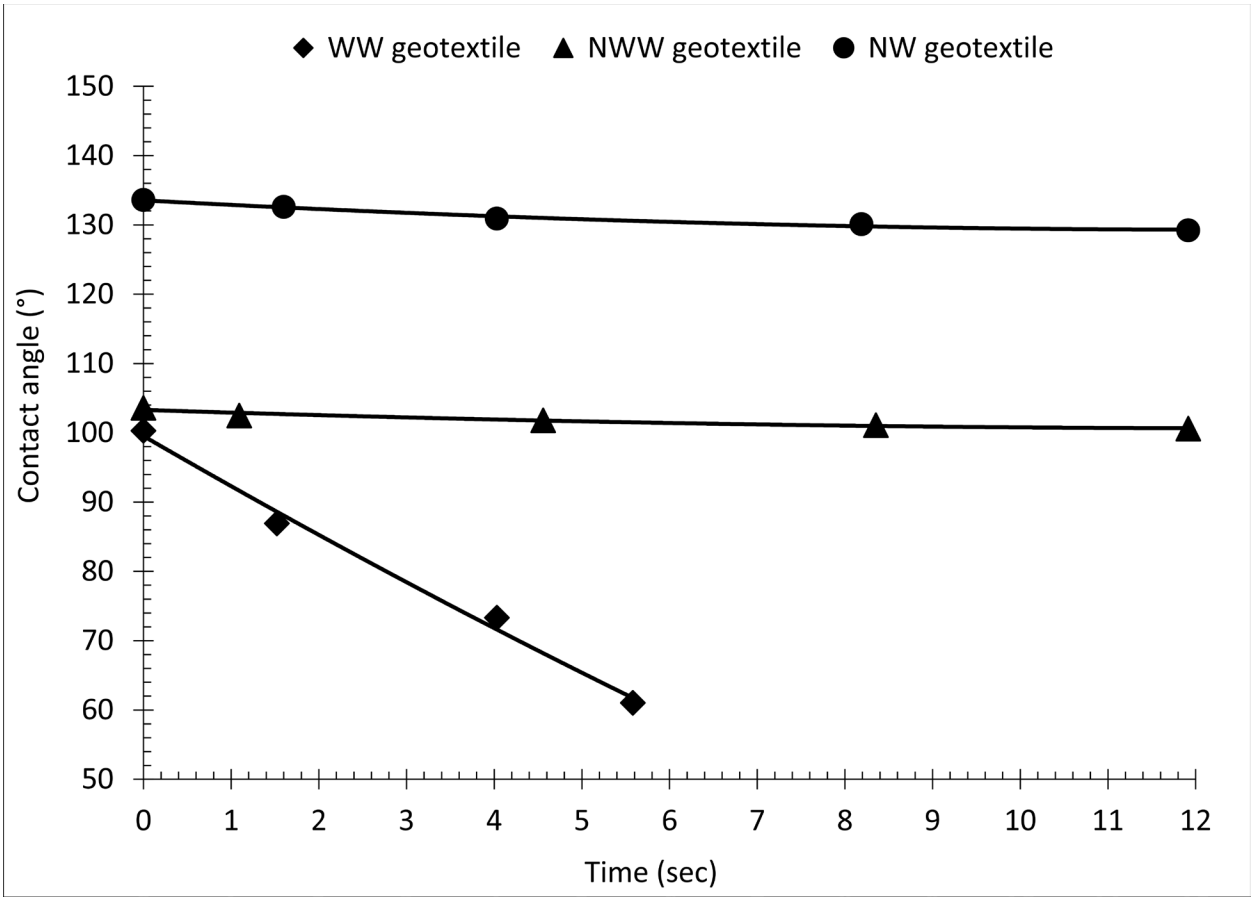

Figure 2.8 Contact angle of water on the disturbed geotextiles compacted with 150 mm thick sand.

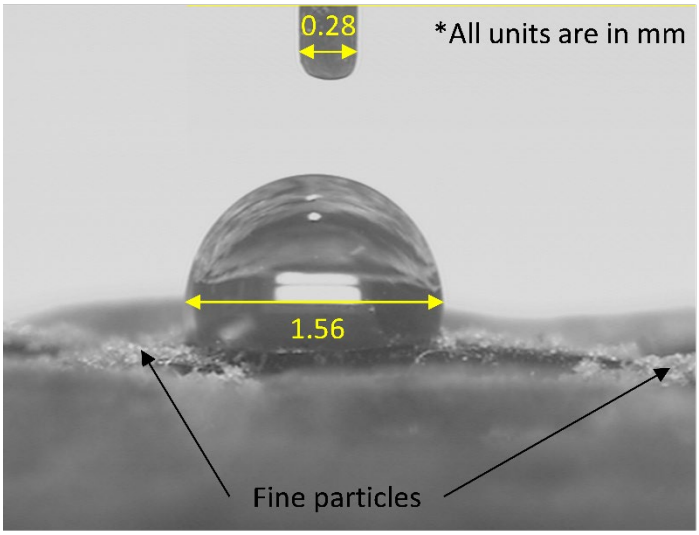

Figure 2.9 2µL water droplet and fine particles on a nonwoven geotextile after compaction with a lift thickness of 150 mm.

2.4 Summary

The simple water droplet method was used in this study to characterize the surface wettability of the wicking woven, non-wicking woven, and nonwoven geotextiles. It was visually observed that the water droplet quickly and fully penetrated the wicking woven geotextile after water dropping while partial penetration was observed in the other two types of geotextiles. The measured contact angles for the wicking woven geotextile were smaller than those for the non-wicking woven geotextile and the nonwoven geotextile after water dropping. The contact angles for the wicking woven geotextile became smaller than 90° after a few seconds of dropping the water droplet while those for the non-wicking geotextile and the nonwoven geotextile stayed larger than 90° or approximately 90° during the observation period. Four possible mechanisms have been identified in this study for the change of contact angle over time: (i) initial spreading of the droplet, (ii) penetration of the droplet into the channels of fibers and gaps between fibers, (iii) evaporation of the droplet, and (iv) wicking ability of fibers due to high capillary forces.

Flattening of the geotextile sheet or fibers and soil intrusion in the geotextile were identified as two contributing factors to the change of contact angles after soil compaction. Their combined effect dominated the increase or reduction of the contact angle. A thicker lift of sand was beneficial to minimize flattening of the geotextile sheet or fibers and increase the amount of fine particles retained on the geotextile, thus reducing the contact angle and improving the wettability of the geotextile.

Chapter 3 Laboratory Investigation of Field Moisture Capacities of Silty Sands at Different Fines Contents

3.1 Introduction

Field capacity (FC) or moisture holding capacity of a soil is well-known terminology in irrigation, agriculture, and physical soil science. It is defined as the upper limit of field soil moisture under free and gravitational drainage within two to three days after rain or irrigation (Veihmeyer and Hendrickson 1931; Colman 1947; Or et al. 2002). The authors think this terminology should be modified into field moisture capacity (FMC) for geotechnical engineering applications highlighting the importance of moisture; therefore, the term "field moisture capacity" or "FMC" for short, is used in this report. The FMC varies from soil to soil and mostly depends on particle size, shape, texture, aggregation, temperature, water table location, evapotranspiration, and organic matter content (Hillel 1971; Hignett et al. 2002). Micropores and macropores control the water-holding capacity and free drainage in natural soil. For example, heavy clay soils have a higher water-holding capacity (i.e., FMC) with poor drainage ability due to the presence of more micropores and fewer macropores, respectively (Zettl et al. 2011; Rai et al. 2017), than granular soils (e.g., sands and gravels). FMC provides important information on soil water storage characteristics for rainfed crop production in dry regions (Ritchie 1981). Under certain conditions, soil retains moisture below the FMC, which is insufficient for plant use and called the lower limit or permanent wilting point (PWP) (Tillotson and Nielson 1984; Cassel and Nielson 1986). The available water capacity (AWC) of soil is estimated by the difference in water content between FMC and PWP (de Oliveira et al. 2015). The FMC concept was introduced to encourage farmers not to irrigate excessively and frequently while taking full advantage of existing moisture in the soil (Veihmeyer and Hendrickson 1931). However, there have been recent arguments among agricultural engineers on the FMC concept due to its

dependency on many factors and difficulty in measuring it in the laboratory or field accurately. Kirkham (2014) stated that FMC is simply the amount of water that a well-drained soil holds against gravitational forces when downward drainage is significantly decreased. He further acknowledged its importance to qualitatively measure the amount of moisture in the soil for irrigation design and scheduling.

Researchers in the agriculture and soil sciences have used different methods to determine the FMCs of various soils both in the field and laboratory. Colman (1947) used small, saturated soil blocks on a porous ceramic cell and drained under 1/3 atmosphere tension. He then determined the retained moisture in the soil block and concluded it was the FMC. In his study, Ritchie (1981) recommended the use of neutron moisture meters to measure the upper limit of soil moisture (i.e., FMC) in the field. Veihmeyer and Hendrickson (1931) mentioned that 24 to 72-hour waiting periods were sufficient for the natural soil to reach the FMC condition. According to the Soil Science Society of America (1984), in situ FMC is defined as the amount of water remaining in the soil for two or three days after being wetted and free drainage to negligible moisture loss. For some coarse-grained soils, this reduction in moisture content may occur within 6 to 24 h (Cassel and Sweeney 1974) whereas some fine-grained soils continue to drain for several weeks (Davidson et al., 1969). Zettl et al. (2011) observed negligible drainage after 18 h in sandy soil containing a small amount of clay (less than 5%). According to Cassel and Nielson (1986), to determine the in-situ FMC, the soil surface was flooded with sufficient water to infiltrate at least 750 mm depth and cover the soil surface with polyethylene sheets to minimize moisture loss due to evaporation. After 48 hours, the sheets were removed and various soil samples from different depths were collected to measure their gravimetric moisture contents as defined in Equation (2.1). Volumetric soil moisture as defined in Equation (2.2) may be used

as an alternative to the gravimetric moisture content. Volumetric soil moisture contents can be obtained using moisture sensors (Guo et al., 2019, 2021; Liu et al. 2022). Zettl et al. (2011) used a double-ring infiltrometer (DRI) in their study to infiltrate the natural soil to determine the FMC.

$$w_w = \frac{M_w}{M_s} \tag{3.1}$$

$$w_v = w_w \times \frac{\rho_b}{\rho_w} = \frac{M_w}{V_a \times \rho_w} \tag{3.2}$$

where w_w = in situ gravimetric moisture content, w_v = in situ volumetric moisture content, M_w = mass of water, M_s = oven-dried mass of soil, ρ_b = soil bulk density, ρ_w = water density, and V_a = bulk soil volume.

Many soil scientists reported soil water pressure corresponding to the FMC condition ranging from -2.5 to -50 kPa (negative sign indicates suction) depending on the soil type (Smith and Browning 1948; Jamison, 1956; McIntyre 1979). Zettl et al. (2011) applied soil water pressure (i.e., suction) ranging from -0.01 to -0.03 MPa for sandy soils in the pressure plate tests to measure FMC in the laboratory. Commonly, soil water pressures of -10 and -33 kPa are chosen by most soil researchers for sandy and clay soils, respectively, at the FMC condition and hence, this value is widely applied in laboratory experiments to drain out water from a wet soil in the pressure plate apparatus to determine the FMC of the soil (Marshall and Stirk 1949; de Oliveira et al. 2015; Rai et al. 2017). However, the applied pressure can be adjusted depending on soil type and if the soil water pressure at the FMC condition is known for any specific soil type. Since plant roots extract moisture from the surrounding soil, the FMC may depend on the root depth of plants. Typically, the FMC is measured at the maximum root depth of any specific

test site, which is commonly taken as 1.0 m (Kimmins and Hawkes 1978; CEMA 2006), for agriculture applications. Rawls et al. (1982) suggested a linear regression equation to estimate the FMC at 1.0 m of suction considering the amount of sand, clay, and organic matter of any soil.

Since soils are often partially saturated under an FMC condition, it is important to understand the unsaturated soil mechanics, which is at the intersection of several disciplines of engineering and science, such as geotechnical engineering, geo-environmental engineering, agricultural science, soil physics, and hydrology (Likos and Lu 2004). The relationship between soil moisture and tension is called the soil moisture characteristic curve (SWCC) and is an important relationship for unsaturated soils. This curve is also known as the soil moisture release curve or retention curve. The capillary suction between soil particles makes the soil unsaturated above the groundwater table. In addition, soils may become unsaturated after the infiltration of water (e.g., rainfall or irrigation). Negative pore-water pressure exists in soils under unsaturated conditions. Even though there have been many advances in unsaturated soil mechanics, it is still difficult to accurately predict the changes in soil properties due to the changes in negative pore-water pressures in soil. Water flow through an unsaturated soil may lead to seepage, settlement, shrinkage-swelling problems, and slope failure due to a decrease in effective stress; therefore, the shear strength of the soil decreases significantly and contributes to the instability, ground cracks, and differential settlements (Fredlund and Rahardjo 1993; Derbyshire 2001; Sun et al. 2009; Xu et al. 2011; Wen and Yan 2014). Many researchers have studied unsaturated soils and investigated partially saturated soil behavior considering soil suction or negative pore-water pressure (Bishop 1959; Sauer and Monismith 1968; Edris and Lytton 1976; Fredlund et al. 1977; Fredlund 2014; Vanapalli and Oh 2015; and Houston 2019). Cassel and Nielson (1986) indicated that the FMC condition is reached when drainage becomes negligible due to a reduction in the

unsaturated hydraulic conductivity or hydraulic gradient. Fredlund (2006) further acknowledged the importance of FMC for water flow measurement in unsaturated soils as it governs the moisture storage capacity of the soil.

Under pavements, subgrade soils and base courses (compacted soils) typically stay under an unsaturated condition during their entire service life. The moisture from precipitation, freeze-thaw, and capillary rise of the groundwater weakens the soil and induces distresses of roadways over time (Zhan 2004; Han and Vanapalli 2015). Several researchers investigated road failures due to the changes in the modulus and strength of the subgrade soil resulting from the changes of the moisture level (Xu et al., 2011; Sahin et al. 2013; Xu et al. 2014; Zhou et al. 2016; Fan et al. 2017; Hou et al. 2018; and Tang et al., 2020). To overcome this problem, a wicking geotextile was introduced to the market to minimize moisture in the soil. The wicking geotextile has special hydrophobic and hygroscopic nylon fibers with many deep-grooved channels that can provide enhanced lateral drainage. This product has demonstrated its excellent moisture-wicking ability (i.e., wicking drainage) as compared with woven and non-woven geotextiles commonly used in several studies (Zhang et al. 2014; Guo et al. 2017; Wang et al. 2017; Zornberg et al. 2017; Lin and Zhang 2020; Biswas et al. 2021; Zaman and Han 2023). Lin and Zhang (2018) studied the drainage efficiency of the wicking geotextile placed in the aggregate containing 14.5% fines where the geotextile worked at a slower wicking rate. Guo et al. (2019) and Guo et al. (2021) performed laboratory soil column tests and large cyclic plate loading tests with the wicking geotextile to remove moisture from the aggregate base with 10% fines. Liu et al. (2022) monitored the field performance of the wicking geotextile between a subgrade and a base course under a concrete pavement and observed a decrease in its wicking ability due to the presence of fine particles in the aggregate base. Furthermore, Zaman et al. (2022a) evaluated the wettability

of the wicking geotextile based on water contact angles, which is essential for initiating lateral drainage.

So far, the wicking geotextile has shown excellent drainage performance in saturated or nearly saturated conditions of the soil as summarized by Zaman et al. (2022b). It is unknown what the limit for this wicking geotextile is to effectively reduce moisture in unsaturated soils at FMC, especially when the soils contain fines. Before evaluating the benefit of the wicking geotextile, a test method should be developed to prepare a soil at an FMC condition. Considering FMC as the upper limit of available water for plants, this research attempts to make a technological shift from the field of irrigation to geotechnical engineering to simulate an FMC condition for unsaturated subgrade soils at different fine contents. This study aimed to develop a simple laboratory test method to determine the FMC profiles of sands with 0%, 5%, 10%, and 15% fines. The authors further studied the effect of soil thickness and layered soils above the groundwater table on the FMC profiles and the sample preparation method using compaction of moist soil. In these tests, moist soil was prepared by mixing the soil with water at the average field moisture capacity, compacting and keeping it undisturbed in the test box for a waiting period of three days to confirm whether the same FMC profile was obtained as in the infiltration method. In addition, soil samples were collected at different depths in the field to verify the FMC profile compared with that found in the laboratory.

3.2 Materials

In this study, Kansas River sand was selected as the main soil material. One type of sandy silt (i.e., pond fill sand) was collected from a local sand quarry in Kansas and mixed with the Kansas River sand to create silty sands at different fine contents for the research purpose. The river sand and sandy silt were classified as poorly graded sand (SP) and silt (ML), respectively,

according to the Unified Soil Classification System (USCS). Figure 3.1 shows the particle size distributions of all the soils used in this study. The collected sandy silt contained approximately 40% fines (smaller than 0.075 mm) while the river sand contained 0% fines. These two soils were mixed at different percentages to prepare silty sands at 5%, 10%, and 15% fines. The prepared soils were used in this study to determine their FMC profiles. Table 3.1 lists the physical properties of the soils. Figure 3.2 shows the standard Proctor compaction test results of the silty sands at different fine contents. Clean sand with 0% fines is not suitable for compaction tests and not included in this figure.

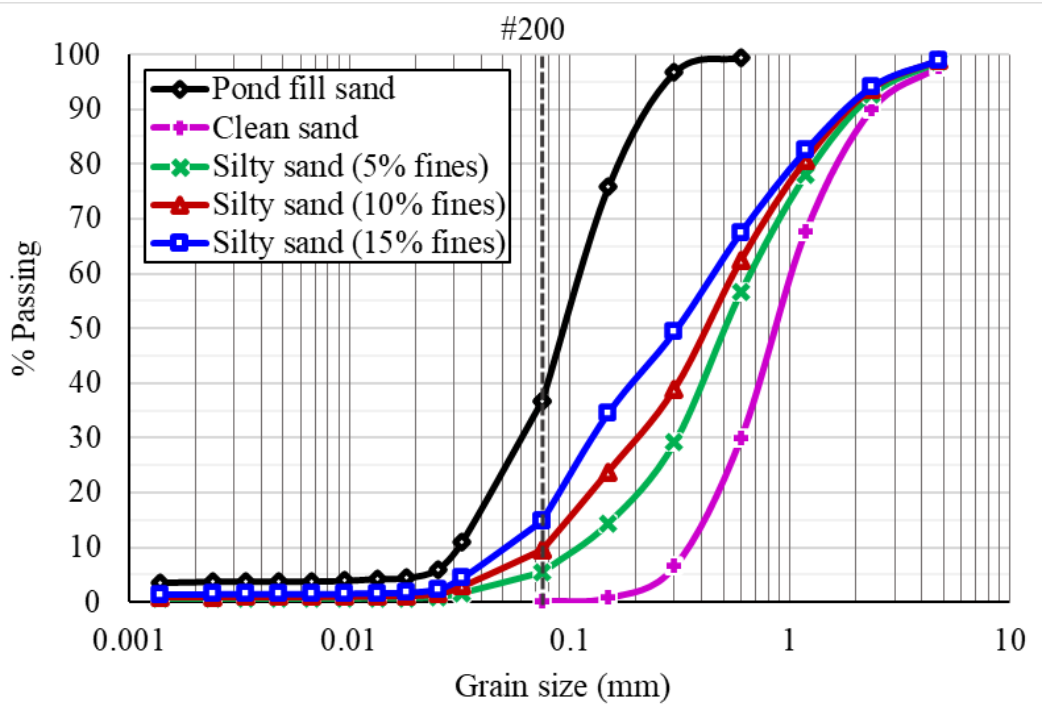

Figure 3.1 Particle size distributions of soils.

Table 3.1 Physical properties of soils

Soil type	D_{10} (mm)	D_{30} (mm)	D_{50} (mm)	D_{60} (mm)	C_u	C_c	G_s	e	$\gamma_{d,max}$ (kN/m^3)
Sand (0% fines)	0.32	0.6	0.85	1	3.13	1.13	2.65	0.44	18.85
Silty sand (5% fines)	0.12	0.30	0.51	0.68	5.67	1.10	2.66	0.43	19.2
Silty sand (10% fines)	0.08	0.20	0.42	0.56	7	0.89	2.67	0.41	20.4
Silty sand (15% fines)	0.05	0.14	0.30	0.45	9	0.87	2.66	0.40	20.25

Note: D_{10}=10% of particles finer than this size (effective particle size); D_{30}=30% of particles finer than this size; D_{50}=50% of particles finer than this size (mean particle size); D_{60}=60% of particles finer than this size; C_u=uniformity coefficient; C_c=coefficient of curvature; G_s=specific gravity; e=void ratio at the relative density of 75%; and $\gamma_{d,max}$=maximum dry unit weight.

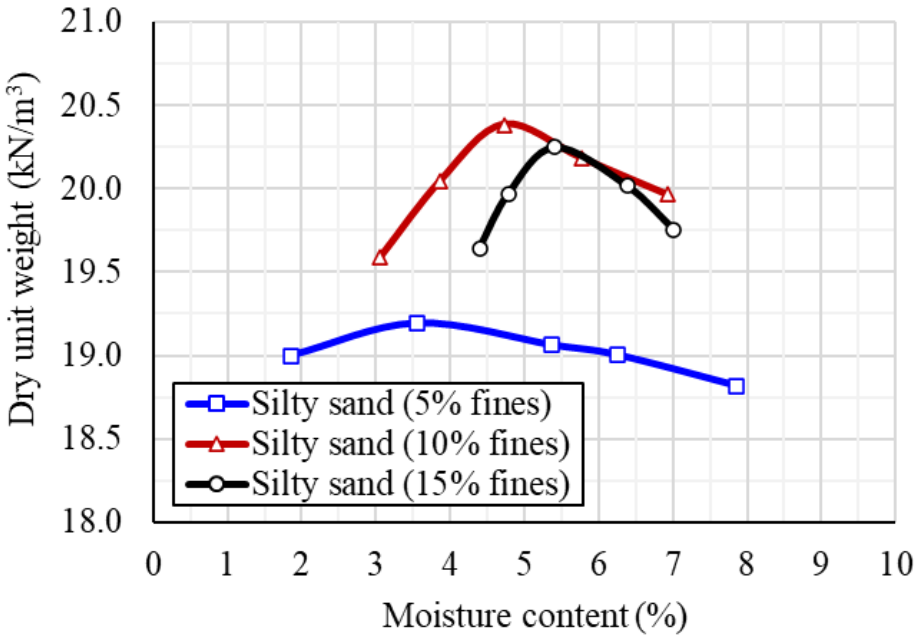

Figure 3.2 Standard Proctor compaction tests to determine maximum dry density.

3.3 Test methods

Naturally, most of the moisture moves downward through the soil after a rainfall event in the field until it reaches the groundwater table. The deeper the moisture travels, the lower the

infiltration rate becomes. It is mainly because the soil closer to the groundwater table is already in a fully or nearly saturated condition due to the capillary rise of the groundwater. Figure 3.3 shows the profile of the moisture content with depth. A stable profile is also referred to as the field moisture capacity (FMC) profile. The moisture area (i.e. the shaded area) divided by the depth (i.e., soil thickness) gives the average field moisture capacity (AFMC) for this specific soil profile and thickness, which was used in this study. The AFMC was used to prepare a compacted soil sample at a certain moisture content to be discussed later.

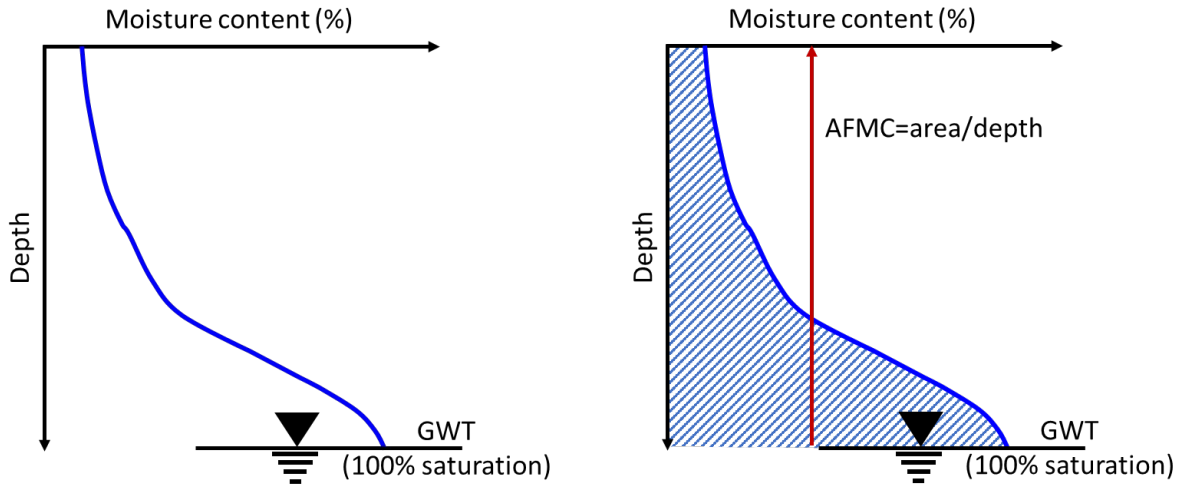

(a) Moisture content variation with depth (b) Average field moisture capacity

Figure 3.3 Profile of field moisture content (capacity) with depth in soil.

In the laboratory, a test column consisting of two boxes with dimensions of 600 mm high, 300 mm wide, and 300 mm long was built using polycarbonate pieces. Many small holes were made at the bottom of the lower box so that water could flow freely under gravity. To retain the soil in the box, a layer of nonwoven geotextile was glued at the bottom to cover the holes. A very thin sticky foam was used to create a uniform gap between the upper and lower boxes. The sticky

foam was covered by a layer of plasticine clay to prevent any leakage through the gaps. To determine the FMC profile of a sand with (i) 0%, (ii) 5%, (iii) 10%, and (iv) 15% fines, dry soil was compacted first to a relative density of 75% for clean sand or relative compaction of 95% for the sand with fines in the polycarbonate box. Water was introduced uniformly and slowly from the top to simulate the rainfall until excess water came out from the bottom. The soil column was stored in the tank as shown in Figure 3.4. Then the top of the box was sealed using a plastic sheet with holes to minimize the evaporation and canopy effect. After a waiting period of 24 hours for clean sand and 48 hours for sand with fines, the FMC of the soil was reached as the drainage from the bottom of the column became negligible. Soil samples at different depths were collected and gravimetric moisture contents were determined. Figure 3.4c shows the soil column cross section for the FMC profile test. Changes in moisture contents with depth were plotted to calculate the AFMC of the soil of that specific thickness (i.e., 600 mm).

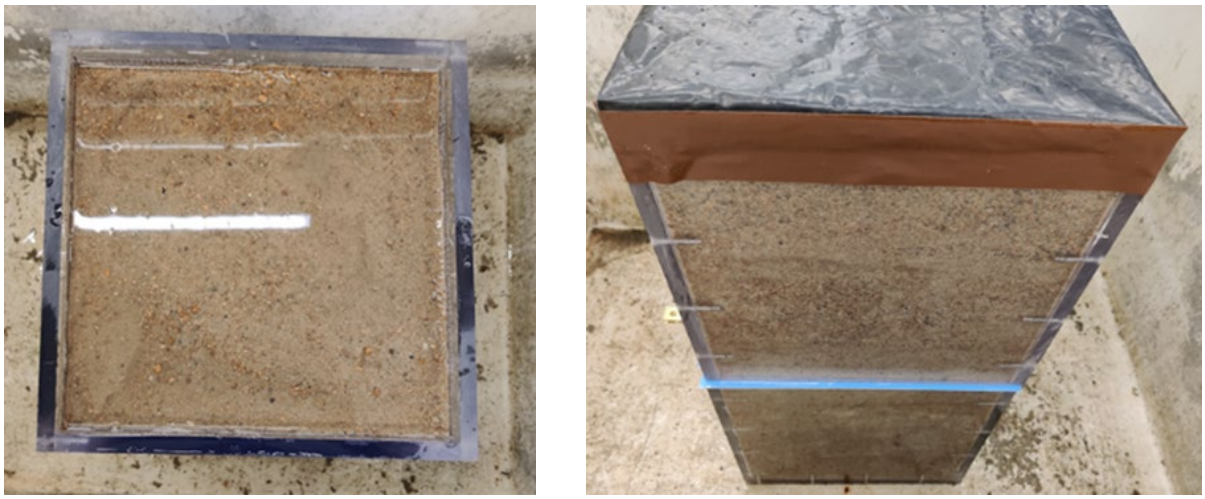

(a) (b)

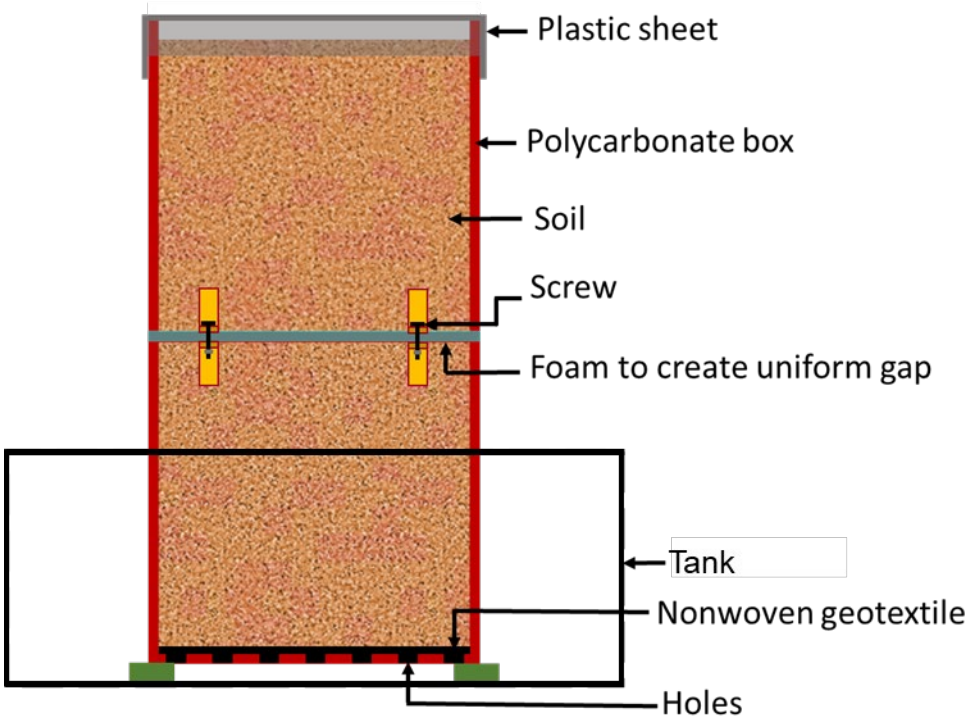

(c)

Figure 3.4 Field moisture capacity test setup: (a) flooding of soil box for full saturation; (b) soil box during the waiting period, and (c) soil column cross section (box dimension: 300 mm x 300 mm x 600 mm).

3.4 Test results and discussion

3.4.1 Measured FMC profile in laboratory

To generate FMC profiles, laboratory tests were performed on four types of soils: (i) sand with 0% fines (i.e., clean sand), (ii) sand with 5% fines, (iii) sand with 10% fines, and (iv) sand with 15% fines using polycarbonate test boxes. Each box was 300 mm long, 300 mm wide, and 300 mm high. Two boxes were stacked together to form a column. The soil column inside the boxes was approximately 575 mm high so that the soil could be compacted easily without coming out of the box.

In the first test, the sand with 0% fines was compacted to approximately 75% relative density in the test boxes in six equal lifts. Water was uniformly and slowly introduced onto the compacted soil for several hours to simulate the rainfall until water infiltrated through the soil column and came out from the bottom of the box. At this moment, the soil column was considered nearly saturated. After the simulated rainfall, the top of the box was sealed with a plastic sheet. The box was kept undisturbed for 24 hours. Excess water continuously came out, was collected by the tank at the bottom of the box, and was cleaned by a dry towel. Due to the gravity and capillary suction effect of the soil particles, water flow and retention in the soil came to an equilibrium condition. As a result, water flow stopped and drainage became negligible. This condition was observed after approximately six hours for the sand with 0% fines. Since this clean sand had large voids and low internal suction, it was quick to reach the moisture equilibrium condition. After 24 hours, representative soil samples were collected at different depths with 100 mm intervals to measure their gravimetric moisture contents. At each depth, nine soil samples were collected for measuring their moisture contents, which were averaged to

calculate one average moisture content at each depth. The moisture contents of the soil at different depths inside the soil column are plotted in Figure 3.5 as the FMC profile.

A similar test methodology was followed to determine the FMC profiles for sands with 5%, 10%, and 15% fines, respectively. Unlike the sand with 0% fines, the soils with fines were compacted to approximately 95% relative compaction to maintain the same compaction level and consistency. For the sands with fines, the soil columns inside the test boxes were kept undisturbed for 48 hours. Since silty sands had higher capillary suction between soil particles and less voids than the sand with 0% fines, it took more time (approximately 16 to 20 hours) to reach the negligible drainage condition than that for the sands with fines. Therefore, a 48-hour waiting period was observed to be satisfactory for these soils. Figure 3.5 includes the FMC profiles for all four types of sand. To examine the degree of saturation of the soil in the column, the degree of saturation at each depth was calculated using Equation (3.3) and is plotted in Figure 3.6, which shows the soil at the bottom of the test box reaching approximately 100% degree of saturation. This elevation can also be considered as the water level.

$$S_r = \frac{w(\%) \times G_S}{e} \tag{3.3}$$

where S_r = degree of saturation, w = moisture content, G_s= specific gravity of soil particles, e = void ratio = $\frac{G_S \times \gamma_w}{\gamma_d} - 1$, γ_w = unit weight of water, and γ_d = dry unit weight of soil.

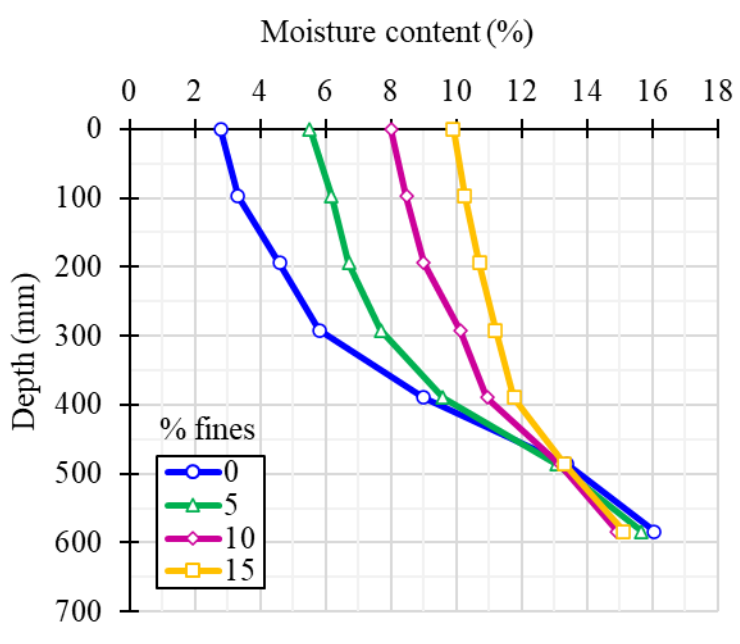

Figure 3.5 Field moisture capacity profiles for four types of soils.

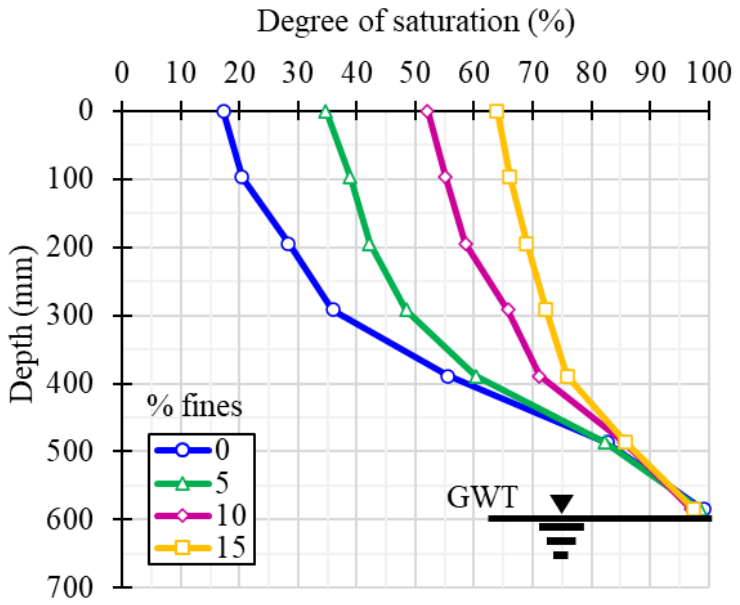

Figure 3.6 Degree of saturation profiles for four types of soils.

Based on the test results in Figure 3.5, the AFMCs were calculated for four types of soils following the procedure in the test methods section and are plotted in Figure 3.7. Figure 3.7

shows that the sand with 0% fines had the lowest AFMC, indicating the least amount of moisture in the soil column. This figure also shows that the AFMC increased with the increase of the fine content in the sand. This result is expected because fine particles have large surface areas that attract and retain water on the surfaces of soil particles. In addition, sand with small particles can create dense particle packing, which results in small voids and high surface tension to retain water and reduce water drainage.

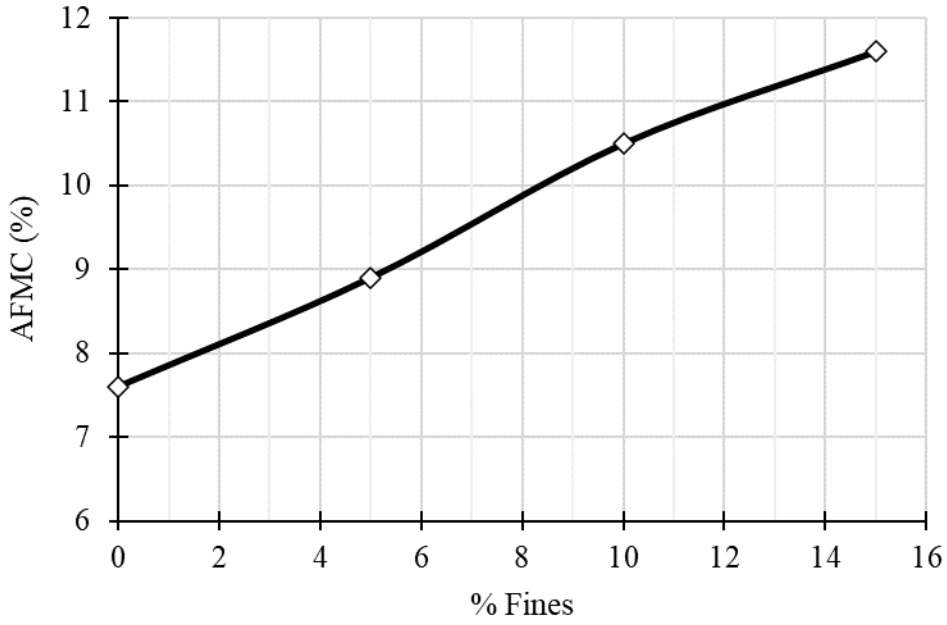

Figure 3.7 Average field moisture capacities of the soils at different fine contents.

3.4.2 Influence of soil thickness

To investigate the effect of the soil thickness on FMC, two more FMC tests were conducted at soil thicknesses of 300 and 900 mm. The 900-mm high soil column required one additional 300 mm high polycarbonate box of added to the 600 mm high box set to make a total height of 900 mm as shown in Figure 3.8. Clean sand was used for this investigation. For the 300

mm high soil column, the soil was compacted in three lifts of equal lift thickness. For the 900 mm soil column, the soil was compacted in nine lifts of equal lift thickness. As described earlier, water was added to the top of the soil column for several hours, which was kept undisturbed for 24 hours before samples were taken at different depths for measuring the gravimetric moisture contents. By repeating the same process, the AFMCs were determined for the clean sand with thicknesses of 300, 600, and 900 mm.

Figure 3.8 Field moisture capacity test on a 900-mm high soil column with clean sand.

Figure 3.9 shows the measured FMC profiles for the clean sand at different soil thicknesses above the water level. Interestingly, the moisture content decreased with the decrease of depth (i.e., the increase of the height from the water table) at a similar rate up to the top of the soil column. In other words, the FMC profile of a thick soil layer can be used to describe that of a thin soil layer starting from the water table. The variation of the moisture content with depth can be explained by two reasons: (1) water flows downward under gravity and (2) soil suction bringing water upward is balanced by soil gravity. These reasons lead to the soil closer to the water table holding more moisture and that farther away from the water table holding less moisture.

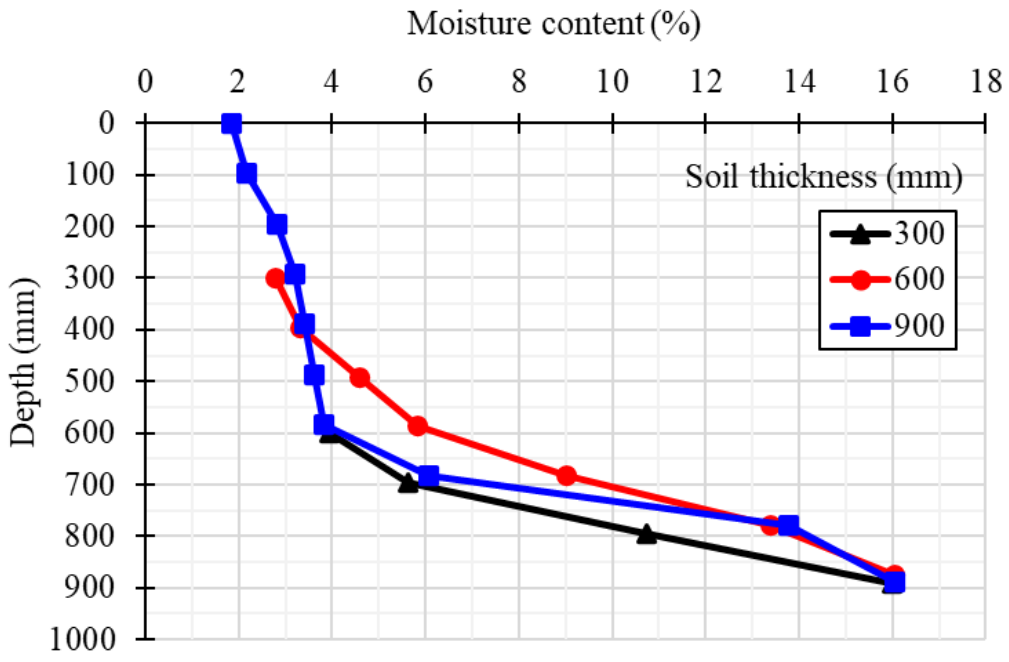

Figure 3.9 Measured field moisture capacities of the clean sand prepared at different soil thicknesses above the water table.

Figure 3.10 shows the AFMCs calculated based on the test results presented in Figure 3.9. The black line presents the actual data obtained from the three tests with 300, 600, and 900 mm soil thicknesses. As discussed earlier, the FMC profile with 900 mm soil thickness might be used to describe those with 300 and 600 mm soil thicknesses. The FMC profile for the clean sand with 900 mm thickness was used to predict the AFMCs for the clean sand with 300 and 600 mm thicknesses as shown in Figure 3.10, which are close to the measured.

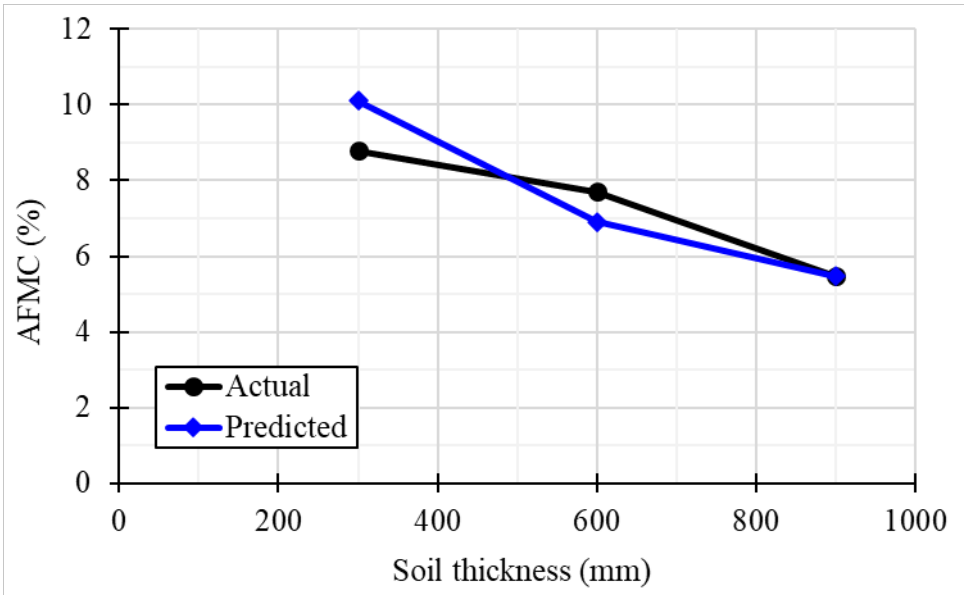

Figure 3.10 Average field moisture capacities of the clean sand at different soil thicknesses.

3.4.3 Layered soil

For pavement applications, a base course is placed above a subgrade. When a geosynthetic layer is used, it is placed between the aggregate base course and the subgrade soil. Therefore, this study further investigated the FMC profile in a two-layer soil column system that consisted of a 300 mm thick aggregate base over a 300 mm thick sand with 10% fines as a subgrade soil. Table 3.2 presents the properties of this aggregate base material.

Table 3.2 Properties of the Aggregate Base Material (Wang et al. 2017)

Properties	**Value**
Coefficient of uniformity, C_u	50
Coefficient of curvature, C_c	2.88
Fine content (%)	10
Liquid limit (%)	20
Plasticity index	7
Unified Soil Classification System (USCS)	CL-ML (fine particle), GW-GC (well graded gravel)
Optimum moisture content (%)	7.2
Maximum dry density, $\gamma_{d\text{-}max}$ (kg/m^3)	2100
Permeability (mm/s)	95×10^{-5}

In this test, the sand with 10% fines was first compacted in three equal lifts to 300 mm in the lower test box. Then the aggregate base material was compacted on the silty sand layer in another three equal lifts to approximately 300 mm. Water was introduced from the top onto the soil column for several hours to ensure full saturation. After that, the top of the box was sealed and kept undisturbed for 48 hours. In this waiting period, excess water from the soil column was collected inside the tank below the soil column. It was observed that drainage became negligible after approximately 24 hours. At the end of the waiting period, soil samples were collected from different depths during exhumation, and then oven-dried to measure their gravimetric moisture contents. Figure 3.11 shows the measured FMC profile of the layered soil column compared with the one-layer sand column. The test results show that the FMC profile for the two-layer soil deviated from that for the one-layer soil at the interface between the base course and the silty

sand subgrade. In other words, the FMC for the aggregate base was lower than that for the silty sand because the aggregate base had larger particle sizes than the silty sand.

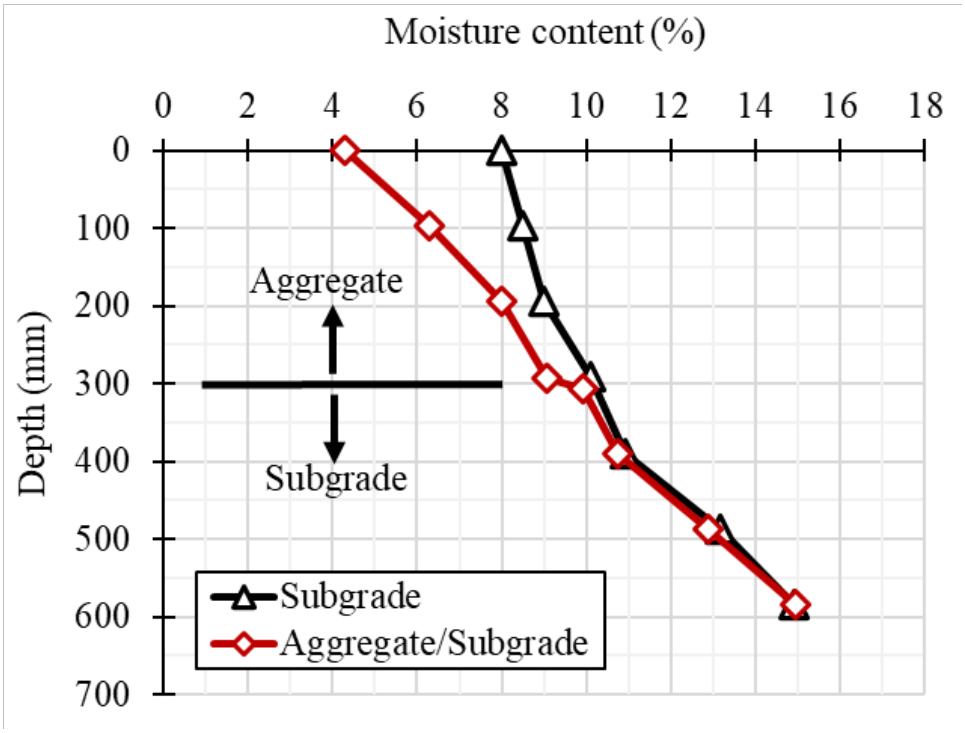

Figure 3.11 Field moisture capacity profiles in the one and two-layer soil columns.

3.4.4 Method of specimen preparation

The above procedure prepared soil samples under a dry condition and then water was introduced to create a saturated condition, which allowed water flow to a field moisture capacity condition. In the field, soils may exist under natural moist conditions or when moist soils are compacted. This study also explored a different method of specimen preparation for FMC profiles. Based on the AFMCs determined for the sands using the previous procedure, the sand was mixed with water at the amount equal to the AFMC. Then the moist soil was placed and compacted into the same polycarbonate test box to meet the same density requirements as the

previous procedure. The soil column was kept undisturbed for three days to ensure moisture distribution and equilibrium. No water was seen coming out from the bottom of the test box containing the moist soil during the waiting period. Soil samples were taken at different depths and measured for moisture contents in the same way as the previous procedure. This method of specimen preparation was adopted for the sands with 0%, 5%, 10%, and 15% fines.

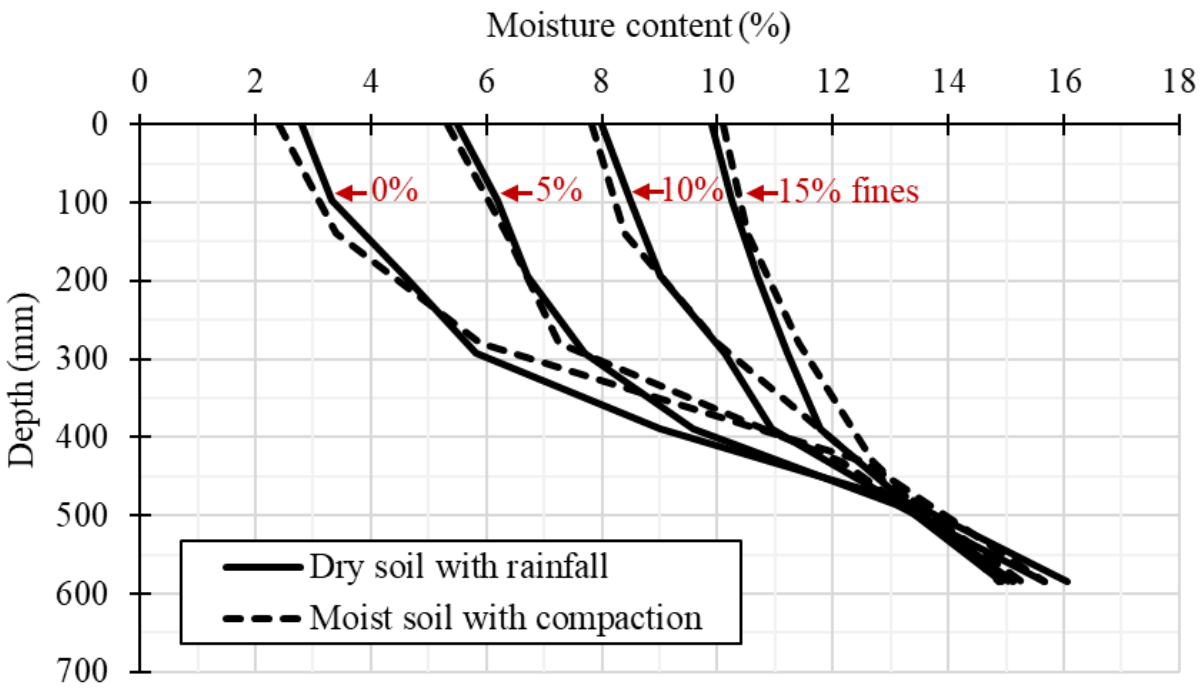

Figure 3.12 FMC profiles for moist soil prepared at AFMC.

Figure 3.12 shows the test results of this investigation, which show that the FMC profiles obtained by the compacting moist sand method were almost the same as those obtained by the rainfall method on dry sands. This investigation verified that the rainfall method adopted in this study is equivalent to the moist soil compaction method and suitable to generate FMC profiles for silty sands in the laboratory. In addition, Figure 3.12 shows that all the curves converged at

the bottom of the soil column (i.e., close to 600 mm depth) and the reduction of fine contents reduced the moisture contents above the bottom of the soil column.

3.4.5 Field measurements

Moisture content of a soil in the field may be influenced by different factors, for example, rainfall, capillary rise from the groundwater table, evaporation, and plant uptake. Therefore, field moisture content is a dynamic parameter that can change over time with season, weather, and land management practice. Field moisture content is crucial for agricultural purposes as it helps in making decisions related to irrigation scheduling, crop management, and water conservation. It is also important for the long-term performance of pavements.

A field study was carried out by this research team in the US-169 highway in Humboldt, Kansas to monitor the soil moisture variations under the pavements to evaluate the long-term performance of a concrete pavement on aggregate bases improved by the wicking geotextile. A number of moisture sensors were placed in the subgrade and the aggregate base during construction of the pavement. Details of this study can be found in the paper by Liu et al. (2022). The research team monitored this pavement for more than three years. Recently, soil samples were collected at different depths of the aggregate base on the slope next to the shoulder of the pavement to measure gravimetric moisture contents. Figure 3.13 presents the gravimetric moisture contents in the aggregate bases collected at different depths in the field in May and August 2023 compared with the laboratory results. Figure 3.13 shows that the measured moisture contents increased with the increase of depth in the field and laboratory tests. The measured moisture contents in the field were lower than those in the laboratory.

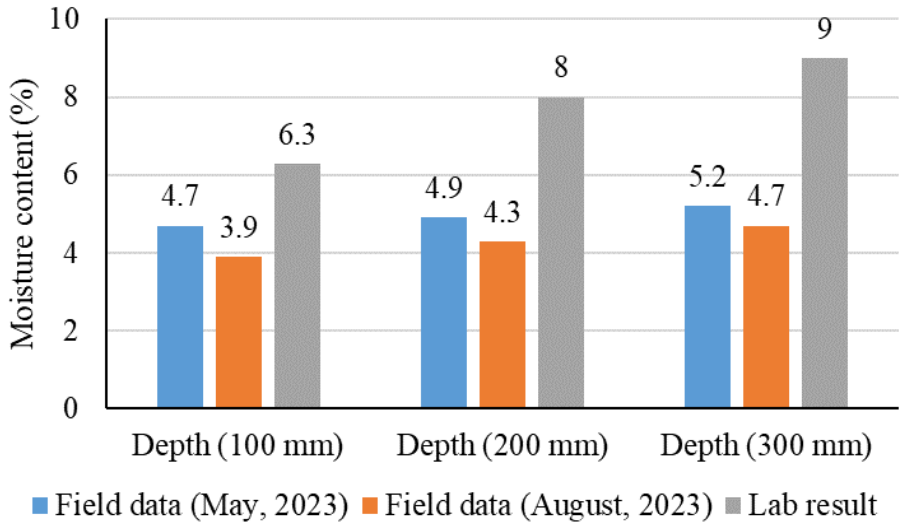

Figure 3.13 Gravimetric moisture contents in the aggregate soil samples collected from field in May and August of 2023.

To investigate this difference, field weather information was gathered and evaluated. Weather conditions, such as precipitation, temperature, relative humidity, and wind speed, are all vital to the moisture content changes in the pavement structure. Figure 3.14 shows the daily air temperature, precipitation, relative humidity, and wind speed from May 1st, 2023 to August 31st, 2023 in Humboldt, Kansas (collected from: https://www.visualcrossing.com), which correspond to the field soil sample collection period for the test results shown in Figure 3.13. Different from random variations of precipitation, relative humidity, and wind speed during this period, the air temperature was relatively low at the beginning of May and then increased, especially from July to August. The highest and lowest daily temperatures were 33.6°C on August 2nd, 2023 and 12.1°C on May 1st, 2023, respectively, while the highest precipitation and wind speed were 73.1 mm on July 13th, 2023, and 42.59 km/h (kph) on July 14th, 2023, respectively. The lowest relative humidity was 38% on May 2nd, 2023. The month of August 2023 had the most days with precipitation heavier than 25 mm (twice as in May).

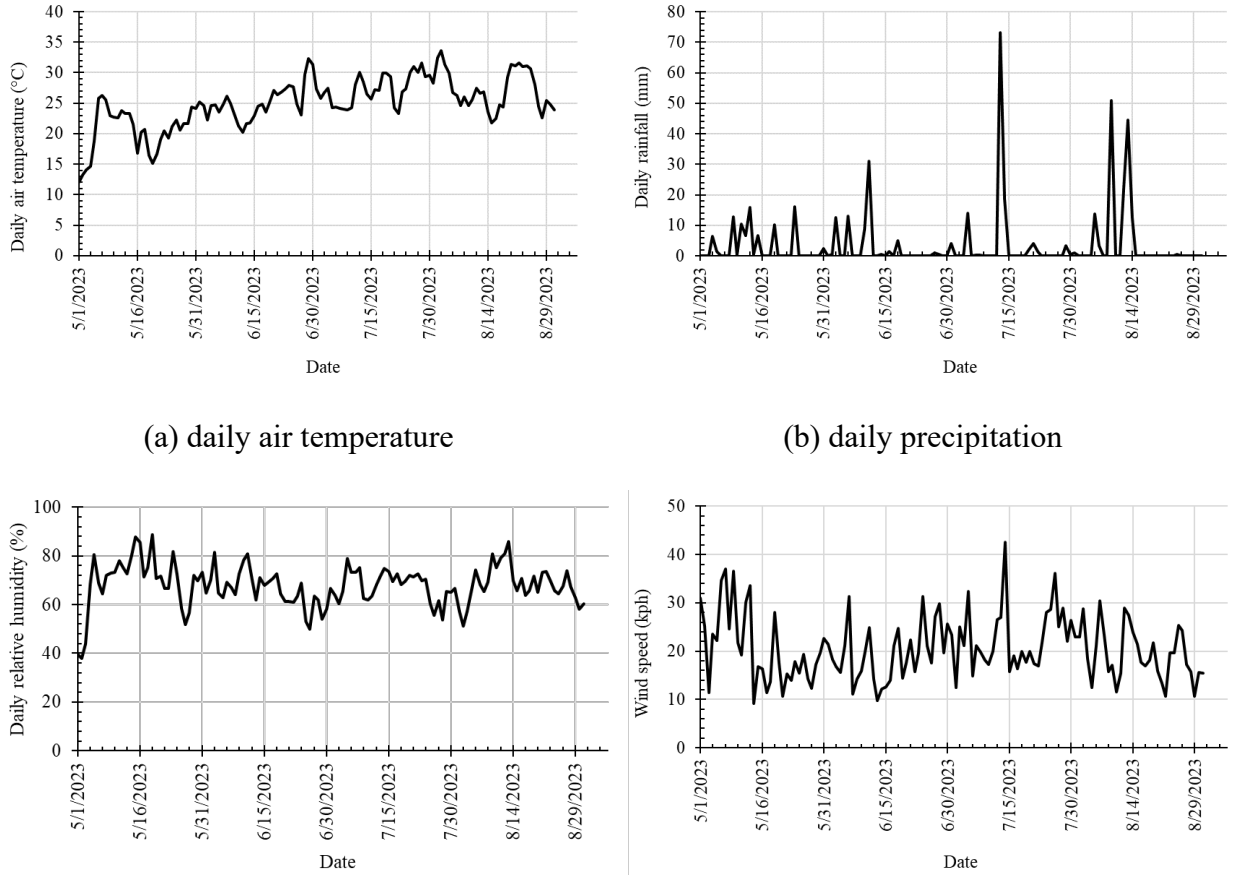

(a) daily air temperature

(b) daily precipitation

(c) daily relative humidity

(d) daily wind speed

Figure 3.14 Weather Condition in Humboldt, KS from May 2023 to August 2023.

Figure 3.15 shows the volumetric moisture content (VMC) readings of the sensors buried in the aggregate base at approximately 250 mm under a concrete pavement shoulder. The VMC readings changed with the precipitations and groundwater rising. Liu et al. (2022) reported the saturated VMC of this material as 27.4%. The sensor readings showed that the aggregate at the mentioned level after moderate rainfalls (greater than 25 mm) did not reach the saturated condition. This was due to the surface runoff of rainwater to the nearby drainage ditch and a small change to the groundwater reservoir. Also, the water infiltration at this level in the aggregate was slower due to the presence of the concrete shoulder above the aggregate layer. To

compare with the VMC readings in the field, soil samples were collected at approximately the same location in May and August 2023 for the data presented in Figure 3.13. On May 18, 2023, the gravimetric moisture content was found to be 5.2% while the corresponding VWC was recorded as approximately 14%. On August 25, 2023, the gravimetric moisture content was found to be 4.7% while the corresponding VWC was recorded as approximately 13%. Based on the relationship established by Liu et al. (2022), the volumetric moisture content of this aggregate was approximately 2.12 times the gravimetric moisture content. Based on this relationship, the gravimetric moisture contents under the concrete shoulder in May and August were 6.6% and 6.1%, which are slightly higher than those reported in Figure 3.13. The possible reason is that the sensors were under the concrete shoulder, which allowed less evaporation, while the soil samples were taken under the aggregate slope, which allowed more evaporation.

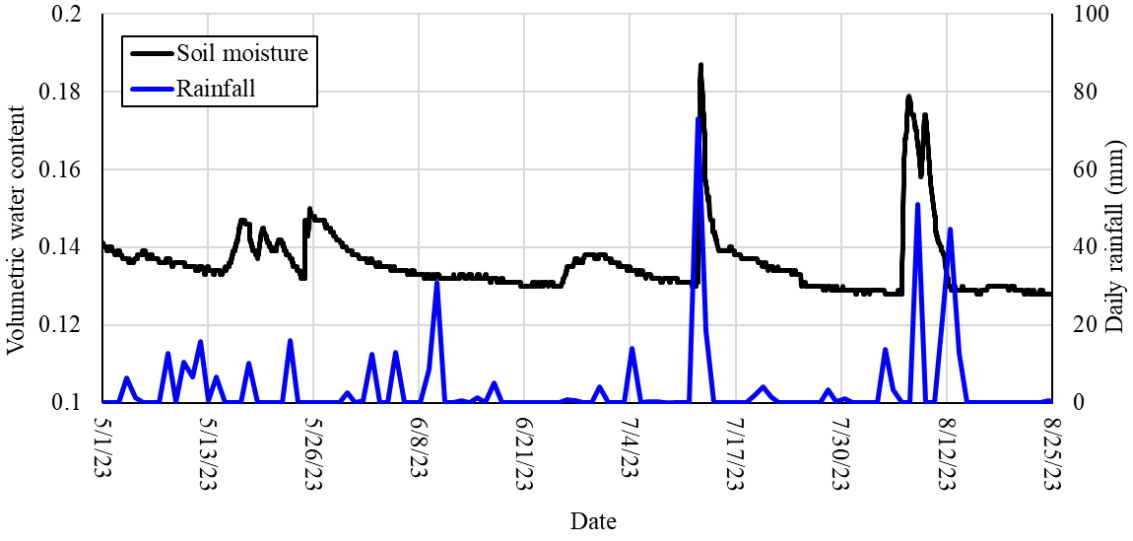

Figure 3.15 VMC readings in the aggregate base at approximately 250 mm under a concrete pavement shoulder from May 1st to August 25th, 2023.

3.5 Summary

This report proposed a simple laboratory method to determine the field moisture capacity (FMC) profile and the average FMC (AFMC). In the laboratory, test boxes were designed, built, and constructed using polycarbonate pieces. FMC profiles were developed to determine the AFMC of the sand with 0%, 5%, 10%, and 15% fines. Furthermore, the changes in the FMC and AFMC due to the change in soil thickness and the use of layered soils were investigated. Another specimen preparation method by compacting moist soils at the AFMC was also investigated. Soil samples were collected from a field project to evaluate the variation of moisture with depth. Volumetric moisture data from the soil moisture sensors in the field were collected and compared with the gravimetric moisture contents measured from the same soil in the laboratory. The following conclusions can be made based on the findings of this study.

(1) FMC profiles for sands with 0%, 5%, 10%, and 15% fines showed the decrease of the moisture content with depth until reaching the water table.

(2) AFMC of the sand increased with the increase of the fine content.

(3) AFMC of the sand decreased with the increase of soil thickness (i.e., distance from the water table).

(4) The FMC profile and AFMC of smaller soil thicknesses could be predicted using those of larger soil thickness obtained from the experimental results on the same soil.

(5) The infiltration method with dry soil produced similar FMC profiles as the moist soil compaction method at the same AFMC.

(6) The soil samples collected at different depths from the field had the moisture content increasing with depth, which was in good agreement with that observed in the laboratory tests.

(7) The field monitoring data showed that the volumetric water contents increased after rainfalls. The gravimetric moisture contents of the collected soil samples from the field also changed with the season including the rainfall event.

Chapter 4 Laboratory Evaluation of Wicking Geotextile for Moisture Reduction in Silty Sands at Different Fines Contents

4.1 Introduction

The textile industry first introduced the concept of moisture "wicking" through fibers. Wicking in textiles is capillary-driven moisture migration (Washburn, 1921). The evolution of the wicking concept and its applications has progressed through research and years, with a more recent focus on understanding moisture management in various fabrics. The textile industry has conducted extensive research on the properties and size and shape of pore structures of fibrous materials as summarized by Zaman et al. (2022a). Several studies indicated that wicking fibers could effectively absorb and transport liquid (Adler and Walsh, 1984; Hsieh, 1995; Nyoni, 2011; Fangueiro et al., 2010; Chatterjee and Singh, 2014). However, the quantity and transport rate of liquid depend on the fiber type, pore structure, internal surface, chemical treatment, and liquid properties (Hollies et al., 1957; Kumar & Das, 2014; Cotorobai et al., 2016). Hsieh (1995) concluded that the geometrical configuration of the fibrous material controlled the liquid travel distance. Nyoni (2011) reported that the penetration and retention of liquid in the fabric depended on the pore size, shape, and orientation. Mhetre and Parachuru (2010) pointed out that the rate of liquid migration between the longitudinal and transverse yarns was a crucial factor in deciding the wicking in woven fabrics. Yanılmaz and Kalaoğlu (2012) concluded that the greater wicking height happened in the fabrics having smaller capillary pores between yarns. In addition, Chatterjee and Singh (2014) concluded that macro-capillaries controlled short-term wicking while microcapillaries controlled long-term wicking in the fabric.

The wicking concept has been adopted by the geosynthetics industry in the last couple of decades. Before the adoption of the wicking concept, the geosynthetics industry used the capillary break concept to manage soil moisture problems. For example, geotextiles made of

hydrophobic polypropylene and polyester repel water, creating a capillary break effect (Henry, 1995; Stormont and Anderson, 1999; Koerner, 2012). These geotextiles have larger pores than base course materials, creating a capillary barrier that restricts water drainage when air gets trapped. Moreover, excess water accumulation at the soil-geotextile interface negates the intended reinforcing function of the geotextiles (Zornberg et al., 2017). To overcome this problem, wicking geotextile was introduced to the market. Wicking geotextile utilizes wicking fibers of hydrophilic and hygroscopic nylon filaments with multichannel cross-sections (Han and Zhang, 2014). Deep groove hydrophilic fibers (Fig. 4.1) have many irregular micro-channels with high surface tension. This mechanism associated with the wicking geotextile addresses moisture-related challenges beyond traditional geosynthetic materials. Several studies have shown that this wicking geotextile product has a highly effective moisture-wicking ability, even under unsaturated soil conditions (Zhang et al., 2014; Guo et al., 2017; Wang et al., 2017; Zornberg et al., 2017; Lin and Zhang, 2020; Biswas et al., 2021). This geotextile also serves for functions of separation, stabilization, reinforcement, and filtration in addition to enhanced lateral drainage.

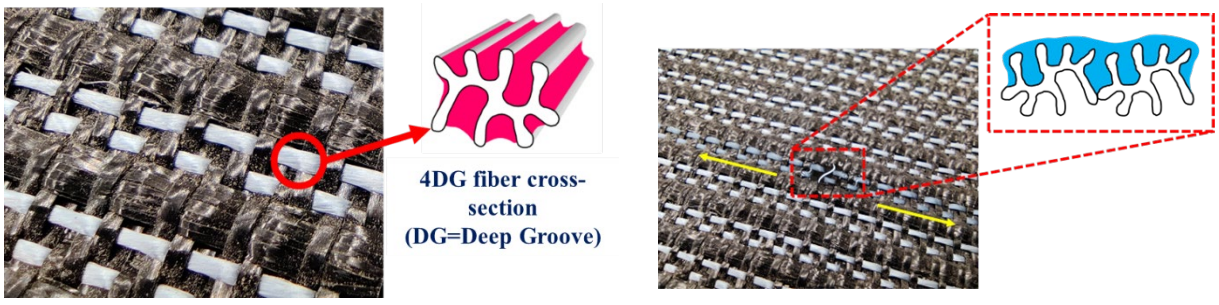

(a) deep groove nylon fibers (b) lateral drainage mechanism

Figure 4.1 Moisture movement mechanism in the wicking geotextile (Zaman et al. 2022b).

Removal of water (e.g., drainage) in an efficient and timely manner is necessary to improve the short-term and long-term performance of earth structures including slopes, walls, and roadways (Iryo and Rowe, 2005; Azevedo and Zornberg, 2013; Lin et al., 2017; Lin and Zhang 2018; Guo et al., 2019). Pavements have joints and cracks due to construction and repeated traffic loads, which allow rainwater to infiltrate into pavement layers. When the moisture that comes from precipitation, thawing, and capillary rise of the groundwater remains within base and subbase courses and subgrade, it weakens the soils and induces distresses of roadways over time (Christopher et al., 2006; Peng et al., 2020; Zhang et al., 2022). Furthermore, issues like pumping of fine-grained soils and soil volume change may arise due to the presence of excessive moisture in soils (Alobaidi and Hoare, 1994; Li et al., 2002; Zornberg and Gupta, 2009; Puppala et al., 2017; Indraratna et al., 2018; Galinmoghadam et al., 2022).

Zaman et al. (2024) demonstrated that natural soil remains at its field moisture capacity condition year-round except the precipitation and freezing-thawing days considering no change in the groundwater level. They also presented a simple laboratory method to determine the average field moisture capacity of soil. Figure 4.2 illustrates how the wicking geotextile under a pavement attracts water from the soil and transports and releases it at the field moisture capacity condition, primarily through high capillary suction followed by enhanced lateral moisture transport to the pavement shoulders. Several studies have been conducted in the laboratory or field to evaluate the effectiveness and performance of the wicking geotextile removing moisture under pavements.

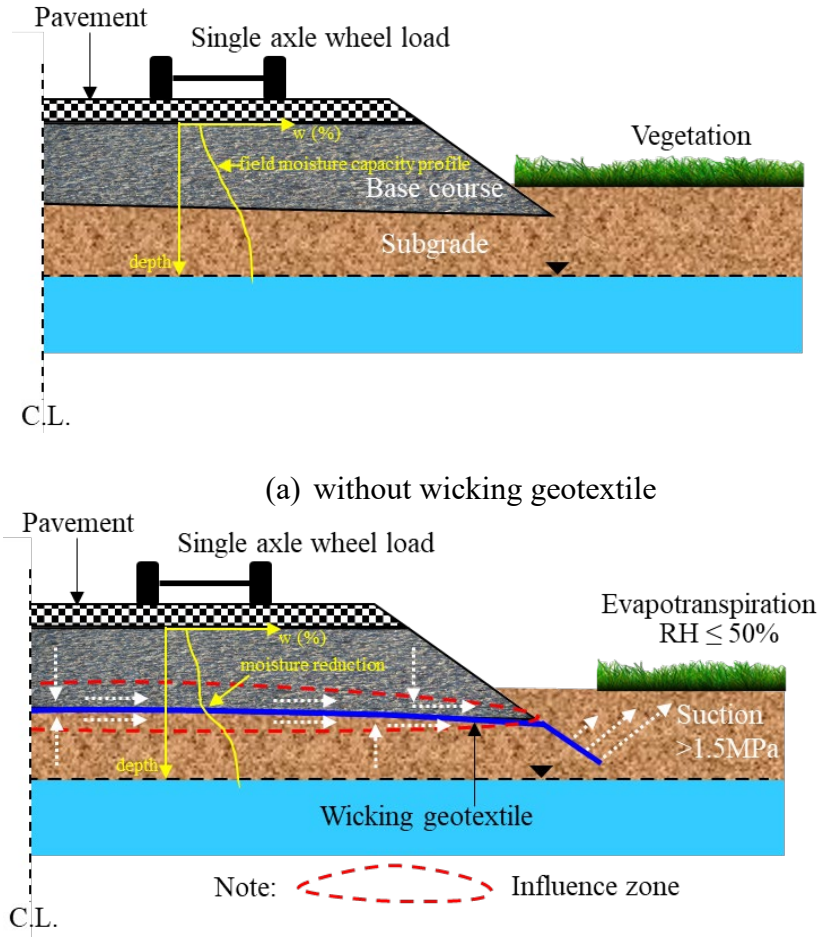

Figure 4.2 Schematic diagram for the coupled soil-water-geotextile system for water transport under a pavement.

Lin et al. (2017) demonstrated the effectiveness of the wicking geotextile in reducing soil moisture during spring thawing in Alaskan pavements. Zornberg et al. (2017) presented case studies showcasing the drainage benefits over non-wicking geotextiles in unsaturated pavement sections. Lin and Zhang (2018) studied the drainage performance of the wicking geotextile in the aggregate with 14.5% fines and observed a slow wicking rate. Guo et al. (2019) performed soil column tests with the aggregate containing 10% fines and reported the effective distance (i.e.,

influence zone) of the wicking geotextile was approximately 200 mm above and below the geotextile. However, Bai et al. (2021) observed the influence zone was more than 50 mm in small soil column tests. Lin et al. (2019) concluded that the wicking geotextile removed approximately 2% of moisture from the base course and resulted in a significant increase in the base resilient modulus. Guo et al. (2021) demonstrated from large cyclic plate loading tests that the unpaved sections with the wicking geotextile had the least permanent deformation compared with the control and non-wicking geotextile sections due to its additional wicking benefit. Zaman and Han (2023) conducted moisture reduction tests with the wicking geotextile inside a clean sand in a large direct shear box and observed obvious moisture reduction below and above the wicking geotextile. Galinmoghadam et al. (2022) reported the use of the wicking geotextile to mitigate pavement pumping issues due to fines migration under repetitive traffic loads. Guzman et al. (2021) observed enhanced wicking drainage in arctic highway embankments during the thawing season. Biswas et al. (2021) reported the moisture reduction within 300 mm distance from the wicking geotextile in the subgrade soils resulted in the reduced permanent deformation in a road section. In addition, Liu et al. (2022) reported the long-term field performance of the wicking geotextile under a concrete pavement in removing moisture from the aggregate base containing fines. In addition to laboratory and field studies, Lin et al. (2021) performed numerical simulations showing that wicking fibers removed soil moisture under light rain, while the geotextile acted as a permeable material under heavy rainfall.

However, water removal efficiency may be limited when the suction in the geotextile is close to or lower than that in the soil, such as for the case when the soil contains fine particles. It is well known that soil suction depends on its fines content (Kermani et al., 2018, 2019). In other words, the effectiveness of the wicking geotextile in reducing moisture depends on the

percentage of fines in the soil. In addition, it is expected that the suction induced by the wicking geotextile decreases with the distance from the geotextile; therefore, there is an influence distance as found by Guo et al. (2019) and Bai et al. (2021). However, there have been limited studies and understanding of how fines affect the effectiveness of the wicking geotextile with regard to moisture reduction and influence distance and whether there is a limit for the fines content beyond which the wicking geotextile becomes ineffective. This study developed a simple test method to evaluate the moisture reduction ability of the wicking geotextile from silty sands with fines (silt particles without plasticity). The objective of this study was to evaluate the moisture reduction ability of the wicking geotextile from silty sands prepared at different fines contents. To ensure a consistent initial condition for all sands in tests, they were prepared at their field moisture capacities. Zaman et al. (2024) investigated the field moisture capacities of the soils used in this study. To demonstrate the benefit of the moisture reduction by the wicking geotextile, a non-wicking woven geotextile was also tested in this study. In addition, control tests without any geotextile were conducted.

4.2 Test materials and methods

In this study, Kansas River sand was selected as the main soil material. One type of sandy silt (also named pond fill sand) was collected from a local sand quarry in Kansas and mixed with the Kansas River sand to create silty sands at different fine contents for the research purpose. The collected sandy silt contained approximately 40% fines (smaller than 0.075 mm) while the river sand contained 0% fines. The river sand and sandy silt were classified as poorly graded sand (SP) and silt (ML), respectively according to the Unified Soil Classification System (USCS). These two soils were mixed at different percentages to prepare silty sands at 5%, 10%, and 15% fines. Figure 4.3 shows the particle size distributions of all these soils used in this

study. The prepared soils were used in this study to evaluate the moisture reduction by the wicking geotextile. Table 4.1 lists the physical properties of these soils. Figure 4.4 shows the standard Proctor compaction test results of the silty sands at different fine contents. Clean sand with 0% fines is not suitable for compaction tests and not included in this figure. The maximum dry density of the clean sand in Table 4.1 was determined using the vibrating table method (ASTM D4253) while the maximum dry densities of the silty sands were determined using the standard Proctor compaction tests.

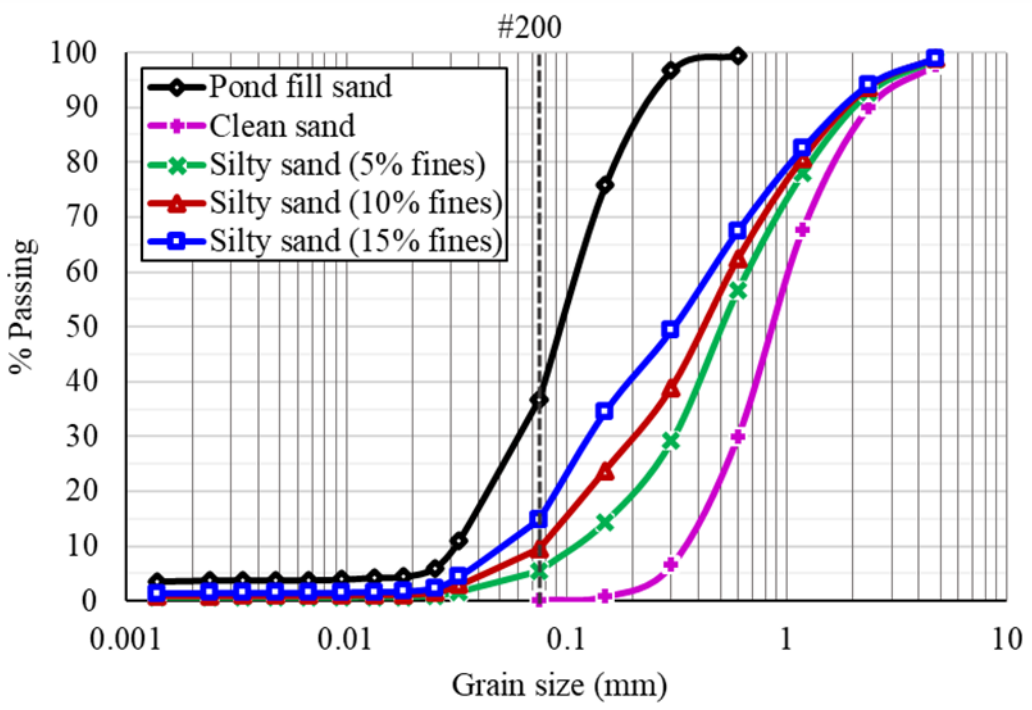

Figure 4.3 Particle size distributions of soils.

Table 4.1 Physical properties of soils

Soil type	D_{10} (mm)	D_{30} (mm)	D_{50} (mm)	D_{60} (mm)	C_u	C_c	G_s	e	$\gamma_{d,max}$ (kN/m^3)
Sand (0% fines)	0.32	0.6	0.85	1	3.13	1.13	2.65	0.44	18.85
Silty sand (5% fines)	0.12	0.30	0.51	0.68	5.67	1.10	2.66	0.43	19.2
Silty sand (10% fines)	0.08	0.20	0.42	0.56	7	0.89	2.67	0.41	20.4
Silty sand (15% fines)	0.05	0.14	0.30	0.45	9	0.87	2.66	0.40	20.25

Note: D_{10}=10% of particles finer than this size (effective particle size); D_{30}=30% of particles finer than this size; D_{50}=50% of particles finer than this size (mean particle size); D_{60}=60% of particles finer than this size; C_u=uniformity coefficient; C_c=coefficient of curvature; G_s=specific gravity; e=void ratio at the relative density of 75%; and $\gamma_{d,max}$=maximum dry unit weight.

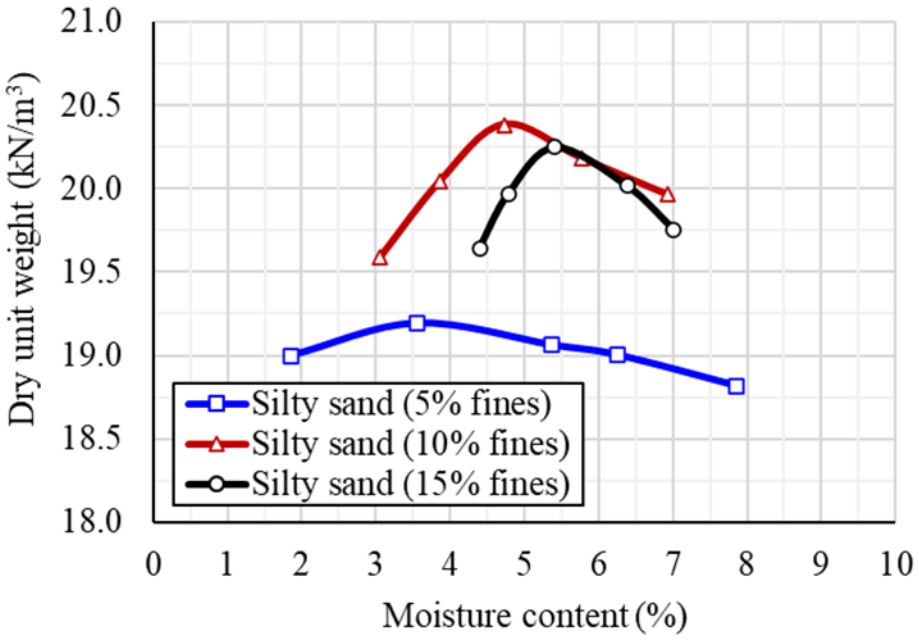

Figure 4.4 Dry density versus moisture content curves of the soils from standard Proctor compaction tests.

This study adopted two different types of geotextiles: (i) wicking woven (WW) geotextile and (ii) non-wicking woven (NWW) geotextile. Table 4.2 provides the basic properties of these geotextile products. In the laboratory, four boxes, each 300 mm long, 300 mm wide, and 600 mm high, were built using polycarbonate pieces. Each box had upper and lower parts that were each 300 mm high.

Table 4.2 Properties of geotextile (provided by the manufacturer)

Geotextile	Property	Unit	Value
Wicking Woven (WW)	Apparent opening size	mm	0.43
	Pore size (O_{50})	Microns	85
	Pore size (O_{95})	Microns	195
	Permittivity	sec^{-1}	0.4
	Flow rate	$l/min/m^2$	1222
	Thickness	mm	1.24
	Unit mass	g/m^2	497
	Specific gravity of fibers	-	0.96
	Porosity	%	58.6
	Tensile strength (2% strain, MD)	kN/m	7
	Tensile strength (2% strain, CD)	kN/m	15.8
	Wet front movement (vertical)	mm	152
	Wet front movement (horizontal)	mm	1862
Non-Wicking Woven (NWW)	Apparent opening size	mm	0.60
	Permittivity	sec^{-1}	0.4
	Flow rate	$l/min/m^2$	1222
	Thickness	mm	1.22
	Unit mass	g/m^2	385
	Specific gravity of fibers	-	0.91
	Porosity	%	65.3
	Tensile strength (2% strain, MD)	kN/m	14
	Tensile strength (2% strain, CD)	kN/m	19.3
	Tensile Strength (ultimate)	kN/m	70

Before a soil was placed into a box, it was mixed with water to prepare a moist condition close to the average field moisture capacity as determined by Zaman et al. (2024). The moist soil was prepared at its field moisture capacity rather than after precipitation because: (1) wicking drainage begins after gravity drainage (Wang et al., 2017) and (2) equal initial moisture content is ensured for better comparison of test results with a wicking geotextile, a non-wicking geotextile, or without any geotextile. The moist soil was kept in a closed container overnight to allow the water to fully penetrate and distribute within the soil.

The prepared moist soil was moved to a control room. In the control room, relative humidity and temperature were maintained approximately at 50% and 10°C, respectively, for all the tests. The moist soil was mixed thoroughly before being placed in the polycarbonate test boxes. The soil was placed in three equal lifts and compacted inside the lower boxes to a relative density of 75% for the clean sand, or a relative compaction of 95% for the sand with fines. The geotextile, if used, was placed at the top of the lower box (at a height of 300 mm). The placed geotextile was extended by approximately 100 mm beyond two side walls of the polycarbonate box. Next, the upper box was placed above the lower box and filled with the soil in the same manner as the lower box. The upper box was filled with soil 275 mm high (i.e. 25 mm space on the top of the box) to ensure better compaction. After compaction to the top, the top of the box was sealed using a plastic sheet with holes to minimize the evaporation and canopy effect. After the desired waiting period, soil samples at different depths inside the box were collected and their gravimetric moisture contents were determined. This process was repeated for all specimens at four fines contents (0%, 5%, 10%, and 15%) and four waiting periods (3, 7, 14, and 28 days), A total of 48 tests were conducted. Figure 4.5 shows the moisture reduction test setup.

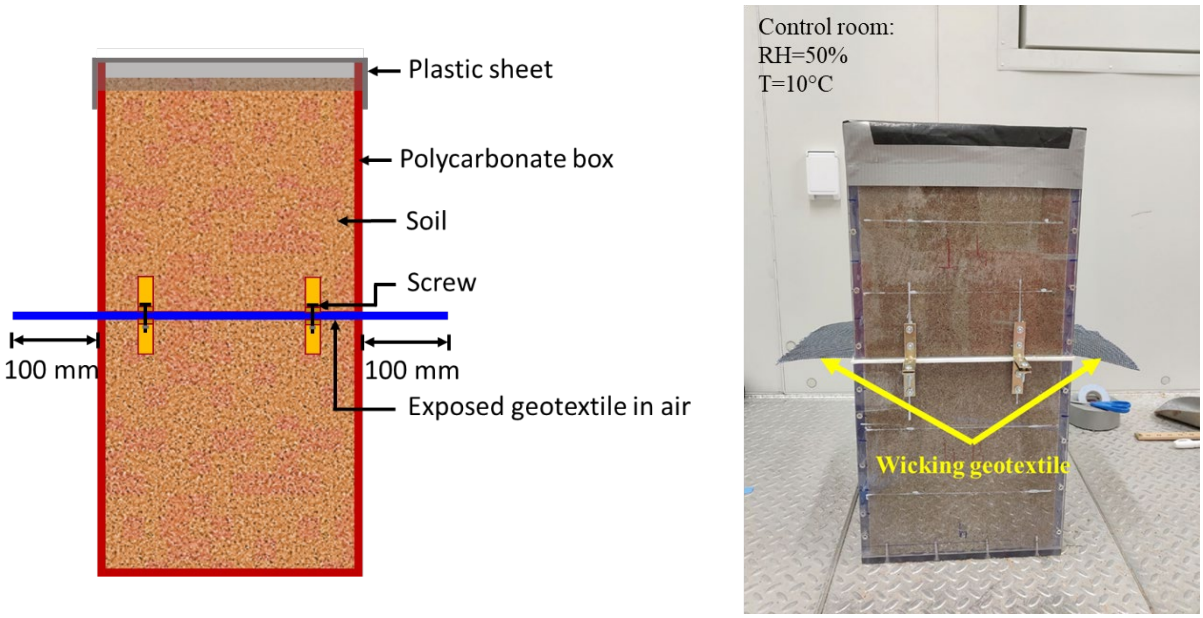

Figure 4.5 Moisture reduction test setup: (a) illustration (drawn not to scale) and (b) photo taken in the laboratory.

4.3 Test Results and Discussion

4.3.1 Gravimetric moisture contents in the moisture reduction tests

In the laboratory, 48 moisture reduction tests were performed using four types of soil: (i) sand with 0% fines (i.e., clean sand), (ii) sand with 5% fines, (iii) sand with 10% fines, and (iv) sand with 15% fines using polycarbonate test boxes. In the tests with the sand containing 0% fines, approximately 7.6% moisture was added to prepare the soil at the moist condition close to the average field moisture capacity (Zaman et al. 2024). In the control tests, no moisture reduction is expected but water flow and retention in the soil came to an equilibrium condition due to the gravity and capillary effect of the soil particles after different waiting periods (i.e., 3, 7, 14, and 28 days). Figure 4.6 shows that for the control tests, no significant moisture content changes were observed for different waiting periods as the soil moisture had already reached an

equilibrium condition after three days. The test results with the NWW geotextile show that the moisture contents of the clean sand above the geotextile were higher than those in the control tests, indicating downward movement of moisture was obstructed by the NWW geotextile. Since the capillary suction in the clean sand was low, soil moisture easily moved downwards. Moisture in the sand accumulated on top of the NWW geotextile. The amount of accumulation increased with the increase in the waiting period. The moisture contents of the sand below the NWW geotextile (i.e., in the lower test box) were lower than those in the control tests because the downward movement of moisture due to gravity was obstructed when the NWW geotextile was used. On the other hand, the test results with the WW geotextile show that the moisture contents of the sands above and below the WW geotextile were lower than those in the control tests and the tests with the NWW geotextile. The rate of moisture reduction increased with the increase in the waiting period. It was found that the soil moisture profiles in these tests after 14 days were close to those after 28 days. Therefore, it can be concluded that the WW geotextile removed the maximum amount of moisture in the clean sand in no more than 14 days. This result indicates that the WW geotextile could not remove moisture from the clean sand above the geotextile when the moisture content was at approximately 1.5%. However, the moisture contents of the sand below the WW geotextile ranged from approximately 3% to 16% (close to saturation at the bottom). Figure 4.6 also shows that the influence zone was approximately 300 mm above and below the WW geotextile.

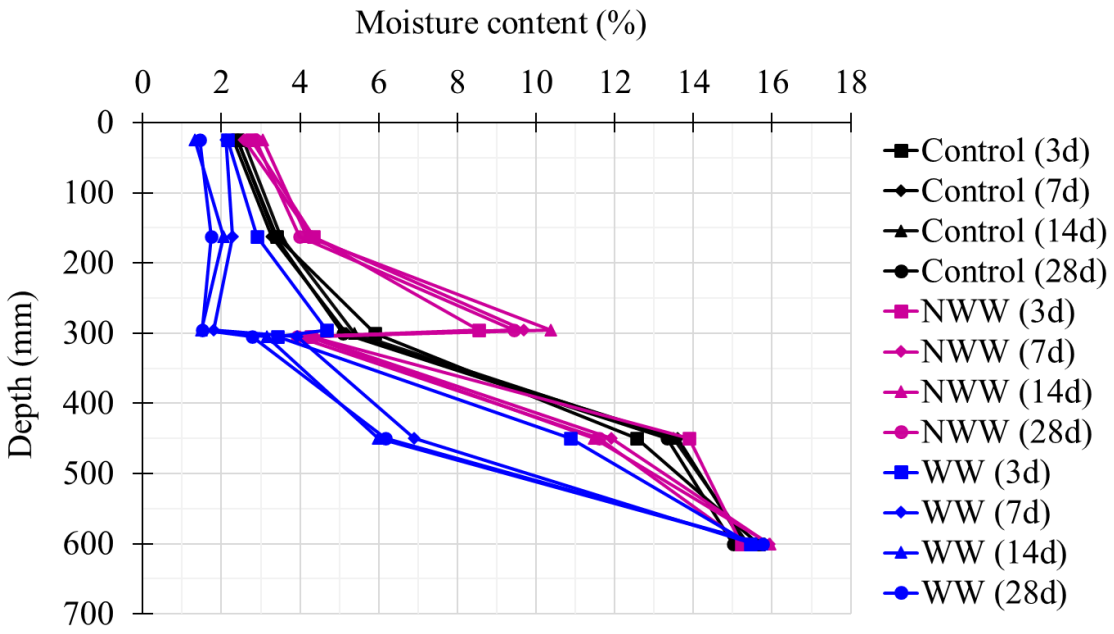

Figure 4.6 Gravimetric moisture content profiles for the sand with 0% fines with and without the geotextile at different waiting periods.

Figure 4.7 shows the moisture reduction test results with the silty sand containing 5% fines. Approximately 8.8% moisture was added to prepare the moist condition close to its average field moisture capacity as determined by Zaman et al. (2024). In the control tests, soil moisture moved downward until a moisture equilibrium condition was achieved depending on the capillary suction of soil particles, gravity, and time. Similar to the tests with the clean sand, moisture in this silty sand was obstructed and accumulated on top of the NWW geotextile and the accumulation rate increased with the increase in the waiting period. However, the WW geotextile collected and removed moisture from the surrounding soil. The moisture reduction rate increased with the increase in the waiting period. It was found that the moisture content profiles were similar after the waiting periods of 14 and 28 days. In the silty sand with 5% fines, the WW geotextile could not remove moisture from the soil above the geotextile when the moisture content was at approximately 5%. However, the moisture content of the silty sand with

5% below the WW geotextile ranged from 5% to 16%. The influence distances above and below the WW geotextile were less than 300 mm.

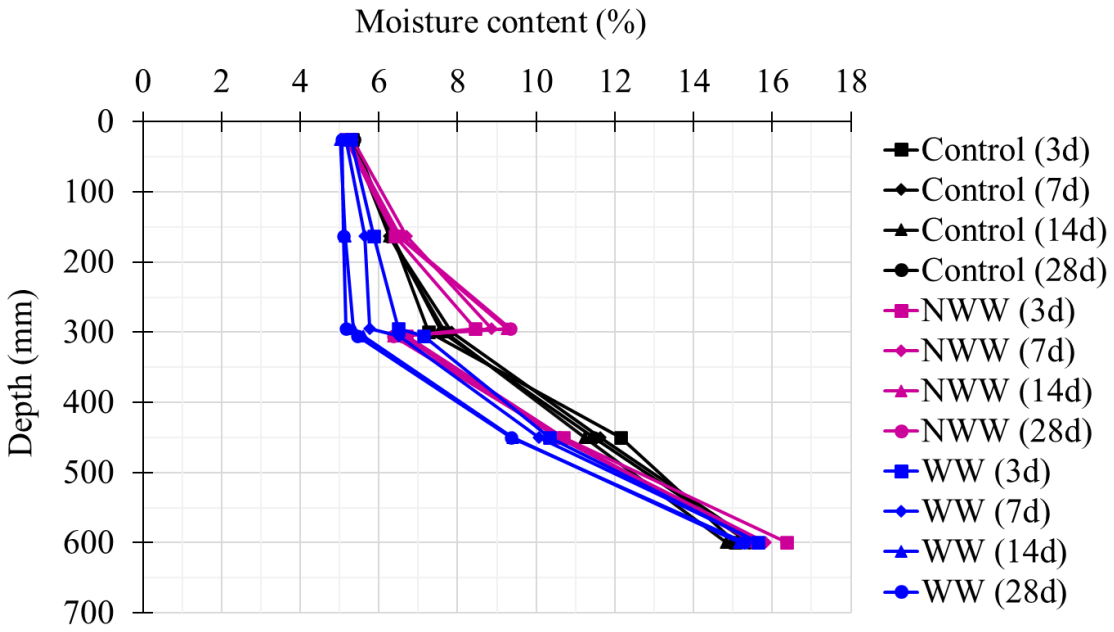

Figure 4.7 Gravimetric moisture content profile for silty sand with 5% fines with and without the geotextile at different waiting periods.

Figure 4.8 shows the moisture reduction test results with the silty sand containing 10% fines. Approximately 10.4% moisture was added to prepare the moist condition close to the average field moisture capacity for this sand as determined by Zaman et al. (2024). In the control tests, soil moisture moved downwards at different waiting periods but eventually reached an equilibrium moisture distribution. In the tests with the NWW geotextile, moisture was seen obstructed and accumulated on top of the NWW geotextile; however, the moisture accumulation rate was less than the rates for the clean sand and the sand with 5% fines at different waiting periods because the downward movement of moisture in this sand was relatively slow due to the presence of a large amount of fines. The WW geotextile did remove moisture above and below

the geotextile; however, the moisture reduction rate decreased compared to the tests with the clean sand and the sand with 5% fines. The WW geotextile was observed to stop functioning when the moisture content above the geotextile was at approximately 8.2%. Figure 4.8 shows that the moisture content profiles at 7-, 14-, and 28-day waiting periods were similar, indicating that the moisture reduction by the WW geotextile was essentially completed after 7 days.

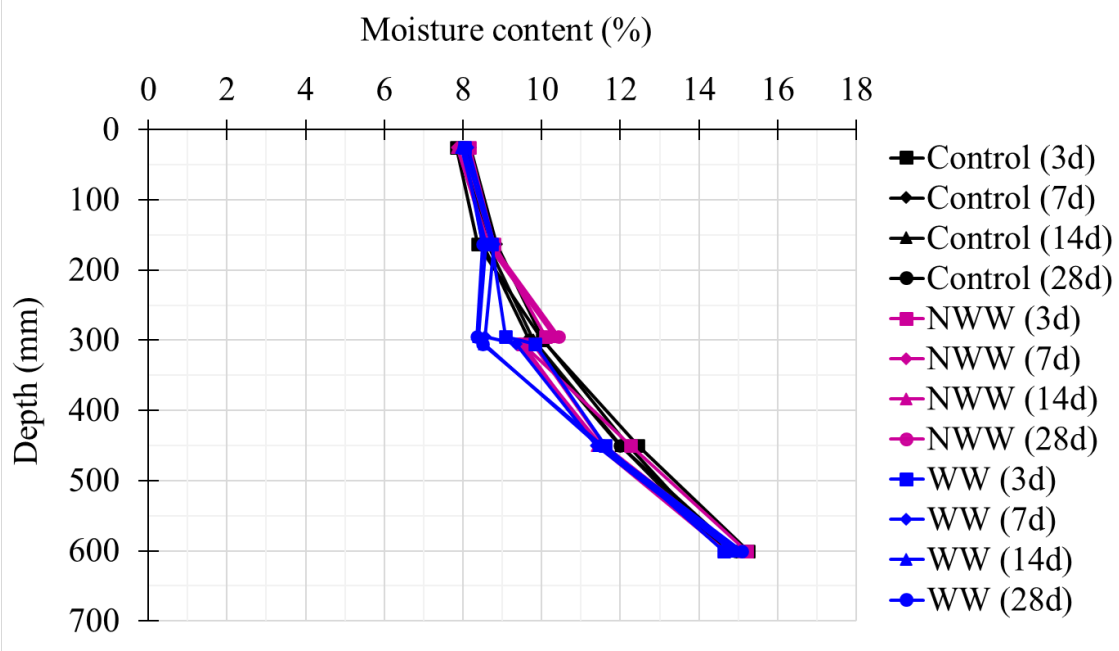

Figure 4.8 Gravimetric moisture content profiles for the silty sand with 10% fines.

Zaman et al. (2024) determined the average field moisture capacity of the silty sand with 15% fines as 11.5%. Figure 4.9 shows the laboratory test results with this soil. Due to the presence of a large amount of fines in the sand, the movement of moisture under the effect of gravity decreased. Therefore, only a small amount of moisture accumulated on top of the NWW geotextile with time. The presence of more fines reduced the size of pore spaces between sand particles, thus reducing the hydraulic conductivity and flow rate in the sand and increased the

soil suction. Figure 4.9 shows that the WW geotextile still removed moisture from the soil above and below the geotextile after three days but had a reduced influence zone. After three days, the average moisture content in the silty sand above the geotextile was approximately 10.2%.

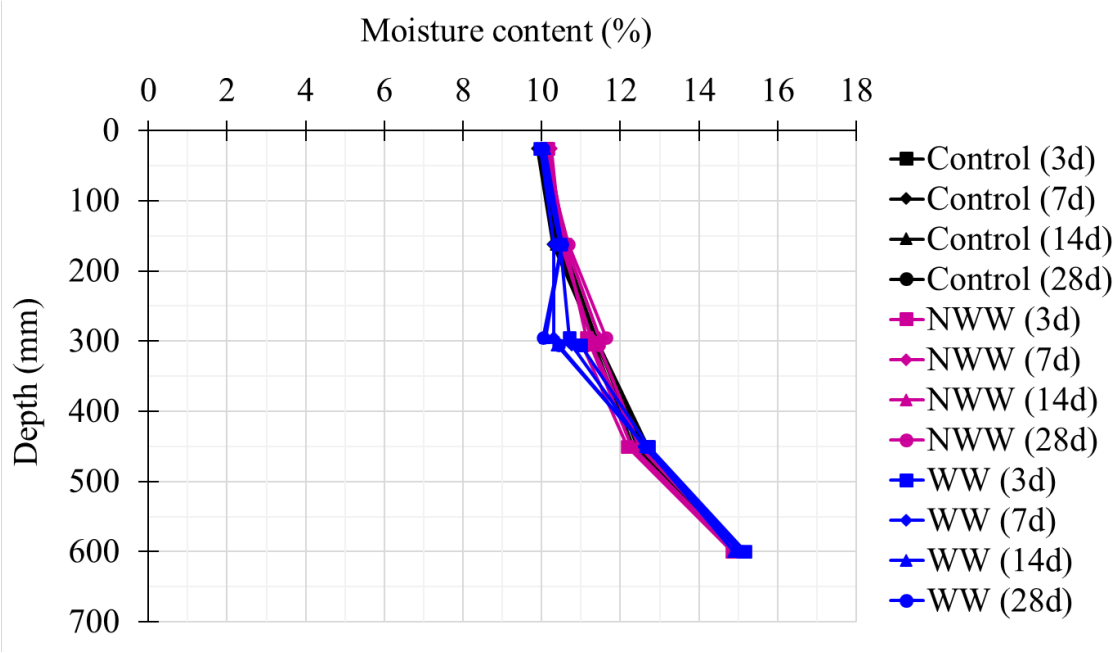

Figure 4.9 Gravimetric moisture content profile for silty sand with 15% fines.

4.3.2 Change of average moisture content with time

The average moisture contents (AMC) in the upper and lower boxes were calculated as the moisture content area from the moisture content profile divided by the soil thickness as shown in Figures 4.6 to 4.9. Figure 4.10 presents the change in the AMC within the upper box (i.e., the soil above the geotextile) with time and indicates that the NWW geotextile worked as a barrier against the downward movement of moisture in the soil above the geotextile. As a result, more moisture was retained in the upper box compared to the tests with no geotextile (i.e., control), in which soil moisture was able to move downward in the lower box. In the control and

NWW geotextile tests, no significant changes were observed in the AMC at different waiting periods, meaning that moisture movement came to an equilibrium condition in the first three days. For example, in the tests with the clean sand (Figure 4.10a), the AMCs for the control and NWW conditions were calculated as approximately 3.8% and 5.1%, respectively in the upper box. On the other hand, the AMC decreased with the waiting period in the tests with the WW geotextile. For example, the AMCs were approximately 3.3% after three days and 1.8% after 28 days for the tests with the WW geotextile. This result indicates that the WW geotextile worked well in the clean sand prepared at the average field moisture capacity in terms of reducing moisture from the soil above the geotextile. Similar results were observed in the tests with the sand containing 5% fines (Figure 4.10b). However, the WW geotextile became less effective when the silty sand with fines was used. Fine particles in the sand had a high moisture retention capacity due to large surface areas, making it more difficult for the WW geotextile to draw moisture away from the soil. Additionally, fines in the sand increased capillary action, causing moisture to move upward against the intended lateral drainage of the WW geotextile, thus counteracting its wicking capability. The test results show that the WW geotextile removed the maximum amount of moisture from the sand with 0% and 5% fines in 14 days. Figures 4.10c and 4.10d present the average soil moisture content in the upper box with the sand containing 10%, and 15% fines, respectively. While the WW geotextile removed a small amount of moisture from the sand with 10% fines, no significant changes in the moisture content were observed in the sand with 15% fines at different waiting periods.

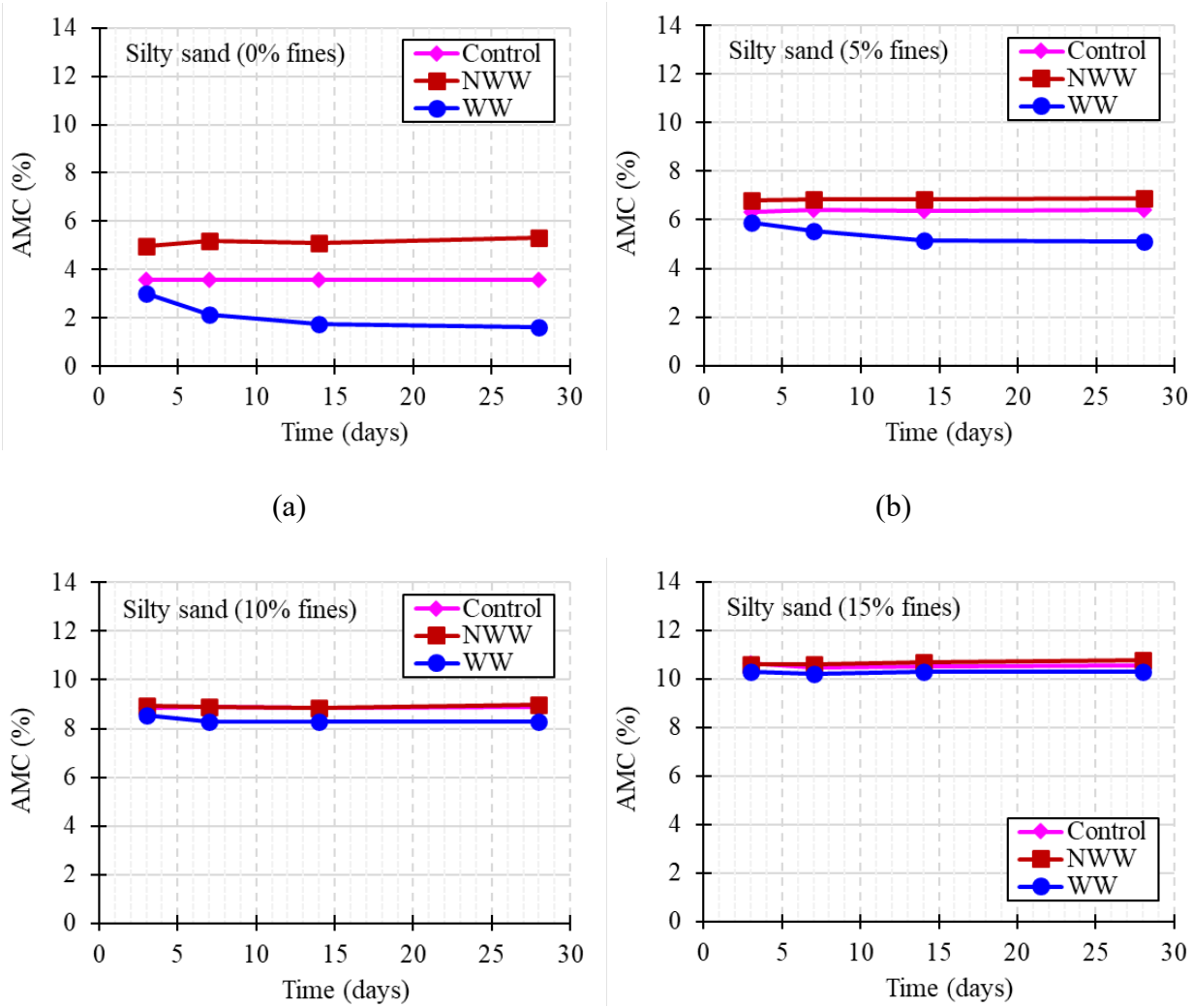

Figure 4.10 Average moisture contents in the soil within the upper box at different waiting periods.

Figure 4.11 presents the change in the average moisture content in the sand below the geotextile or in the lower test box. The results for the control and NWW geotextile tests show a constant level of AMC in the lower box as there was no reduction in the moisture content. In the sand with 0% and 5% fines (Fig. 4.11a and 4.11b), moisture moved down more easily under gravity; therefore, more moisture accumulated within the lower box. However, the control tests

had higher AMCs than the NWW geotextile tests as the NWW geotextile impeded downward moisture flow from the upper box. The control and NWW geotextile tests show similar levels of moisture content when the sand with 10% and 15% fines were used due to the reduced hydraulic conductivity and increased moisture retention capacity when a larger amount of fines existed in the silty sand (Fig. 4.11c and 4.11d). The presence of 10% or more fines in the silty sand restricted moisture flow; therefore, moisture could not travel downward easily, leading to the same moisture content profile at different waiting periods. In the case of the sand with 0% fines, the AMC within the lower box decreased from approximately 12% in 3 days to 8% in 28 days by the WW geotextile (Fig. 4.11a). The WW geotextile reduced the AMC within the lower box from approximately 11% in 3 days to 10% in 28 days when the silty sand with 5% fines was used (Fig. 4.11b). However, there was no significant reduction of moisture content from the soil within the lower box in case of the silty sand containing 10% or 15% fines (Fig. 4.11c and 4.11d).

Figure 4.12 shows the effect of the fines content on the AMCs of the sand above and below the WW geotextile. From 3 to 14 days, the AMCs in the soil above the geotextile were reduced by approximately 1.5%, 1.0%, and 0.5% in the silty sand containing 0%, 5%, and 10% fines, respectively. No significant change was observed when the sand containing 15% fines was used. Similar observations were obtained in the soil below the geotextile from a 3 to 14-day waiting period. The test results further indicate that soil moisture content did not change much between 14 and 28 days. This phenomenon happened because the wicking geotextile reached its maximum moisture reduction capacity as no additional moisture (e.g., rainfall) was added to the unsaturated soil prepared initially at the average field moisture capacity condition.

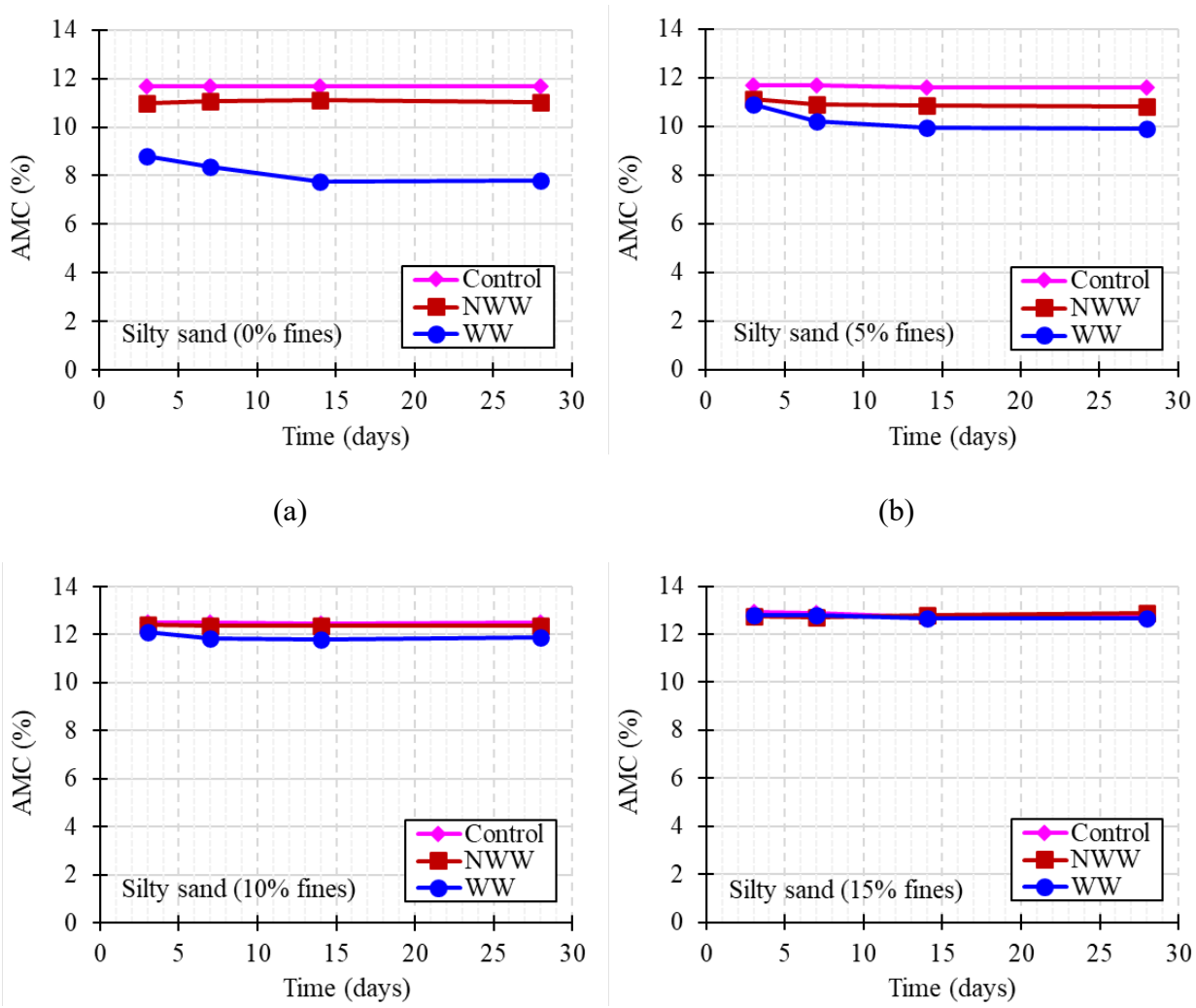

Figure 4.11 Average moisture contents in the soil within the lower box at different waiting periods.

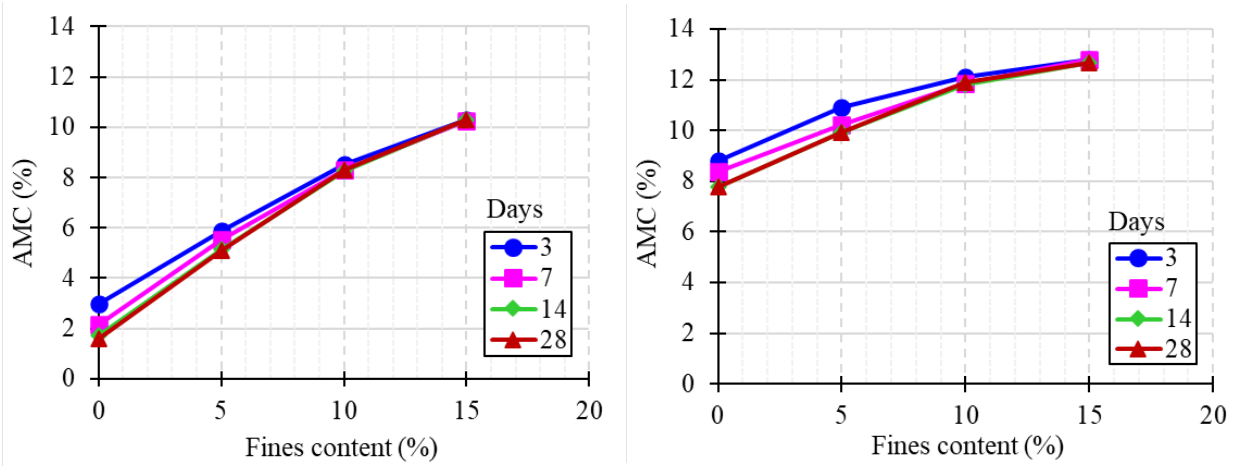

(a) above geotextile (b) below geotextile

Figure 4.12 Effect of fines content on the average moisture contents of the sand with the wicking woven geotextile at different waiting periods.

4.3.3 Influence zone of wicking geotextile in silty sand

In the moisture reduction tests, the influence zone and influence distances, d_i above and below the WW geotextile were identified from the moisture content profiles for the silty sand containing different amounts of fines. It was observed that the influence zone below the geotextile was smaller than that above the geotextile due to capillary action and gravity. Above the geotextile, downward movement of moisture was facilitated by gravity and capillary action of wicking fibers in the WW geotextile. Below the geotextile, gravity drove moisture downward, counteracting the upward movement facilitated by the wicking action from the WW geotextile. In other words, the combination of capillary action by wicking fibers and gravity driving moisture downward resulted in a larger influence zone above the wicking geotextile than that below the geotextile. Figure 4.13 presents the influence distances for the wicking geotextile in the silty sands containing different amounts of fines. The influence distance decreased with the

increase in the fines content in the silty sand. The influence distance in the clean sand was estimated as at least 300 mm above and below the geotextile, which was the total soil thickness placed in the test box, i.e. the maximum distance that could be evaluated.

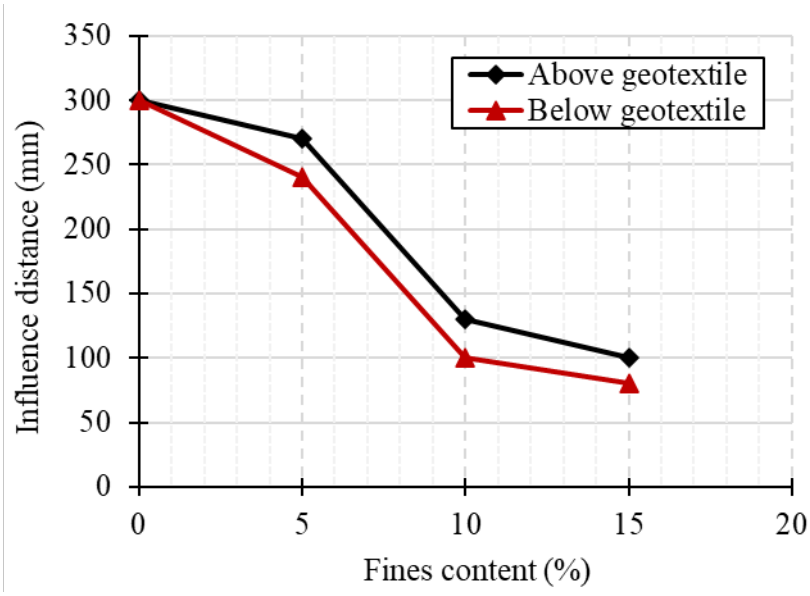

Figure 4.13 Effect of the fines content on the influence distance of the wicking geotextile.

4.3.4 Average moisture content within the influence zone

Average moisture content (AMC) was also calculated within the influence zone to investigate the effectiveness of the wicking geotextile in reducing moisture from the silty sand containing fines at different waiting periods. Figure 4.14 shows that the sand with a lower fines content had lower AMC within the influence zone than that with a higher fines content. The AMC of the sand above the WW geotextile was lower than that of the same sand below the geotextile. Figure 4.14a shows the change in the AMC within the influence zone above the WW geotextile in the silty sands containing different amounts of fines. It was observed that the moisture reduction was faster in the soil containing 5% or less fines whereas the moisture

reduction was slower in the soil containing 10% or more fines. Figure 4.14b shows the change in the AMC within the influence zone below the WW geotextile in the silty sands containing different amounts of fines. The wicking phenomena were similar to those seen within the influence zone above the geotextile.

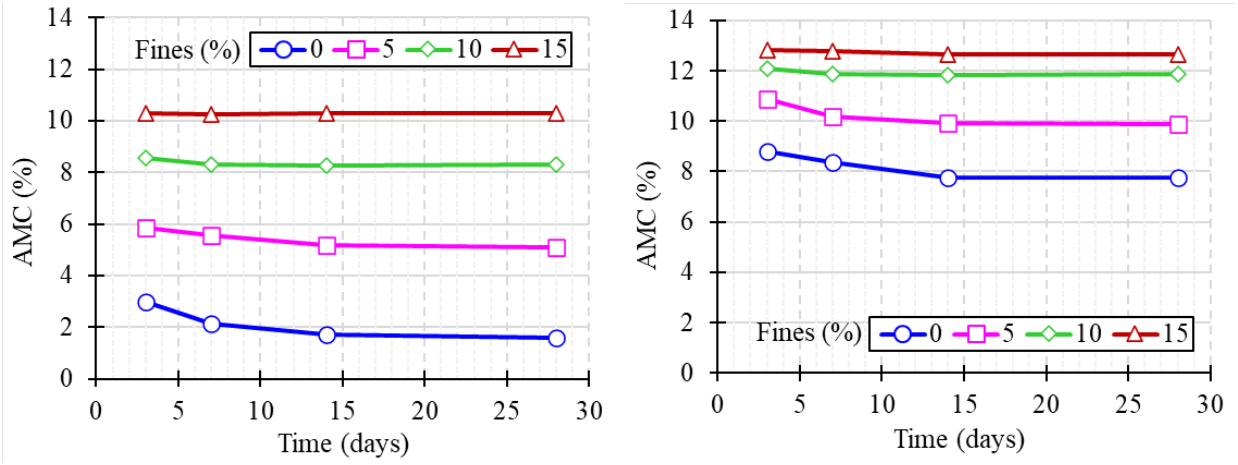

(a) above geotextile (b) below geotextile

Figure 4.14 Average moisture content in the influence zone of wicking geotextile.

4.3.5 Percentage moisture content reduction by wicking geotextile

To further evaluate the benefit of the wicking geotextile in reducing the moisture content of the sand, percentage moisture content reduction (MCR) by the WW geotextile was calculated using the following equation based on the test results obtained in this study:

$$MCR\ (\%) = \left(\frac{W_0 - W_1}{W_0}\right) \times 100 \qquad (4.1)$$

where W_0 = the AMC in the soil without geotextile and W_1 = the AMC in the soil with the WW geotextile. Note the AMC used in this calculation is for the soil above or below the geotextile in the test boxes.

Figure 4.15 presents the calculated MCRs by the WW geotextile, clearly showing that MCR decreased with the increase of the fines content. Within the soil above and below the geotextile, Figure 4.15 shows that MCR increased with the increase in the waiting period in the silty sand containing fines up to 10%. In the silty sand with 15% fines, MCRs were independent of the waiting period and their values were lower than 3%, indicating low efficiency of the wicking geotextile in reducing moisture in the silty sand containing 15% fines; therefore, 15% fines content can also be considered the limit for the effectiveness of this WW geotextile.

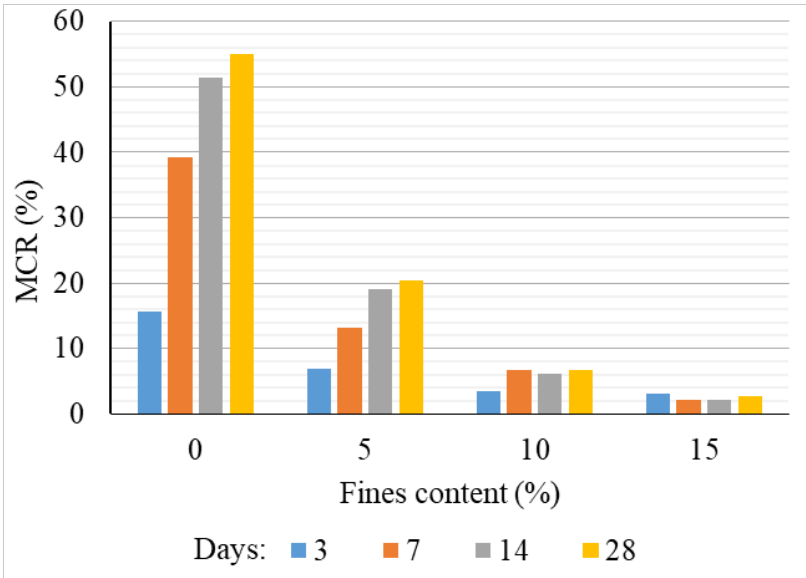

(a) above geotextile

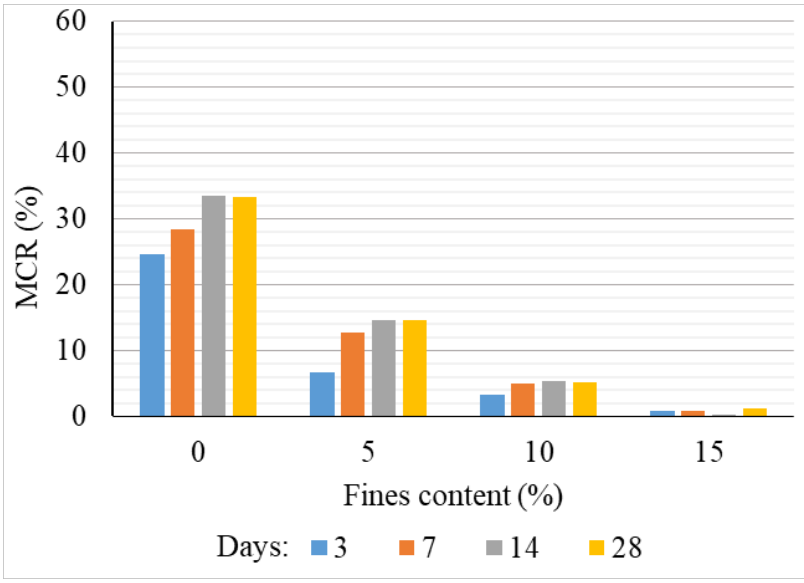

(b) below geotextile

Figure 4.15 Percentage moisture content reduction by the wicking geotextile compared to the control test.

4.4 Summary

This report presents a simple laboratory method to evaluate the moisture reduction from silty sands by the wicking geotextile. Polycarbonate test boxes were designed, built, and used for the experiments conducted in a controlled room (approximate relative humidity of 50% and temperature of 10°C). Three types of test conditions were investigated with the silty sands containing 0%, 5%, 10%, and 15% fines: (i) soil without any geotextile (i.e., control), (ii) soil with a non-wicking woven geotextile, and (iii) soil with a wicking woven geotextile. Silty sand was mixed with water to prepare a moist condition close to the average field moisture capacity. Moisture content profiles were developed based on the measured gravimetric moisture contents after 3, 7, 14, and 28 days of waiting periods. The AMCs within the soils above and below the geotextile were calculated and analyzed for different waiting periods. Furthermore, the influence zones and distances for the wicking geotextile in the silty sands were determined from the moisture reduction test results. The changes in the AMC within the influence zone were also investigated. The percentage moisture content reduction (MCR) by the wicking geotextile was calculated for silty sands with different fine contents and at different waiting periods. The following conclusions can be made based on the findings of this study.

1. The wicking geotextile removed moisture from the silty sands prepared at their average field moisture capacities while moisture accumulated on top of the non-wicking woven geotextile as a barrier.
2. Moisture reduction was more pronounced when the silty sand contained fines up to 5%. The wicking geotextile was able to reduce moisture in the silty sand with 10% fines but at a slower rate and smaller amount.

3. The influence zone above the wicking geotextile was larger than that below the geotextile and the influence distance decreased with the increase of fines in the silty sands.
4. The wicking geotextile reduced the maximum amount of moisture from the silty sand containing fines up to 5% at 14 days and from silty sand containing fines 10% or more by 7 days.
5. MCR in the silty sand by the wicking geotextile decreased significantly as the fines content increased from 0% to 15%. The 15% fines content is considered the limit for the effectiveness of this wicking geotextile.

Chapter 5 Conclusions and Recommendation

5.1 Conclusions

The following conclusions can be made from this study:

(1) The contact angles for the wicking woven geotextile became smaller than 90° after a few seconds of dropping the water droplet while those for the non-wicking woven geotextile and the nonwoven geotextile stayed larger than 90° or approximately 90° during the observation period.

(2) The wicking geotextile showed better surface wettability due to high capillary forces by the wicking fibers compared to non-wicking woven and nonwoven geotextiles.

(3) Flattening of the geotextile sheet or fibers and soil intrusion in the geotextile were identified as two contributing factors to the change of contact angles after soil compaction.

(4) A simple laboratory method was developed to determine the field moisture capacity (FMC) profiles for soils.

(5) The average field moisture capacity (AFMC) of a silty sand increased with the increase of its fines content. The AFMC of the sand decreased with the increase of soil thickness (i.e., distance from the water table).

(6) The FMC profile and AFMC of smaller soil thicknesses could be predicted using those of larger soil thickness obtained from the experimental results on the same soil.

(7) Moisture reduction experiments showed that the wicking geotextile removed moisture from the silty sands prepared at their average field moisture capacities while moisture accumulated on top of the non-wicking woven geotextile as a barrier.

(8) Moisture reduction was more pronounced when the sand contained fines up to 5%. The wicking geotextile was able to reduce moisture in the silty sand with 10% fines but at a slower rate and smaller amount.

(9) The influence zone above the wicking geotextile was larger than that below the geotextile and the influence distance decreased with the increase of fines in the silty sands.

(10) The moisture content reduction (MCR) in the silty sand by the wicking geotextile decreased significantly as the fines content increased from 0% to 15%. The 15% fines content is considered the limit for the effectiveness of this wicking geotextile.

5.2 Recommendation for Future Work

The following research is recommended for future work:

(1) This study adopted one type of clean sand and one type of pond fill sand to prepare silty sands at different fines contents by mixing them together. Different types of soils may have different field moisture capacities, which may affect the effectiveness of the wicking geotextile. Future work is needed to verify the experimental results obtained in this study.

(2) The experimental results obtained in this study were mainly based on one specific type of wicking geotextile. Other types of wicking geotextile may have different behavior; therefore, they should be evaluated in future research.

(3) This study simulated field conditions after rainfall precipitation. Performance of the wicking geotextile in other applications, such as being used as a capillary barrier, for frost-heave reduction, and for fines pumping mitigation, may be different; therefore, it should be investigated in future studies.

References

1. ASTM Committee D-18 on Soil and Rock. (2016). Standard test methods for maximum index density and unit weight of soils using a vibratory table. ASTM International.

2. ASTM D5261-10, 2018. Standard Test Method for Measuring Mass per Unit Area of Geotextiles. Annual Book of ASTM Standards. ASTM International, West Conshohocken, PA.

3. ASTM D6767-21, 2021. Standard Test Method for Pore Size Characteristics of Geotextiles by Capillary Flow Test. Annual Book of ASTM Standards. ASTM International, West Conshohocken, PA.

4. ASTM D7334-08, 2013. Standard Practice for Surface Wettability of Coatings, Substrates and Pigments by Advancing Contact Angle Measurement. Annual Book of ASTM Standards. ASTM International, West Conshohocken, PA.

5. Alobaidi, I., and Hoare, D. J. (1994) Factors affecting the pumping of fines at the subgrade subbase interface of highway pavements: a laboratory study. Geosynthetics International, 1(2), 221-259.

6. Adler, M. M., & Walsh, W. K. (1984) Mechanisms of transient moisture transport between fabrics. Textile Research Journal, 54(5), 334-343.

7. Aydilek, A., D'Hondt, D., & Holtz, R., 2007. Comparative Evaluation of Geotextile Pore Sizes Using Bubble Point Test and Image Analysis. Geotechnical Testing Journal, 30 (3), 173-181.

8. Azevedo, M., & Zornberg, J.G., 2013. Capillary barrier dissipation by new wicking geotextile. In: Caicedo, et al. (Eds.), Advances in Unsaturated Soils Proceedings, First Pan-American Conference on Unsaturated Soils. Taylor & Francis Group, London, pp. 559-565.

9. Bai, M., Liu, Z., Zhang, S., Liu, F., Lu, L., & Zhang, J. (2021) Experimental study on the effect of fabric parameter on drainage performance of wicking geotextile. Fibers and Polymers, 22(7), 2044-2051.

10. Bishop, A. W. (1959) The principal of effective stress. Teknisk ukeblad. 39, 859-863.

11. Biswas, N., Puppala, A. J., Khan, M. A., Congress, S. S. C., Banerjee, A., & Chakraborty, S. (2021) Evaluating the performance of wicking geotextile in providing drainage for flexible pavements built over expansive soils. Transportation Research Record, 2675(9), 208-221.

12. Bouazza, A., 2014. A simple method to assess the wettability of nonwoven geotextiles. Geotextiles and Geomembranes. 42 (4), 417–419.

13. Cassel, D. K., & Nielsen, D. R. (1986) Field capacity and available water capacity. Methods of soil analysis: Part 1 Physical and mineralogical methods. 5, 901-926.

14. Cassel, D. K., & Sweeney, M. D. (1974) In situ soil water holding capacities of selected North Dakota soils. Bulletin. 495, 25.

15. Colman, E. A. (1947) A laboratory procedure for determining the field capacity of soils. Soil science, 63(4), 277-284.

16. Cumulative Environmental Management Association (CEMA), (2006) Land capability classification system for forest ecosystems in the oil sands. Fort McMurray, AB, Canada.

17. Chatterjee, A., & Singh, P. (2014) Studies on wicking behaviour of polyester fabric. Journal of Textiles.

18. Chen, X., Kornev, K.G., Kamath, Y.K., & Neimark, A.V., 2001. The Wicking Kinetics of Liquid Droplets into Yarns. Textile Research Journal. 71 (10), 862–869.

19. Christopher, B. R., C. W. Schwartz, R. Boudreaux, and R. R. Berg. (2006) Geotechnical aspects of pavements. Washington, DC: Federal Highway Administration.

20. Clarke, A., Blake, T. D., Carruthers, K., & Woodward, A., 2002. Spreading and imbibition of liquid droplets on porous surfaces. Langmuir. 18 (8), 2980-2984.

21. Cotorobai, V. F., Zgura, I., Birzu, M., Frunza, S., & Frunza, L. (2016) Wicking behavior of fabrics described by simultaneous acquiring the images of the wet region and monitoring the liquid weight. Colloids and Surfaces A: Physicochemical and Engineering Aspects, 497, 146-153.

22. Davis, S. H., & Hocking, L. M., 2000. Spreading and imbibition of viscous liquid on a porous base. II. Physics of fluids. 12 (7), 1646-1655.

23. Davidson, J. M., Stone, L. R., Nielsen, D. R., & Larue, M. E. (1969) Field measurement and use of soil‐water properties. Water Resources Research. 5(6), 1312-1321.

24. Drelich, J. 1997. “The effect of drop (bubble) size on contact angle at solid surfaces”, J. Adhesion, 63, 31.

25. de Oliveira, R. A., Ramos, M. M., & de Aquino, L. A. (2015) Irrigation management. Sugarcane. Academic Press. 161-183.

26. Derbyshire, E. (2001) Geological hazards in loess terrain, with particular reference to the loess regions of China. Earth-Science Reviews. 54(1-3), 231-260.

27. Edris, E. V., & Lytton, R. L. (1976) Dynamic properties of subgrade soils, including environmental effects. Interim Report No. TTI-2-18-74-164-3. Texas A&M University.

28. Elton, D.J., & Hayes, D.W., 2008. The significance of the contact angle in characterizing the pore size distribution of geotextiles. Geosynthetics International. 15 (1), 22–30.

29. Elton, D.J., & Hayes, D.W., 2007. The Bubblepoint Method for Characterizing Geotextile Pore Size. In: Geosynthetics in Reinforcement and Hydraulic Applications, 1–10.

30. Fatema, N., & Bhatia, S.K., 2020. Comparisons between Geotextile Pore Sizes Obtained from Capillary Flow and Dry Sieving Tests. Geotechnical Testing Journal. 43 (4), 20180203.

31. Fangueiro, R., Filgueiras, A., Soutinho, F., & Meidi, X. (2010) Wicking behavior and drying capability of functional knitted fabrics. Textile Research Journal, 80(15), 1522-1530.

32. Fan, X., Xu, Q., Scaringi, G., Li, S., & Peng, D. (2017) A chemo-mechanical insight into the failure mechanism of frequently occurred landslides in the Loess Plateau, Gansu Province, China. Engineering Geology, 228, 337-345.

33. Fredlund, D. G. (2006) Unsaturated soil mechanics in engineering practice. Journal of geotechnical and geoenvironmental engineering. 132(3), 286-321.

34. Fredlund, D. G. (2014) The emergence of unsaturated soil mechanics. Canadian Geotechnical Journal. 51(12), ix-x.

35. Fredlund, D. G., & Rahardjo, H. (1993) An overview of unsaturated soil behaviour. Geotechnical special publication, 1-1.

36. Fredlund, D. G., Bergan, A. T., & Wong, P. K. (1977) Relation between resilient modulus and stress conditions for cohesive subgrade soils. Transportation Research Record. pp. 642.

37. Galinmoghadam, J., Liu, J., Zhang, X., Lin, C., & Guo, Y. (2022) Mitigating Pumping in Pavement Shoulder Using Wicking Geotextile: An Experimental Study. Transportation Research Record, 2676(11), 145-159.

38. Ghali, K., Jones, B., & Tracy, J., 1994. Experimental Techniques for Measuring Parameters Describing Wetting and Wicking in Fabrics. Textile Research Journal. 64 (2), 106–111.

39. Guo, J., Wang, F., Zhang, X., & Han, J. (2017) Quantifying water removal rate of a wicking geotextile under controlled temperature and relative humidity. Journal of Materials in Civil Engineering, 29(1), 04016181.

40. Guo, J., Han, J., Zhang, X., & Li, Z. (2019) Evaluation of moisture reduction in aggregate base by wicking geotextile using soil column tests. Geotextiles and Geomembranes, 47(3), 306-314.

41. Guo, J., Han, J., Zhang, X., & Li, Z. (2021) Experimental evaluation of wicking geotextile-stabilized aggregate bases over subgrade under rainfall simulation and cyclic loading. Geotextiles and Geomembranes, 49(6), 1550-1564.

42. De Guzman, E. M. B., Alfaro, M. C., Doré, G., Arenson, L. U., & Piamsalee, A. (2021) Performance of highway embankments in the Arctic constructed under winter conditions. Canadian Geotechnical Journal, 58(5), 722-736.

43. Harnett, P. R., & Mehta, P. N. (1984). A survey and comparison of laboratory test methods for measuring wicking. Textile research journal, 54(7), 471-478.

44. Hachem, A.E., & Zornberg, J.G., 2019. Enhanced Lateral Drainage Geotextile to Mitigate the Effects of Moisture Migration from a High-Water Table. In: Geo-Congress 2019. 227–234.

45. Han, J., & Zhang, X. (2014) Recent advances in the use of geosynthetics to enhance sustainability of roadways. 20th International Conference on Advances in Civil Engineering for Sustainable Development. Suranaree University of Technology Nakhon Ratchasima, Thailand. pp. 29-39.

46. Han, J., & Giroud, J.P., 2016. Field evaluation of the performance of unpaved roads incorporating geosynthetics - Planning. Geosynthetics. 34 (2), 27-41.

47. Han, Z., & Vanapalli, S. K. (2015) Model for predicting resilient modulus of unsaturated subgrade soil using soil-water characteristic curve. Canadian Geotechnical Journal, 52(10), 1605-1619.

48. Henry, K., & Patton, S., 1998. Measurement of the Contact Angle of Water on Geotextile Fibers. Geotechnical Testing Journal. 21 (1), 11-17.

49. Henry, K. S. (1995) The use of geosynthetic capillary barriers to reduce moisture migration in soils. Geosynthetics International, 2(5), 883-888.

50. Hignett, C., Evett, S. R., Dane, J. H., & Topp, G. C. (2002) Neutron thermalization. Methods of soil analysis. Part 4, 501-521.

51. Hillel, D. (1971) Research within the coordinated programme on the application of radiation techniques in water use efficiency studies. International Atomic Energy Agency. No. IAEA-R--328-F.

52. Hou, X., Vanapalli, S. K., & Li, T. (2018) Water infiltration characteristics in loess associated with irrigation activities and its influence on the slope stability in Heifangtai loess highland, China. Engineering Geology. 234, 27-37.

53. Houston, S. L. (2019) It is time to use unsaturated soil mechanics in routine geotechnical engineering practice. Journal of Geotechnical and Geoenvironmental Engineering. 145(5), 02519001.

54. Hollies, N. R., Kaessinger, M. M., Watson, B. S., & Bogaty, H. (1957) Water transport mechanisms in textile materials: Part II: Capillary-type penetration in yarns and fabrics. Textile Research Journal, 27(1), 8-13.

55. Hsieh, Y. L. (1995) Liquid transport in fabric structures. Textile Research Journal, 65(5), 299-307.

56. Indraratna, B., Israr, J., & Li, M. (2018) Inception of geohydraulic failures in granular soils–an experimental and theoretical treatment. Geotechnique, 68(3), 233-248.

57. Iryo, T., & Rowe, R. K. (2005) Hydraulic behaviour of soil–geocomposite layers in slopes. Geosynthetics International, 12(3), 145-155.

58. Jamison, V. C. (1956) Pertinent factors governing the availability of soil moisture to plants. Soil Science, 81(6), 459-472.

59. Jeon, H.-Y., & Bouazza, A., 2007. Tensile strength of plasma-treated nonwoven geotextiles. Geosynthetics International. 14 (4), 244–247.

60. Kermani, B., Xiao, M., Stoffels, S. M., & Qiu, T. (2018) Reduction of subgrade fines migration into subbase of flexible pavement using geotextile. Geotextiles and Geomembranes, 46(4), 377-383.

61. Kermani, B., Xiao, M., Stoffels, S. M., & Qiu, T. (2019) Measuring the migration of subgrade fine particles into subbase using scaled accelerated flexible pavement testing–a laboratory study. Road Materials and Pavement Design, 20(1), 36-57.

62. Kimmins, J. P., & Hawkes, B. C. (1978) Distribution and chemistry of fine roots in a white spruce–subalpine fir stand in British Columbia: implications for management. Canadian Journal of Forest Research. 8(3), 265-279.

63. Kirkham, M. B. (2014) Field capacity, wilting point, available water, and the nonlimiting water range. Principles of soil and plant water relations. 153-170.

64. Koerner, R. M. (2012) Designing with geosynthetics. Vol. 1. Xlibris Corporation.

65. Kumar, B., & Das, A. (2014) Vertical wicking behavior of knitted fabrics. Fibers and Polymers, 15, 625-631.

66. Kumar, S. M., & Deshpande, A. P., 2006. Dynamics of drop spreading on fibrous porous media. Colloids and Surfaces A: Physicochemical and Engineering Aspects. 277 (1-3), 157-163.

67. Kung, C.H., Sow, P.K., Zahiri, B., & Mérida, W., 2019. Assessment and Interpretation of Surface Wettability Based on Sessile Droplet Contact Angle Measurement: Challenges and Opportunities. Advanced Materials Interfaces. 6 (18), 1900839.

68. Kutilek, M., & Nielsen, D.R., 1994. Soil Hydrology. Verlag, Germany, 370p.

69. Le, C.V., Ly, N.G., & Stevens, M.G., 1996. Measuring the Contact Angles of Liquid Droplets on Wool Fibers and Determining Surface Energy Components. Textile Research Journal. 66 (6), 389–397.

70. Li, J., & Cameron, D. A. (2002) Case study of courtyard house damaged by expansive soils. Journal of performance of constructed facilities, 16(4), 169-175.

71. Lin, C., Galinmoghadam, J., Han, J., Liu, J., & Zhang, X. (2021) Quantifying and Incorporating the Benefits of Wicking Geotextile into Pavement Design. Journal of Transportation Engineering, Part B: Pavements, 147(3), 04021044.

72. Lin, C., & Zhang, X. (2018) Laboratory drainage performance of a new geotextile with wicking fabric. Journal of Materials in Civil Engineering, 30(11), 04018293.

73. Lin, C., & Zhang, X. (2020) Numerical simulation of seasonal variations of base course resilient modulus in pavement structures in nonfrost regions. Journal of Transportation Engineering, Part B: Pavements, 146(3), 04020038.

74. Lin, C., Presler, W., Zhang, X., Jones, D., & Odgers, B. (2017) Long-term performance of wicking fabric in Alaskan pavements. Journal of Performance of Constructed Facilities, 31(2), D4016005.

75. Lin, C., & Zhang, X. (2020) Comparisons of Geotextile-Water Characteristic Curves for Wicking and Non-Wicking Geotextiles. In Geo-Congress 2020 (pp. 629-636). Reston, VA: American Society of Civil Engineers.

76. Lin, C., Zhang, X., & Han, J. (2019) Comprehensive material characterizations of pavement structure installed with wicking fabrics. Journal of Materials in Civil Engineering, 31(2), 04018372.

77. Liu, H., Han, J., Al-Naddaf, M., Parsons, R. L., & Kakrasul, J. I. (2022) Field monitoring of wicking geotextile to reduce soil moisture under a concrete pavement subjected to precipitations and temperature variations. Geotextiles and Geomembranes, 50(5), 1004-1019.

78. Likos, W. J., & Lu, N. (2004) Hysteresis of capillary stress in unsaturated granular soil. Journal of Engineering mechanics. 130(6), 646-655.

79. Marmur, A. 2006. Soft contact: measurement and interpretation of contact angles. Soft Matter 2, 12-17.

80. Marshall, T. J., & Strik, G. B. (1949) Pressure potential of water moving downward into soil. Soil Science. 68(5), 359-370.

81. McIntyre, D. S., Cunningham, R. B., Vatanakul, V. I., & Stewart, G. A. (1979) Measuring hydraulic conductivity in clay soils: methods, techniques, and errors. Soil Science. 128(3), 171-183.

82. Melki, S., Biguenet, F., & Dupuis, D., 2019. Hydrophobic properties of textile materials: Robustness of hydrophobicity. The Journal of the Textile Institute. 110 (8), 1221–1228.

83. Mhetre, S., & Parachuru, R. (2010) The effect of fabric structure and yarn-to-yarn liquid migration on liquid transport in fabrics. The Journal of The Textile Institute, 101(7), 621-626.

84. Miller, B., & Young, R.A., 1975. Methodology for Studying the Wettability of Filaments. Textile Research Journal. 45 (5), 359–365.

85. Nyoni, A. B. (2011) Liquid Transport in Nylon 6.6. Woven Fabrics Used for Outdoor Performance Clothing. Advances in modern woven fabrics technology. 1st ed. InTech, 211-240.

86. Or, D., Wraith, J. M., & Warrick, A. W. (2002) Soil water content and water potential relationships. Soil physics companion. 1, 49-84.

87. Peng, J., Zhang, J., Li, J., Yao, Y., & Zhang, A. (2020) Modeling humidity and stress-dependent subgrade soils in flexible pavements. Computers and Geotechnics, 120, 103413.

88. Pimanpang, S., Wang, P.-I., Senkevich, J.J., Wang, G.-C., & Lu, T.-M., 2006. Effect of hydrophilic group on water droplet contact angles on surfaces of acid modified SiLK and Parylene polymers. Colloids and Surfaces A: Physicochemical and Engineering Aspects. 278 (1–3), 53–59.

89. Puppala, A. J., Pedarla, A., Pino, A., & Hoyos, L. R. (2017) Diffused double-layer swell prediction model to better characterize natural expansive clays. Journal of Engineering Mechanics, 143(9), 04017069.

90. Rai, R. K., Singh, V. P., & Upadhyay, A. (2017) Planning and evaluation of irrigation projects: methods and implementation. 1st Edition. Elsevier.

91. Rawls, W. J., Brakensiek, D. L., & Saxtonn, K. E. (1982) Estimation of soil water properties. Transactions of the ASAE. 25(5), 1316-1320.

92. Rani, K.V., Chandwani, N., Kikani, P., Nema, S.K., Sarma, A.K., & Sarma, B., 2018. Optimization and surface modification of silk fabric using DBD air plasma for improving wicking properties. The Journal of The Textile Institute. 109 (3), 368–375.

93. Ritchie, J. T. (1981) Soil water availability. Plant and soil. 327-338.

94. Rollin, A., & Lombard, G., 1988. Mechanisms affecting long-term filtration behavior of geotextiles. Geotextiles and Geomembranes. 7 (1–2), 119–145.

95. Sarah, K., & Ulrich, H., 2018. Short timescale wetting and penetration on porous sheets measured with ultrasound, direct absorption and contact angle. RSC advances. 8 (23), 12861-12869.

96. Sahin, H., Gu, F., Tong, Y., Luo, R., & Lytton, R. L. (2013) Unsaturated soil mechanics in the design and performance of pavements. Advances in Unsaturated Soils. 1, 87.

97. Sauer, E. K., & Monismith, C. L. (1968) Influence of soil suction on behavior of a glacial till subjected to repeated loading. Highway Research Record. 215, 8-23.

98. Shim, M.H., Kim, J., & Park, C.H., 2014. The effects of surface energy and roughness on the hydrophobicity of woven fabrics. Textile Research Journal. 84 (12), 1268–1278.

99. Smith, R. M., & Browning, D. R. (1948) Soil moisture tension and pore space relations for several soils in the range of the "field capacity". Soil Science Society of America Journal. 12(C), 17-21.

100. Stormont, J.C., Henry, K.S., & Evans, T.M., 1997. Water Retention Functions of Four Nonwoven Polypropylene Geotextiles. Geosynthetics International. 4 (6), 661–672.

101. Stormont, J.C., & Morris, C.E., 2000. Characterization of Unsaturated Nonwoven Geotextiles. In: Advances in Unsaturated Geotechnics. 153–164.

102. Stormont, J. C., & Anderson, C. E. (1999) Capillary barrier effect from underlying coarser soil layer. Journal of Geotechnical and Geoenvironmental Engineering, 125(8), 641-648.

103. Sun, P., Peng, J. B., Chen, L. W., Yin, Y. P., & Wu, S. R. (2009) Weak tensile characteristics of loess in China—an important reason for ground fissures. Engineering Geology. 108(1-2), 153-159.

104. Tang, C., Lu, Z., Duan, Y., & Yao, H. (2020) Dynamic responses of the pavement-unsaturated poroelastic ground system to a moving traffic load. Transportation Geotechnics. 25, 100404.

105. Tillotson, P. M., & Nielsen, D. R. (1984) Scale factors in soil science. Soil Science Society of America Journal. 48(5), 953-959.

106. The European Committee for Standardization (CEN), 2000. CEN EN 13562:2000 Geotextiles and geotextile-related products - Determination of resistance to penetration by water (hydrostatic pressure test).

107. Van Der Meeren, P., Cocquyt, J., Flores, S., Demeyere, H., & Declercq, M., 2002. Quantifying Wetting and Wicking Phenomena in Cotton Terry as Affected by Fabric Conditioner Treatment. Textile Research Journal. 72 (5), 423–428.

108. Vanapalli, S., & Oh, W. (2011) Simple techniques for the estimation of suction in compacted soils in the range of 0 to 60,000 kPa. Geotechnical Testing Journal. 34(6), 765-774.

109. Veihmeyer, F. J., & Hendrickson, A. H. (1931) The moisture equivalent as a measure of the field capacity of soils. Soil Science. 32(3), 181-194.

110. Wang, F., Han, J., Zhang, X., & Guo, J. (2017) Laboratory tests to evaluate effectiveness of wicking geotextile in soil moisture reduction. Geotextiles and Geomembranes, 45(1), 8-13.

111. Washburn, E. W. (1921) The dynamics of capillary flow. Physical review, 17(3), 273.

112. Wen, B. P., & Yan, Y. J. (2014). Influence of structure on shear characteristics of the unsaturated loess in Lanzhou, China. Engineering Geology. 168, 46-58.

113. Xu, L., Dai, F.C., Tham, L.G., Tu, X.B., Min, H., Zhou, Y.F., Wu, C.X. and Xu, K. (2011) Field testing of irrigation effects on the stability of a cliff edge in loess, North-west China. Engineering Geology. 120(1-4), 10-17.

114. Xu, L., Dai, F., Tu, X., Tham, L. G., Zhou, Y., & Iqbal, J. (2014) Landslides in a loess platform, North-West China. Landslides. 11, 993-1005.

115. Yanılmaz, M., & Kalaoğlu, F. (2012) Investigation of wicking, wetting and drying properties of acrylic knitted fabrics. Textile Research Journal, 82(8), 820-831.

116. Yuan, H., 2017. Effectiveness of Wicking Geotextile in Mitigating Freeze-thaw Problems of Aggregate Bases with Fines. Master's thesis. Dept. of Civil, Environmental, and Architectural Engineering. The University of Kansas.

117. Zaman, M. W., Han, J., & Zhang, X. (2022a) Technical Review of Development and Applications from Wicking Fabric to Wicking Geotextile. In Geo-Congress'22 Proceedings. American Society of Civil Engineers. pp. 587-596.

118. Zaman, M. W., Han, J., & Zhang, X. (2022b) Evaluating wettability of geotextiles with contact angles. Geotextiles and Geomembranes. 50(4), 825-833.

119. Zaman, M. W., and Han, J. (2023) Investigation of Moisture Reduction in Sandy Soil using Geotextiles. Geosynthetics'23 Conference. Advanced Textile Association. pp. 305-314.

120. Zaman, M. W., Han, J., & Kabir, M. U. (2024) Laboratory Investigation of Field Moisture Capacities of Silty Sands at Different Fine Contents. Geotechnical Testing Journal. Under review.

121. Zettl, J., Lee Barbour, S., Huang, M., Si, B., & Leskiw, L. A. (2011) Influence of textural layering on field capacity of coarse soils. Canadian Journal of Soil Science. 91(2), 133-147.

122. Zhan, T. L., & Ng, C. W. (2004) Analytical analysis of rainfall infiltration mechanism in unsaturated soils. International Journal of Geomechanics. 4(4), 273-284.

123. Zhang, J., Peng, J., Zhang, A., & Li, J. (2022) Prediction of permanent deformation for subgrade soils under traffic loading in Southern China. International Journal of Pavement Engineering, 23(3), 673-682.

124. Zhang, X., Presler, W., Li, L., Jones, D., & Odgers, B. (2014) Use of wicking fabric to help prevent frost boils in Alaskan pavements. Journal of Materials in Civil Engineering, 26(4), 728-740.

125. Zhou, C., & Ng, C. W. W. (2016) Simulating the cyclic behaviour of unsaturated soil at various temperatures using a bounding surface model. Géotechnique. 66(4), 344-350.

126. Zornberg, J. G., & Gupta, R. (2009) Reinforcement of pavements over expansive clay subgrades. In Proceedings of the 17th International Conference on Soil Mechanics and Geotechnical Engineering (Volumes 1, 2, 3 and 4). IOS Press. pp. 765-768.

127. Zornberg, J. G., Azevedo, M., Sikkema, M., & Odgers, B. (2017) Geosynthetics with enhanced lateral drainage capabilities in roadway systems. Transportation Geotechnics, 12, 85-100.